ABSTRACT.

The Shubnikov de Haas effect has proven to be a useful tool in the determination of the band structure of semiconductors, yielding such parameters as Lande g-factor, carrier concentration and effective mass. The effect itself, exhibits some interesting unexplained behaviour and this has been a source of interest for some time.

In this work, samples of homogeneously doped Indium Antimonide having carrier concentrations varying from $5x10^{15}$ to $5x10^{16}cm^{-3}$ were produced by Neutron Transmutation Doping. Magnetoresistance measurements were made up to a field of 12 Tesla. The influence of sample orientation on the oscillation profile was investigated and the results were found to be in agreement with previous workers, i.e., in the longitudinal position the higher-field peaks in the spin-split doublets have a much reduced amplitude. The Dingle temperatures of the samples were determined from the mobilities and by computer fit to the experimental curves. The values obtained by each method were found to be significantly different.

In addition, the mechanism of magnetic freeze-out was seen in two samples, and a $B^{1/3}$ dependence of the donor binding energy observed. The variation of Hall coefficient with magnetic field, at high magnetic fields was investigated. There was no indication of a sign reversal in the data.

ELECTRON TRANSPORT IN SEMICONDUCTORS IN HIGH MAGNETIC FIELDS

A Thesis

presented by

Jackie Staromlynska B.Sc.

to the

University of St.Andrews

in application for the Degree of

Doctor of Philosophy

Certificate

We certify that Jackie Staromlynska, B.Sc. has spent nine terms at research work in the School of Physical Sciences in the University of St.Andrews under our direction, that she has fulfilled the conditions of the Resolution of the University Court, 1967, no 1, and that she is qualified to submit the accompanying thesis in application for the Degree of Doctor of Philosophy. She was admitted as a research student under Ordinance General no 12 on 1st October 1978 and as a Ph.D. student under Resolution of the University Court, 1967, no 1 on 3rd October 1979.

Research Supervisors

Declaration

I hereby certify that this thesis has been composed by me, and is a record of work done by me, and has not previously been presented for a Higher Degree. The research was carried out in the Physics Department of St.Andrews University under the supervision of Professor R.A. Stradling and Dr. D.M. Finlayson.

Jackie Staromlynska

ACKNOWLEDGEMENTS.

I wish to thank Prof. R. A. Stradling for suggesting the project and for his subsequent help and useful discussions. My thanks is also due to Prof. J. W. Allen for many helpful suggestions on the handling of InSb, and to Mr. R. H. Mitchell for his advice on cryomagnetic systems.

I would especially like to extend my thanks to my supervisor, Dr. D. M. Finlayson, for his advice and guidance throughout the project and for his unfailing patience and good humour.

In addition I wish to express my appreciation of the moral support given to me during my time at St. Andrews by my friends and family. Finally I thank Mr. H. M. Robb for kindly supplying the typing facilities and my hard working typist, Miss Evelyn Dearie, for her speedy and efficient typing.

CONTENTS.

CHAPTER FOUR: SPIN SPLITTING IN S.D.H. OSCILLATIONS.

CHAPTER FIVE: MAGNETIC FREEZE-OUT IN InSb.

CHAPTER 1.

MAGNETIC QUANTUM EFFECT.

1.1 INTRODUCTION.

The most interesting magnetic effects occurring in solids are due to the profound changes in the density of states of the conduction electrons induced by the magnetic quantisation of the energy levels. The energy level structure consists of a set of magnetic sub-bands, known as Landau[1] levels, having energies (neglecting spin).

$$\epsilon(p) = (p+\tfrac{1}{2})\hbar\omega + \frac{\hbar^2 k_z^2}{2m^*} \qquad 1.1$$

where $\epsilon(p)$ = energy of p^{th} Landau level.

p = Landau quantum number = 0, 1, 2, ...

k_z = wave vector in z-direction = direction of magnetic field.

m^* = electron effective mass.

ω = cyclotron frequency = eB/m^*, B = magnetic field.

These sub-bands are separated by $\hbar\omega$ (figure 1.1) and have a singularity in the density of states at the bottom of each band i.e. at $k_z = 0$. In degenerate materials with a well defined Fermi energy, when the magnetic field is increased, the energy of each Landau level increases until the bottom of the sub-band crosses the Fermi level, at which point $k_z = 0$ and the density of states becomes infinite (figure 1.2). This leads to a quasi- periodicity in 1/B in the density of states at the Fermi level and this is reflected in a number of properties.

One of the best known of the oscillatory effects is the de Haas van Alphen[2] effect which is oscillations in the magnetic susceptibility of the material. Oscillations in the magnetoresistance of Bismuth were

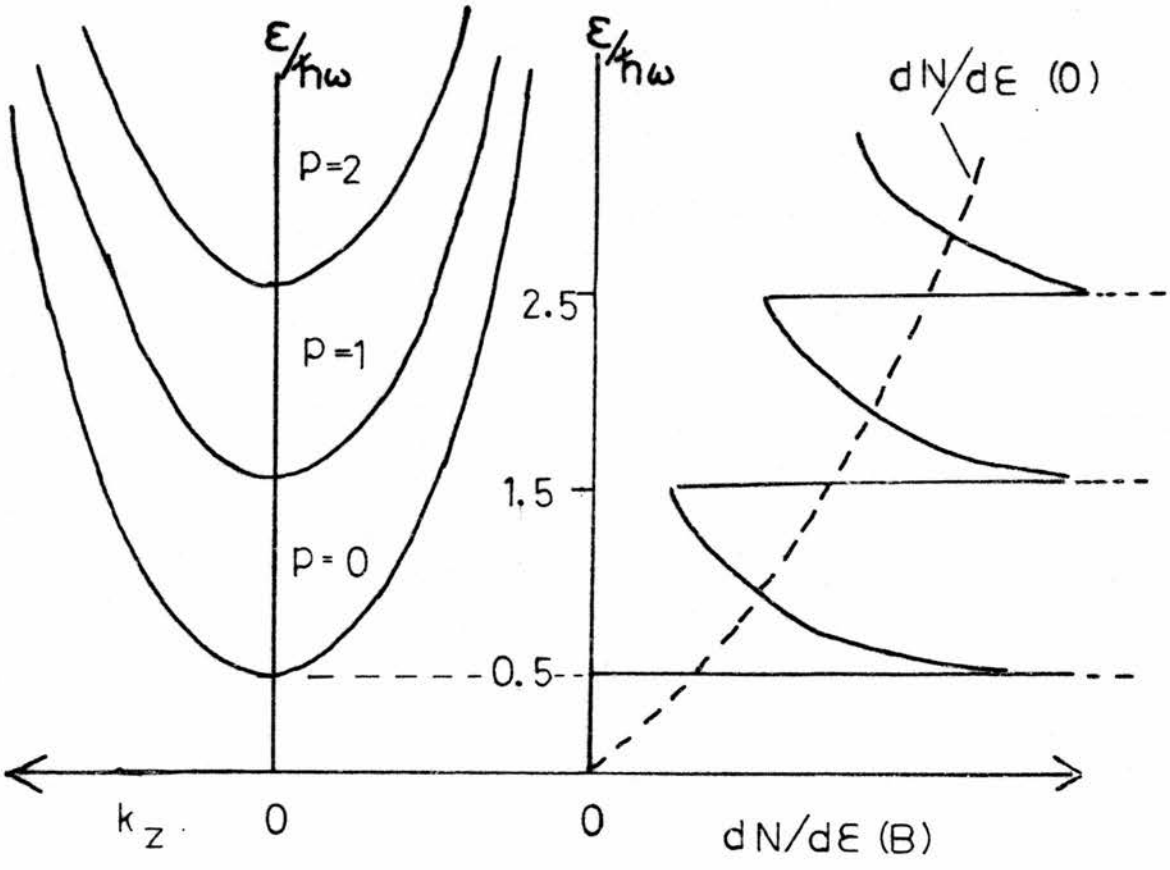

FIGURE 1·1

FIGURE 1·2

ENERGY BANDS FOR A SIMPLE SEMICONDUCTOR IN A MAGNETIC FIELD (FIG.I.1)

DENSITIES OF STATES FOR A SIMPLE SEMICONDUCTOR IN A MAGNETIC FIELD (FIG.I.2).

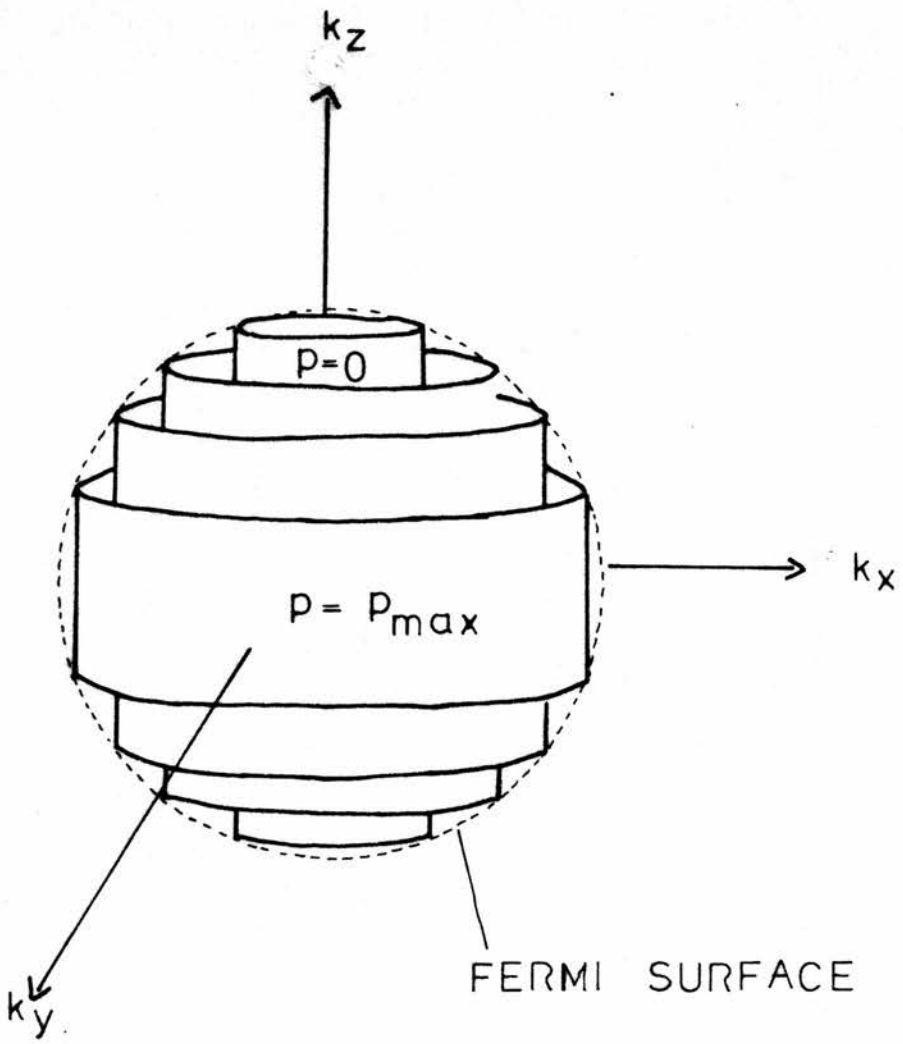

FIGURE 1·3

THE LANDAU LEVELS: ALLOWED ENERGY STATES OF FREE ELECTRONS IN A MAGNETIC FIELD WHICH IS IN THE Z-DIRECTION.

discovered by Shubnikov and de Haas[3] slightly earlier than the de Haas-van Alphen effect. Both effects have proved to be very useful tools in the probing of the band structure of metals and semi-conductors. Analogous oscillations have been observed in other physical properties such as the optical[4] and thermomagnetic[5] properties and the specific heat[6].

For the observation of magnetoresistance oscillations certain conditions have to be fulfilled. These are

$$\omega\tau >> 1 \qquad 1.2$$

and $$\hbar\omega >> kT \qquad 1.3$$

where τ = mean relaxation time.

k = Boltzmann Constant.

T = Temperature

Under the above conditions the quantisation of the electronic energy levels is not blurred either by collisions with impurities or by the thermal spread of the electron distribution. An additional condition for the observation of the Shubnikov-de Haas oscillations is that of degenerate statistics i.e.

$$E_F >> kT \qquad 1.4$$

where E_F = Fermi energy.

The existence of magnetoresistance oscillations in such semiconductors as InSb and InAs, which are degenerate at low temperatures, is a consequence of their small effective masses and small donor binding

energies. The small effective mass enables the condition $\omega\tau >> 1$ to be fulfilled at relatively low magnetic fields and the small donor binding energy means that the carriers do not freeze out until very high magnetic fields and/or very low temperatures. For large enough magnetic fields the electrons are all in the lowest quantum state and the quantum limit is reached where there are smooth field variations of the magnetoresistance, characteristic of the scattering mechanism. The quantum limit is defined by the relation (neglecting spin):

$$E_F < \tfrac{1}{2}\hbar\omega \qquad 1.5$$

where E_F = Fermi energy.

and ω = cyclotron frequency

Further increasing of the magnetic field away from the quantum limit region leads to the ultra-quantum limit where freeze-out of the carriers occurs. An important point to note is that from the quantum limit region onwards, the degeneracy temperature decreases with increasing field, so that it is possible that the statistics of the semi conductor may change as a function of magnetic field, B. The statistics in the magnetic freeze-out region are generally treated as being non-degenerate. Adams and Holstein[7] have produced equations giving the functional forms for the transverse, (electric and magnetic fields perpendicular), and longitudinal, (electric and magnetic fields parallel), magnetoresistances in the quantum limit for several types of scattering and both types of statistics. They predicted that for ionised impurity scattering and for degenerate statistics, both the longitudinal and transverse magnetoresistance have a B^3T^0 dependence. In contrast to this, they also predicted that for non-degenerate (i.e. classical) statistics, and ionised impurity scattering the longitudinal and transverse magnetoresistances would vary as $B^0T^{-3/2}$. These equations are wrong

in detail as has been pointed out in a review by Kubo[8].

The Shubnikov-de Haas effect is a very useful tool for gaining information on semi conductors, where it has the advantage over the de Haas-van Alphen effect in that it is an experimentally less complicated procedure to measure the magnetoresistance than it is to measure the magnetic susceptibility. For example the Fermi surface of a material may be probed by measuring the period of the oscillations which is given by

$$\Delta(1/B) = \frac{2\pi e}{\hbar A(F)} \qquad 1.6$$

where $\Delta(1/B)$ = period of unsplit oscillations

$A(F)$ = cross sectional area of Fermi surface normal to $\underline{B}$

By measuring the period of the unsplit oscillations as a function of crystallographic orientation the shape of the Fermi surface may be deduced. A natural extension of this is that the carrier concentration, n, of a semiconductor may also be deduced from $\Delta(1/B)$. i.e. (for a spherical conduction band).

$$n = \frac{1}{3\pi^2} \frac{(2e)^{3/2}}{(\hbar\Delta(1/B))^{3/2}} \qquad 1.7$$

The measurement of $\Delta(1/B)$ to determine n is a method commonly employed by many workers. It overcomes the need for the knowledge of the sample thickness and is not greatly influenced by contact effects, both of which occur in the Hall effect, and hence is intrinsically more accurate. One important property of the Shubnikov-de Haas effect is that the low order maxima (i.e. $p < 3$) in InSb may be split into two maxima (p^+ and p^-), each representing an electron orientation, against, or in the same direction as, the magnetic field. Measurement of the magnetic

field positions of these spin-split maxima allows the determination of the Lande g factor. The energy levels, now including spin, are given by

$$\epsilon(p,\pm) = (p+\tfrac{1}{2}\pm\tfrac{1}{2}\nu)\hbar\omega+\frac{\hbar^2 k_z^2}{2m^*} \qquad 1.8$$

where ν = spin splitting factor = $\frac{1}{2}gm^*/m$

From equation 1.8 it can be seen that the spin splitting factor ν (and hence g) may be calculated assuming knowledge of m^*, from the peak magnetic field positions and the relation

$$\nu = 1/\Delta(1/B)\left[\frac{1}{B_p^+} - \frac{1}{B_p^-}\right] \qquad 1.9$$

where B_p^+ and B_p^- are the magnetic field positions of the p^+ and p^- maxima respectively.

Quantum limit and ultra-quantum limit measurements also provide important information on material properties. The temperature and magnetic field dependence of the magnetoresistance in the Quantum limit (i.e. before freeze-out) give an indication of the scattering mechanism present, whilst temperature and magnetic field dependent measurements of the Hall coefficient and resistance in the freeze-out region gives values of the donor binding energy. For clarity each effect, (i.e. Shubnikov-de Haas and magnetic freeze-out), its uses, associated problems and anomalies shall be discussed in separate sections, with a final section outlining the theoretical formalism of the Shubnikov-de Haas effect.

1.2 THE SHUBNIKOV-DE HAAS EFFECT.

The Shubnikov-de Haas effect is widely employed to explore the band

structure of degenerate semiconductors. In particular, the temperature dependence of the amplitude of the oscillations has been used to determine effective masses, and the spin-splitting of the high field doublets used to determine the Lande g-factor. The technique has been used on a large variety of materials such as Mercury Telluride[9], Cadmium Mercury Telluride[10], Zinc Mercury Selenide[11] and many others[12-16].

There are many problems associated with the technique which must be considered when using it to evaluate band parameters. Any inhomogeneities in the electron distribution will serve to broaden and decrease the amplitudes of the maxima, which will decrease the resolution of the spin-split peaks resulting in greater errors of the measured g-value. Hence one of the most important requirements for the use of the technique is a homogeneously doped sample. Evaluation of the Lande g-factor is usually achieved by measuring the magnitude of the spin-splitting of the $1^{\pm}$ doublet in the transverse magnetoresistance. This imposes restrictions on the lower limit of the donor concentration of the sample. Since the magnitude of the splitting is proportional to B, (equation 1.8), the magnetic field at which the doublet falls, it follows that $p=1^{\pm}$ doublets occuring at low magnetic fields may be completely unresolved, or only partially resolved. From equations 1.1 and 1.7 it can be seen that the field at which any particular Landau level passes through the Fermi surface varies $n^{2/3}$ (n= carrier concentration) i.e. (neglecting spin)

$$(p+\tfrac{1}{2})\hbar\omega \propto n \qquad 1.10$$

$$\text{ie} \quad Bp \propto n^{2/3} \qquad 1.11$$

where Bp = field at which p^{th} Landau level crosses Fermi surface.

Hence it can be seen that for small values of n, the peaks fall at low magnetic fields with the result that the 1± doublet may not be resolved. For InSb, samples having a carrier concentration less than $10^{16}cm^{-3}$ do not exhibit resolved 1± maxima, for carrier concentrations between 10^{16} and $10^{17}cm^{-3}$ the 1± doublet is partially resolved and at $>10^{17}cm^{-3}$ the 1± maxima are fully resolved.

The high magnetic field peaks are subject to shifts away from the resonance condition, the shifts arising from three different sources. The Fermi energy is not a constant at high magnetic fields but rather increases with magnetic field. The other forms of shifting maybe understood by considering the functional form of the magnetoresistance which is given by

$$\rho_{zz}/\rho_0 = 1+\sum_{r=1}^{\infty} br\cos\left[\frac{2\pi rF}{B} - \pi/4\right] \qquad 1.12$$

$$\rho_{xx}/\rho_0 = 1+5/2\sum_{r=1}^{\infty} b_r\cos\left[\frac{2\pi rF}{B} - \pi/4\right] + R \qquad 1.13$$

where

$$b_r = (-1)^r\left(\frac{r}{2FB}\right)^{1/2} \frac{\beta Tm'\cos(\pi\nu r)}{\sinh(r\beta Tm'/B)} \exp-(r\beta T_D m'/B) \qquad 1.14$$

$$R = 3/4\left(\frac{B}{2F}\right)\left[\sum_{r=1}^{\infty} br\left[A\cos\left(\frac{2\pi rF}{B}\right)+C r\sin\left(\frac{2\pi rF}{B}\right)\right]-\ln(1-\exp-(\beta T_D m'/B))\right] \qquad 1.15$$

$$A_r = 2r^{1/2}\sum_{s=1}^{\infty}\frac{1}{[s(r+s)]^{1/2}} \exp-(2\beta T_D m'S/B) \qquad 1.16$$

$$C_r\, r^{1/2}\sum_{s=1}^{r-1}\frac{1}{[s(r-s)]^{1/2}} \qquad 1.17$$

$$\beta = 2\pi^2 km/\hbar e \qquad 1.18$$

$$F = E_F B/\hbar\omega \qquad 1.19$$

$$m' = m^*/m \qquad 1.20$$

T_D = Dingle temperature

By examining equations 1.12 and 1.13 it can be seen that there is a phase factor $\pi/4$ included in the main cosine term. The phase factor is a consequence of contributions to the scattering from all the Landau levels lying below the Fermi energy. When only a few levels remain occupied this phase factor changes and essentially becomes a function of magnetic field. Again this means that the positions of the high field peaks change. The third type of shifting is known as experimental phase-shifting and is discussed in detail in chapters 2 and 4. It arises from the fact that the cosine term is pre-multiplied by the term b_r which is a complicated function of the magnetic field. This term changes the turning points of the maxima from the values defined by the cosine term. The shifting is not constant throughout the oscillation profile and in general is larger for the low order (i.e. high field) maxima. All the above effects destroy the periodicity ($\Delta(1/B)$) of the low order maxima, this means that in the determination of n, the carrier concentration, from the oscillations, only the low field maxima should be used. The dependence of the Fermi energy and phase factor, ϕ on the magnetic field, at high magnetic fields, shift the 1^+ and 1^- peaks with respect to each other and this introduces inaccuracies into the evaluation of the g-factor from the spin-split doublet. The experimental phase shifting is not such a vital factor in the evaluation of g since it is likely that the 1^+ and 1^- peaks are shifted by an equal amount with this effect.

Apart from being used to investigate the band structure of semiconductors, the Shubnikov-de Haas effect has in itself been studied since it exhibits some still unexplained behaviour. The main anomaly

appears on rotation from the transverse, (ρ_{xx}), to the longitudinal, (ρ_{zz}), orientation. In ρ_{zz} the higher magnetic field peaks in the doublets are either much smaller than their ρ_{xx} counterparts, (as in the case for InSb), or appear to be completely missing (as has been reported for Grey Tin). In addition to this the higher field maximum of the doublet in ρ_{zz} seems to fall at a higher field than the corresponding transverse maximum, although its position is difficult to measure as it generally appears as a barely discernible shoulder on the lower field maximum of the doublet.

One other major difference between ρ_{xx} and ρ_{zz} is the absence of the lower maximum in the p=0 doublet in ρ_{zz} (from now on the lower field maxima will be designated by p^- and the higher field by p^+). This has been satisfactorily explained by assuming no momentum relaxation in the z-direction within the level as it is about to empty and a very small spin-flip scattering probability. Several workers have observed the existence of a very small amplitude peak in the region of the position of the 0^- maximum in ρ_{zz}. Suggestions have been made that it is a remnant of the 0^- peak arising from poor orientation and/or large donor concentration spatial inhomogeneities causing non-parallel current paths. Both of these would result in components of σ_{xx} mixing in with σ_{zz} thus resulting in the manifestation of σ_{xx} characteristics. Again, the measurement of the position of this peak is difficult due to its very small amplitude which is superimposed on a rapidly varying background and to date it has not been proved conclusively that it is a remnant of the 0^- peak.

Further unexplained peaks have been observed in the oscillation profiles of the transverse and longitudinal magnetoresistance. No extensive experimental investigations have as yet been performed to determine their dependence on carrier concentration magnetic field etc., and no

serious attempt to explain their existence has yet been formulated.

1.3 MAGNETIC FREEZE-OUT InSb.

At very high magnetic fields i.e. $\hbar\omega > E_F$ the free carriers begin to freeze-out into bound states on the donor atoms. The free carrier concentration falls, the Hall voltage-magnetic field relationship becomes non-linear and the magnetoresistance increases much more rapidly with magnetic field than it does in the quantum limit region where ionised impurity scattering dominates. The ground state donor binding energy, which varies as $B^{1/3}$, may be obtained from the equation

$$\frac{n+N_A}{N_D-N_A-n} = \frac{N_c}{n}\exp - (E_D/kT) \qquad 1.14$$

where n = free carrier concentration

N_D = Donor concentration

N_A = Acceptor concentration

E_D = Donor binding energy

T = Temperature.

and $N_c = (2\pi m^* kT)^{1/2} eB/\hbar^2$ 1.15

By simply measuring n, the free carrier concentration, as a function of magnetic field the donor binding energy may be evaluated as a function of field. Many theories have been developed to predict the donor binding energy, the simplest of which is the Yafet Keyes and Adams (YKA) theory assuming a parabolic band and ignoring such effects as screening and band tailing. Agreement between the theoretical YKA values and experiment is poor, the reason being due to the many influencing effects (such as non-parabolicity and screening) ignored by the theory. Other theories exist, which include one or two, but not

all, of the influencing factors and in general it has been found that better agreement exists between these theories and experiment. It has been suggested that to some extent these disagreements are due to sample inhomogeneity, and the need for homogeneously doped samples has been stressed.

The above has been a description of the well-known effect of magnetic freeze-out. However it has been found that behaviour of the magnetotransport properties of InSb in the ultra-quantum limit region do not always follow this characteristic pattern. Observations have been made of a sign change in the Hall coefficient and a saturation of the magnetoresistance, at fields greater than 2 Tesla depending on sample temperature and carrier concentration. Much controversy exists over this anomalous behaviour with one group of workers claiming it is merely due to a surface conduction layer being formed during contacting and others stating that it is a bulk effect associated with a mechanism of asymmetric scattering of spin-polarised electrons at ionised impurities known as skew scattering. Both sets of workers contacted in different ways, (both of which involve heating the sample to some extent), and both sets of workers have consistently observed vastly different behaviour.

1.4 AIMS OF THIS WORK.

The aim of this study was to investigate the magneto-quantum transport properties and the associated anomalies of InSb in a controlled and systematic manner. The need for sample homogeneity has been stressed throughout this chapter and for this reason samples were fabricated from high-purity, single crystal InSb, and were subsequently doped by the method of neutron transmutation doping which produces a much better spacial uniformity of doping (to $\sim$ 3%) and allows a much greater control over the degree of doping than the more conventional methods. NTD is

described along with sample preparation in chapter 3. The method proved to be moderately successful with homogeneous samples being produced, although the control over the degree of doping was less successful than was hoped. The crystals were doped to densities lying between $5x10^{15}cm^{-3}$ and $5x10^{16}cm^{-3}$, this giving a range of carrier concentrations with which both the Shubnikov-de Haas effect (including spin-splitting), and magnetic freeze-out could be studied. The minimum of interference with the surface of the samples was achieved by contacting with a Silver epoxy, this being a different system than those adopted by previous workers. It was hoped that by neutron transmutation doping and contacting with the Silver epoxy. (which required no heating), that any observed behaviour could not be attributed to sample inhomogeneity or surface effects. The advantages of NTD are made apparent by figure 1.4 which compares the oscillation profiles of two samples with similar carrier concentrations, one of which has been doped conventionally and one by NTD. Notice how the amplitudes of the maxima in the NTD doped sample are larger than those for the conventionally doped sample. Also notice how the $1\pm$ doublet is spin-split in the NTD sample whereas for the other sample the doublet is an unresolved broad maximum.

The technique of double differentiation was employed to accentuate the higher frequency components of the Fourier series. This enabled some useful measurements to be made. Firstly, under the correct conditions the $1\pm$ doublet in ρ_{xx} was fully resolved allowing accurate measurement of the spin-splitting, ν. Secondly in some cases it was also possible to resolve the $2\pm$ doublet enabling g to be measured without all the attendant problems of a changing Fermi energy and phase, ϕ. By comparing the g values obtained from both doublets it was possible to get an indication of the magnitude of the inaccuracies introduced into the g value obtained from the $1\pm$ doublet due to these effects.

COMPARISON OF MAGNETORESISTANCE PROFILES EXHIBITED BY A CONVENTIONALLY DOPED AND N.T.D. SAMPLE

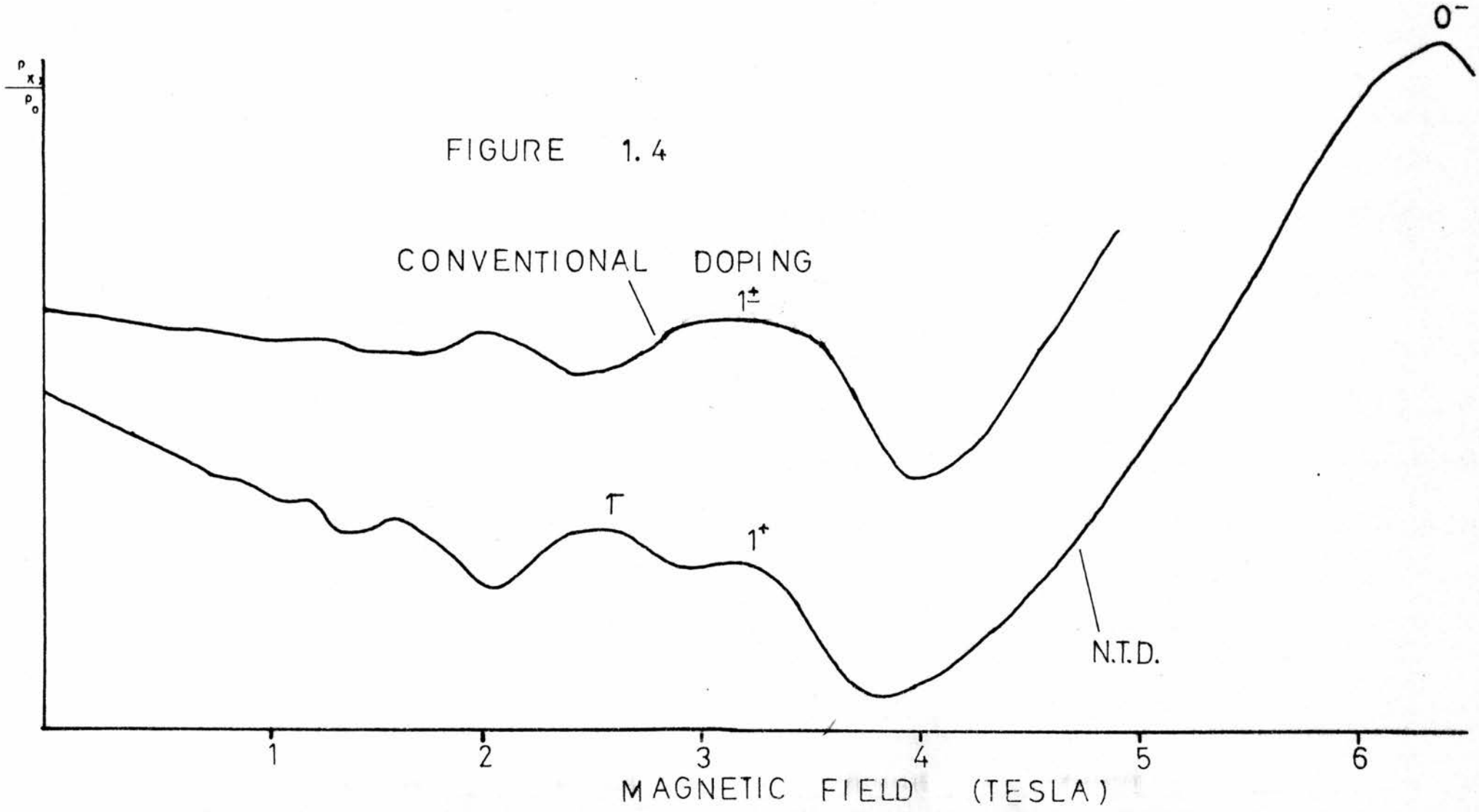

FIGURE 1.4

The double differentiation also resolved other features of the oscillation profiles such as the $1^{\pm}$ doublet in ρ_{zz} and intermediate orientations and also the peaks in ρ_{zz} appearing in the region of the 0^{-}. This again allowed measurement of their magnetic field positions, thus making the identification of the peaks and the study of their behaviour much easier.

1.5 THEORY OF THE SHUBNIKOV-DE HAAS EFFECT.

THE DENSITY OF STATES.

To understand the oscillatory behaviour of the magnetoresistance an understanding of the electron density of states is necessary. Considering the case of a free electron of spin s, mass m*, g-factor g and charge (-e) in a uniform magnetic field B in the z-direction, the Hamiltonian for such a system is

$$H_0 = \frac{1}{2m^*} (\underline{P} + \underline{A})^2 + g\mu_b \underline{S}.\underline{B} \qquad 1.16$$

where $\underline{A}$ = the vector potential describing the magnetic field i.e. $\underline{B} = \nabla \times \underline{A}$

$\underline{P} = m^*\underline{v} - e\underline{A}$

$\mu_b = e\hbar/2m$ m = free electron mass.

Choosing the Landau gauge of

$$\underline{A} = (0, Bx, 0)$$

P_y and P_z commute with the Hamiltonian giving the energy eigenstates

$$\psi_{pk}(r) = (L_y L_z)^{-\frac{1}{2}} \phi_p(x - X_k) \exp i(k_y Y + k_z z) \qquad 1.17$$

Where $\underline{k} = (k_y k_z)$ is the 2-dimensional wave vector associated with the y and x components of the motion of the electron, and $L_y L_z$ are the corresponding normalisation lengths. The oscillator quantum number p, has the values 0, 1, 2 etc. The $\phi p(x-X\ k)$ are the normalised wave functions of a simple harmonic oscillator having angular frequency ω centred at the point.

$$X(k) = -(\hbar/eB)k_y = (m^*/\hbar)\omega k_y \qquad 1.18$$

The energy eigenvalues are now, including spin

$$\varepsilon(p,k\pm) = (p+\tfrac{1}{2}\pm\tfrac{1}{2}\nu)h\omega+\frac{\hbar^2k_z^2}{2m^*} \qquad 1.19$$

where $\nu = m^*g/2m$

This shows that the energy in the x-y plane is quantised in units of $\hbar\omega$, with the energy in the z-direction taking any value. The energy in the x-y plane alone may also be expressed as

$$\varepsilon(p\pm) = (p+\tfrac{1}{2}\pm\tfrac{1}{2}\nu)h\omega = (\hbar^2/2m^*)(k_x^2 + k_y^2) \qquad 1.20$$

In k-space the allowed energy states lie on the surfaces of right cylinders whose cross-section satisfy.

$$A = \frac{2\pi eB}{\hbar}\,(p+\tfrac{1}{2}\pm\tfrac{1}{2}\nu) \qquad 1.21$$

This is illustrated (neglecting spin) in figure 1.5. The density of states is drastically changed in the presence of a magnetic field. Applying periodic boundary conditions and going to a continuous k-space, the density of orbital states per unit range of the wave number k_z with given quantum number p is

$$dN/dk_z = eB/(2\pi)^2\hbar \qquad 1.22$$

The density of states per unit energy interval ε, which is defined by

$$dN/d\varepsilon = \frac{1}{\Omega}\sum_{pk\pm}\delta(\varepsilon(p,k,\pm)-\varepsilon) \qquad 1.23$$

Where Ω is the volume and $\epsilon(p,k,\pm)$ is given by equation 1.19. Using 1.23 we then have

$$dN/d\epsilon = \frac{(2m^*)^{1/2}}{\hbar} \frac{eB}{(2\pi)^2\hbar} \sum_{p,\pm} [\epsilon-(p+\tfrac{1}{2}\pm\tfrac{1}{2}\nu)\hbar\omega]^{-1/2} \qquad 1.24$$

Where the sum extends over all non-negative integers, p, for which the summand is real. The density of states (neglecting spin) is presented graphically in figure 1.2 which displays the well-known periodic character. It can be seen from both equation 1.24 and figure 1.2 that there is a singularity in the density of states at the bottom of each magnetic sub-band. This divergence has a profound effect on the scattering rates and is responsible for the oscillatory behaviour of the transport properties. The density of states in zero magnetic field is also shown figure 1.2 and is given by

$$dN_0/d\epsilon = 2/\Omega[\sum_k \delta(\epsilon_k-\epsilon)] = [(2m^*/\hbar^2)^{3/2}/2\pi^2]\epsilon^{1/2} \qquad 1.25$$

where the factor 2 is for spin. The analytic relationship between the densities of states is obtained through the use of the Poisson summation formula and for $\epsilon/\hbar\omega>1$ the following expression is obtained

$$dN/d\epsilon = dN_0/d\epsilon[1+(\hbar\omega/2\epsilon)^{1/2}\sum_{r=1}^{\infty}(-1)^r/r^{1/2}[\cos(2\pi\epsilon r/\hbar\omega-\pi/4)\cos(\pi\nu r)] \qquad 1.26$$

The effects of imperfections such as impurities and phonons in the solid must be considered. The imperfections affect the motion of the electrons causing scattering and broadening. In the presence of imperfections the infinite discontinuities in $dN/d\epsilon$ are rounded over. By replacing the delta function in 1.25 by a Lorentzian with a constant width Γ and constant energy shift Δ we get

$$dN/d\epsilon = (1/\Omega)\mathrm{Tr}(1/\pi)\Gamma/((E-H_0-\Delta)^2+\Gamma^2) \qquad 1.27$$

where Tr stands for trace. Carrying out the summation over $\underline{k}$ and neglecting Δ for the case of parabolic bands with effective mass m* and neglecting spin

$$dN/d\varepsilon = (m^*/\hbar^2)^{\frac{1}{2}} \sum_{p=0}^{\infty} \frac{\varepsilon-(p+\frac{1}{2})\hbar\omega+[(\varepsilon-(p+\frac{1}{2})\hbar\omega)^2+\Gamma^2]^{\frac{1}{2}}}{(\varepsilon-(p+\frac{1}{2})\hbar\omega)^2+\Gamma^2} \qquad 1.28$$

Again for $\varepsilon/\hbar\omega>1$ and by use of the Poisson summation formula the density of states in zero magnetic field and $dN/d\varepsilon$ may be connected by the expression

$$dN/d\varepsilon = dN_0/d\varepsilon[1+(\hbar\omega/2\varepsilon)^{\frac{1}{2}} \sum_{r=1}^{\infty}((-1)^r/r^{\frac{1}{2}})\exp-(2\pi\Gamma r/\hbar\omega)\cos(2\pi\varepsilon r/\hbar\omega-\pi/4)$$

$$\times \cos(\pi\nu r) \qquad 1.29$$

This is the same as the oscillatory part of equation 1.26 except that the amplitude of the r^{th} term is diminished by $\exp-(2\pi\Gamma r/\hbar\omega)$.

The oscillations can only be distinguished if their separation is greater than the broadening. If $\Gamma>>\hbar\omega$ the oscillations are smeared out. This result was first obtained by Dingle[17] who took

$$\Gamma = \hbar/2\tau \qquad 1.30$$

Where $1/\tau$ = average transition rate for scattering by impurities and is assumed independent of energy. The constant Γ result is most useful in interpreting oscillatory phenomena, but gives divergent results in some situations such as the quantum limit. More rigorous treatments were carried out by Bychkov[18] and Kubo et al[8] whose work was primarily concerned with infinitely localised impurity potentials. The effects of the electron-electron interactions on the density of states was considered by Luttinger[19], who treating the interaction as a

perturbation found that for $\varepsilon >> \hbar\omega, kT$, the period and amplitude of the oscillations in the density of states is correctly given by the above model.

TRANSPORT EFFECTS.

Before discussing the quantum mechanical view of the electrical conductivity it is worth examining the classical picture. In the case of parallel electric and magnetic fields (longitudinal conductivity) the classical electron paths are helices. The effect of the electric field is to accelerate the electron in the direction of the fields. Collisions with crystalline impurities intermittently stop the motion and thus limit the current. The longitudinal conductivity is given by, (magnetic and electric fields in z-direction)

$$\sigma_{zz} = ne\mu \quad ,n = \text{carrier concentration, } \mu = \text{mobility.} \qquad 1.31$$

and the resistivity by

$$\rho_{zz} = \sigma_{zz}^{-1} \qquad 1.32$$

In the case of electric and magnetic fields, (B in z-direction), the conductivity tensor is given by

$$\sigma = \frac{\sigma_0}{1+v^2}\begin{vmatrix} 1 & +v \\ -1 & 1 \end{vmatrix} \qquad 1.33$$

where $\sigma = ne\mu = ne^2\tau/m^*$

$v = \omega\tau$

The unusual situation arose where the component of current along the electric field is produced and enhanced by collisions. This may be seen from the conductivity tensor which gives

$$\sigma_{xx} = \sigma_0/(1+\omega^2\tau^2) \qquad 1.34$$

In the limit of $\omega\tau>>1$, it can be seen that the conductivity is proportional to τ^{-1} the amount of scattering. The transverse resistivity is given by

$$\rho_{xx} = \frac{\sigma_{xx}}{\sigma_{xx}^2+\sigma_{yx}^2} \qquad 1.35$$

which for higher magnetic fields may be approximated to

$$\sigma_{xx}/\sigma_{yx}^2 \qquad 1.36$$

The Hall coefficient R(H) is given by

$$R(H) = -\frac{1}{B}\frac{\sigma_{yx}}{\sigma_{xx}^2+\sigma_{yx}^2} \qquad 1.37$$

$$\sim -1/B\sigma_{yx}$$

In the quantum mechanical calculation of the conductivity tensor for electrons in a high magnetic field the longitudinal and transverse effects present somewhat different problems. The longitudinal magneto-conductivity was calculated by Argyres and Adams[20,21] and by Barrie[22] using a straight forward generalisation of Boltzmann transport theory. The principle effect is due to the change in the relaxation rate due to the altered density of states in the magnetic field. For the transverse conductivity the Boltzmann equation approach is inadequate for describing the effects of quantisation. This was first considered by Titeica[23] who adopted a semi-classical approach and assumed the transverse current to be produced by the drift of centres of the cyclotron orbits due to the electric field and scattering. The same method was followed by other workers. The full quantum mechanical

approach for the transverse current has been carried through by Kubo[24] et al, Adams and Holstein[7], Argyres and Roth[25] and others[26,27]. These approaches are based on the calculation of the density matrix which can be expanded in powers of the scattering potential. Kubo et al[8] made a number of refinements to the theory to include such effects as level broadening.

THE LONGITUDINAL MAGNETORESISTANCE.

Defining the one-electron density matrix, g, by

$$ihdg/dt = [H_o+V,g]+eE_x[x,f(H_o+V] \qquad 1.38$$

Where H_o is given by equation 1.16, V is the scattering potential, and f is the Fermi distribution. The current density is given by

$$\underline{J} = -\frac{e}{\Omega}(Tr g\underline{v}) \qquad 1.39$$

with $\underline{v} = (m^*)^{-1}(\underline{p}+e\underline{A})$, the velocity operator.

Allowing μ to represent p, $\underline{k}$ $\pm$ collectively, the Boltzmann transport equation gives

$$\sum_{\mu} W_{\mu\nu}g_{\mu}(1-g_{\nu})-W_{\nu\mu}g_{\nu}(1-g_{\mu}) = eE_z V_{\mu}^{z} \frac{df(\varepsilon_{\mu})}{d\varepsilon_{\mu}} \qquad 1.40$$

where $W_{\mu\nu}$ are transition probabilities in the Born approximation between Landau states μ and ν. Assuming a standard solution of the form

$$g_{\mu} = f(\varepsilon_{\mu})+\phi_{\mu}df(\varepsilon_{\mu})/d\varepsilon_{\mu} \qquad 1.41$$

where $df/d\varepsilon = -(1/kT)f(1-f)$, to 1st order in ϕ it follows.

$$\sum_{\nu} W_{\mu\nu} f_{\mu}(1-f_{\nu})(\phi_{\mu}-\phi_{\nu}) = eE_z v f_{\mu}(1-f_{\mu}) \qquad 1.42$$

For ionised impurity scattering with impurity potential $V(\underline{r}) = \sum_i v(r-r_i)$ the transition probability is

$$W_{\mu\nu} = W_{\nu\mu} = \frac{2\pi}{\hbar} \left| V_{\mu\nu} \right|^2 \delta(\varepsilon_{\mu}-\varepsilon_{\nu}) \qquad 1.43$$

The matrix element $\left| V_{\mu\nu} \right|^2$ is averaged over the random positions of scattering centres which are assumed to be distributed homogeneously in the crystal. For μ and ν having the same spin we have

$$V(p\underline{k},p'\underline{k}')^2 = (Ni/\Omega)\sum_{q} w(q) \langle p\underline{k}|\exp(iq.\underline{r})|p'k'\rangle^2 \qquad 1.44$$

where N_i is the concentration of scattering centres and

$$w(\underline{q}) = \int v(\underline{r})\exp(-i\underline{q}.\underline{r})d\underline{r} \qquad 1.45$$

is the Fourier Transform of the scattering potential for each centre. A model often used in the calculations is

$$v(\underline{r}-\underline{r}_i) = a\delta(\underline{r}-\underline{r}_i) \qquad 1.46$$

where a is the strength of the delta function. The quantity $m^* a/2\pi\hbar^2$ is known as the scattering length. For elastic collisions, as is the case for ionised impurity scattering the Fermi factors in equation 1.42 cancel

$$\sum_{\nu} W_{\mu\nu}(\phi_{\mu}-\phi_{\nu}) = eE_z v \qquad 1.47$$

For a solution of equation 1.47 of the form $\Phi\mu = k_z$ times a function of energy ε_μ, the scattering may be expressed as

$$\sum_\nu W_{\mu\nu}(\Phi_\mu - \Phi_\nu) = \Phi_\mu/\tau_\mu \qquad 1.48$$

where

$$1/\tau(p,k,\pm) = \sum_{p'k'} W(p,k\pm,p'k'\pm)(1-k_z'/k_z) \qquad 1.49$$

With the use of equations 1.47 and 1.39 we obtain

$$\rho_{zz}^{-1} = \sigma_{zz} = (-e^2/\Omega)\Sigma\ df/d\varepsilon(pk\pm)\tau^{\pm}(\varepsilon(p,k))(v)^2 \qquad 1.50$$

For the Shubnikov-de Haas effect the forward and backward scattering probabilities are equal, thus the relaxation time is equal to the lifetime i.e.

$$1/\tau(p,k,\pm) = \sum_{p'k'} W(pk\pm,p'k'\pm) = CdN/d\varepsilon(p,k,\pm) \qquad 1.51$$

Here $dN/d\varepsilon(p,k,\pm)$ is the density of states for each spin in the presence of a magnetic field with the constant $C=(2\pi/\hbar)a^2Ni$. In the the absence of the magnetic field the relaxation time is $\tau_0^{-1}=\frac{1}{2}CdN_0/d\varepsilon$ with $dN_0/d\varepsilon$ being given by equation 1.25 and the factor $\frac{1}{2}$ giving the spin density of states. Thus it can be seen that the effect of the magnetic field is given directly through its effect on the density of states. Hence ρ_{zz} as given by equation 1.50 is found for $\hbar\omega >> kT$ to be

$$\rho_{zz}^{-1} = \rho_0^{-1}\frac{4Efo}{p\hbar\omega}^{\frac{1}{2}} \sum_{\pm} \frac{p\pm}{\sum_p [E_f-(p+\frac{1}{2}\pm\frac{1}{2}\nu)\hbar\omega]} \qquad 1.52$$

where E_{FO} is the Fermi energy is zero magnetic field,

$\rho_0 = m^*/ne^2\tau_0(\varepsilon_0)$, is the resistivity for zero magnetic field and $p^{\pm}$ is the density of electrons with spin $\pm$. The resistivities for $E_F >> \hbar\omega$ may be approximated by simply averaging the relaxation rates for the two cases. It is then found that

$$\rho_{zz} = \rho_d\left[1+\sum_1^{\infty} b_r \cos(2\pi r E_F/\hbar\omega - \pi/4)\right] \qquad 1.53$$

$$\text{where } b_r = \left((-1)^r/r^{1/2}\right)(\hbar\omega/2E_F)^{1/2} \frac{(2\pi rkT/\hbar\omega)}{(\sinh(2\pi^2 rkT/\hbar\omega))} \cos(\pi\nu r) \times \exp-(2\pi\Gamma r/\hbar\omega) \qquad 1.54$$

which includes the term for collision broadening.

TRANSVERSE MAGNETORESISTANCE.

For the calculation of the transverse magnetoresistance the simplest procedure is to expand the steady-state density matrix g in powers of the scattering interaction. This is possible because the magnetic field limits the mean acceleration of electrons by the electric field and thus a finite steady-state current is present. The current is perpendicular to both $\underline{B}$ and $\underline{E}$ and is equal to the classical value of

$$J_y = neE_x/B \qquad 1.55$$

and it can be shown that to second order in v this value of J_y does not change. The conductivity in the direction of the electric field is given by

$$\sigma_{xx} = (e^2/(2kT\Omega))\sum_{\mu\nu} f_\mu(1-f_\nu)W_{\mu\nu}(X_\mu - X_\nu)^2 \qquad 1.56$$

A more general form of σ_{xx} correct to all orders in v has been obtained by Kubo et al[24] for the case of elastic scattering

$$\sigma_{xx} = (\pi e^2/h\Omega)\int_{-\infty}^{\infty} d\epsilon df/d\epsilon Tr(\delta(\epsilon-H)[V,X]\delta(\epsilon-H)[V,X])$$

where $H = H_0+V$ and X is the operator for the x-component of the orbit centre whose eigen values are X_μ. The transverse conductivity may be written in the simple form of

$$\sigma_{xx} = (-e^2/2\Omega)\Sigma\ df/d\epsilon(pk\pm)W(pk\pm,p'k'\pm)(X_k - X_{k'})^2$$

which maybe expressed as

$$\sigma_{xx} \sim \int d\epsilon \Sigma \frac{Lpp'(\epsilon)df/d\epsilon}{\sqrt{[(\epsilon-p+\frac{1}{2})\hbar\omega]}\sqrt{[\epsilon-(p'+\frac{1}{2})\hbar\omega]}}$$

One main problem with the above expression is that it gives a logarithmic divergence which arises from the two density of states factors coinciding when p=p'. There are several mechanisms which can be responsible for cutting off the divergence such as collision broadening, in elastic scattering and non-Born scattering. These have been discussed by Roth and Argyres[25] and Adams and Holstein[7]. Only collision broadening shall be discussed here as it is the most pertinent to this work. The effect of collision broadening is to remove the infinite discontinuities in the densities at ϵ_z=0. The cutoff occurs when ϵ_z is of the order of the width, Γ, of the levels. This argument was originally due to Davydov and Pomeranchuk[28] and was later applied by Kubo et al[8] who found that for the model of a short range potential and scattering length $f=m^*a/2\pi\hbar^2$

$$\varepsilon_c \sim (\hbar^2\omega/\tau_0 E_{f0}^{1/2})^{2/3}$$

where $1/\tau_0 = N_i 4\pi f^2 (2E_{f0}/m^*)^{1/2}$

is the mean free time for an electron in zero magnetic field and E_{fo} is the Fermi energy in zero magnetic field. For isotropic scattering σ_{xx} may be expressed in terms of the relaxation time of equation 1.51 giving

$$\sigma_{xx} = (-e^2 l^2/\Omega) \sum_{pk\pm} df/d\varepsilon(pk\pm)(p+\tfrac{1}{2}) \quad (\varepsilon(pk\pm))^{-1}$$

Evaluating the above equation at 0^oK and using 1.51 gives

$$\rho_{xx} = \rho_0 \frac{3(\hbar\omega)^3}{16(E_{fo})^2} \sum_{p,p'} \frac{p+\tfrac{1}{2}}{[E_f-(p+\tfrac{1}{2}\pm\tfrac{1}{2}\nu)\hbar\omega]^{1/2}} \frac{1}{[E_f-(p'+\tfrac{1}{2}\mp\nu)\hbar\omega]^{1/2}}$$

For any finite temperature, integration over energy must be performed which is E_f in this case. This has been done by Miyake for collision broadening and the result is

$$\rho_{xx} = \rho_0[1+5/2\sum_{r=1}^{\infty} b_r \cos(2\pi r E_f/h\omega-\pi/4)+R$$

Where R and b_r are given by equations 1.12 to 1.20

The term R is the contribution to the conductivity from transitions which do not change the Landau quantum number p. It diverges if the level width Γ disappears and is relatively unimportant when the higher harmonics are damped out. The second term in the cosine term is the contribution to the oscillatory part of ρ_{xx} due to transitions in which the quantum number p does change.

CHAPTER 2

EXPERIMENTAL METHODS

2:1 INSERT DESIGN.

On each sample, Hall voltage, D.C. conductivity and magnetoresistance were measured at 4.2^{o}k in a superconducting solenoid producing fields up to 12.7T. The magnetoresistance measurements were made with the sample parallel and perpendicular to the magnetic field and at intermediate orientations. For these purposes an insert for use in conjunction with the 12.7T magnet was designed, incorporating a rotating sample holder, screened leads and a variable temperature facility for possible future use.

Figures 2.1 and 2.2 illustrate the basic features of the insert. Six, non-magnetic stainless steel tubes carry 42swg. enamelled, double silk, copper leads from the BNC connections at the top of the insert down to the brass mounting. The leads pass down through holes in the mounting and are soldered to the first set of gold sockets in the P.T.F.E. block. This block contains two sets of six sockets, one at each end, electrically connected by copper wires running on its underside. Electrical contact from the sample to the insert is made via the nylon sample holder and the six tinned copper posts riveted through it. On the top side of the sample holder the sample is mounted and its wires soldered to the six posts, on the underside, six 38swg. double silk copper wires, with pins on one end, lead from the posts. It then just remains for the gold pins to be plugged into the second set of sockets in the P.T.F.E. block for connection to be made between the sample and the BNC sockets at the top of the insert.

TOP HALF OF LOW TEMPERATURE INSERT

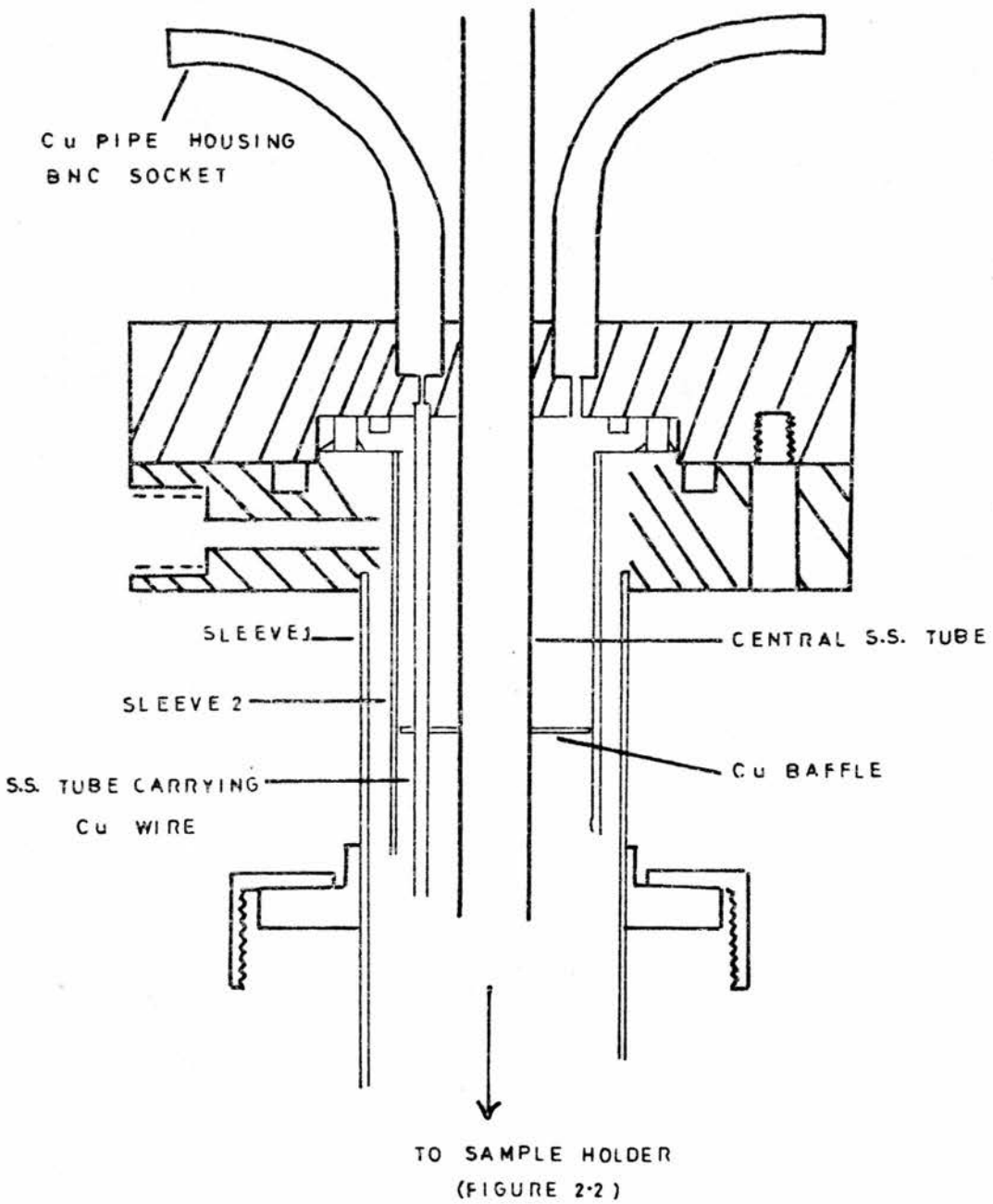

FIGURE 2·1

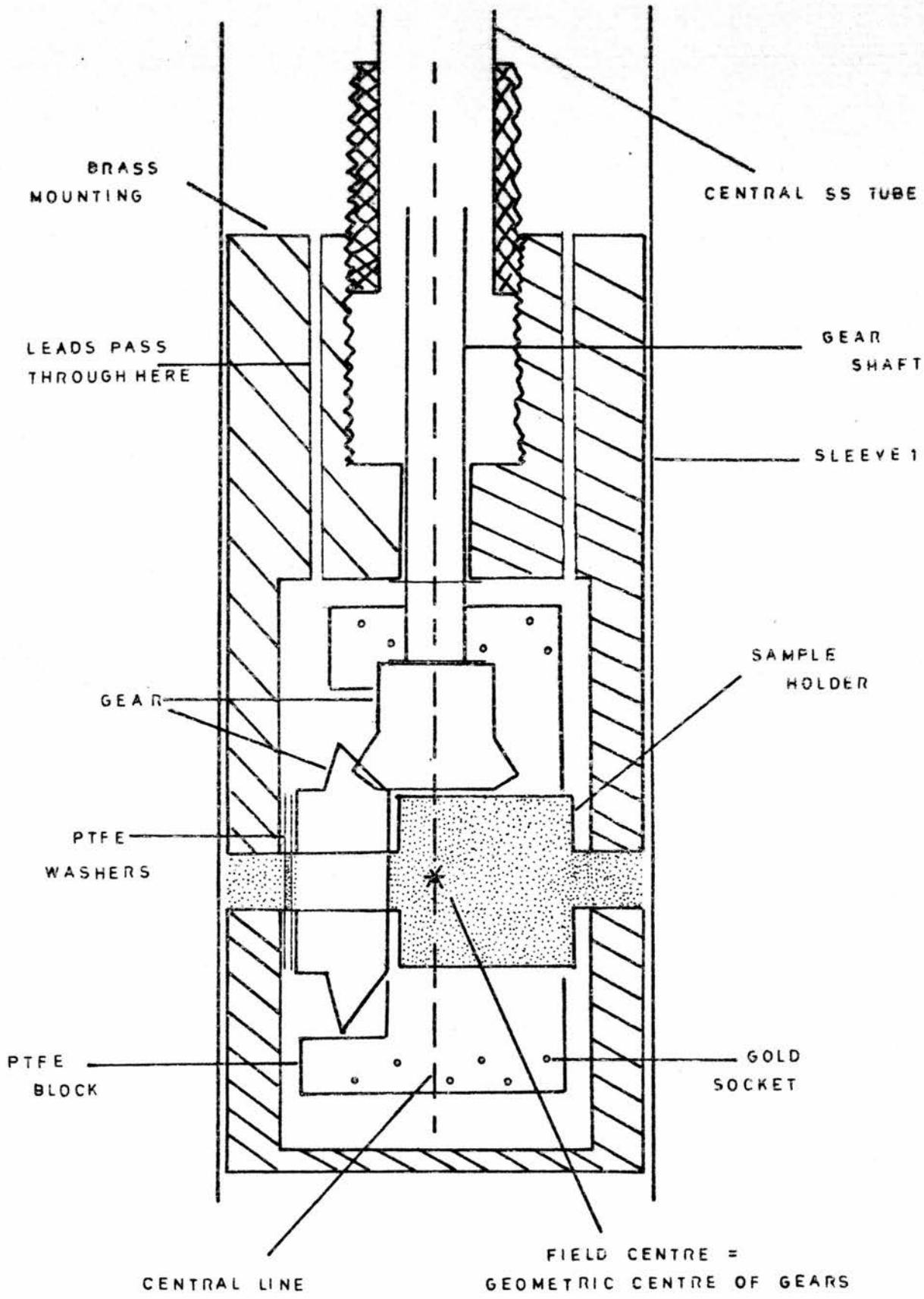

FIGURE 2·2
LOWER HALF OF INSERT SHOWING SAMPLE HOLDER

Rotational motion is achieved through brass bevel gears having a ratio of 2:1, and a central stainless steel shaft running the length of the insert to drive them. This shaft is housed in the middle stainless steel tube and is hollow for most of its length to reduce heat conduction down the insert. The brass mounting is the framework which supports the rotational set-up, the dimensions are such that the geometric centre of the gears, the centre of a mounted sample, and the magnetic field centre of the 12.7 Tesla magnet, all coincide. The mounting screws onto the end of the 10mm tube thus allowing easy removal should it be necessary to change the entire assembly. The sample holder has two cylindrical 'arms', one of which passes through gear B, both arms then slot into the arrangement in the brass structure illustrated in figure 2.3. By adjusting the tension of the nuts it is possible to control the required force applied to the shaft to produce rotation. The top end of the shaft has a pointer and this used together with a graduated scale gives an indication of the angle through which the sample is rotated [figure 2.4]. The scale is not calibrated in units of degrees but has numbers round its circumference ranging form 0 to 100, with a change of 100 units equalling a ratio of 360 degrees. With the gear rotations of 2:1 it follows that a change of 50 units results in the sample being rotated through an angle of 90 degrees.

Sleeves one and two [figure 2.1] allow the sample temperature to be varied from 4.2^{o}K upwards whilst the insert is submerged in liquid Helium. By evacuating the outer sleeve (sleeve one) the sample is placed in thermal isolation and the temperature may then be varied at will. It should be noted that the dimensions of the rotational assembly are not compatible with those of the inner sleeve and that for temperature dependent measurements an alternative sample mounting must be used. For operation at 4.2^{o}K the outer sleeve alone is

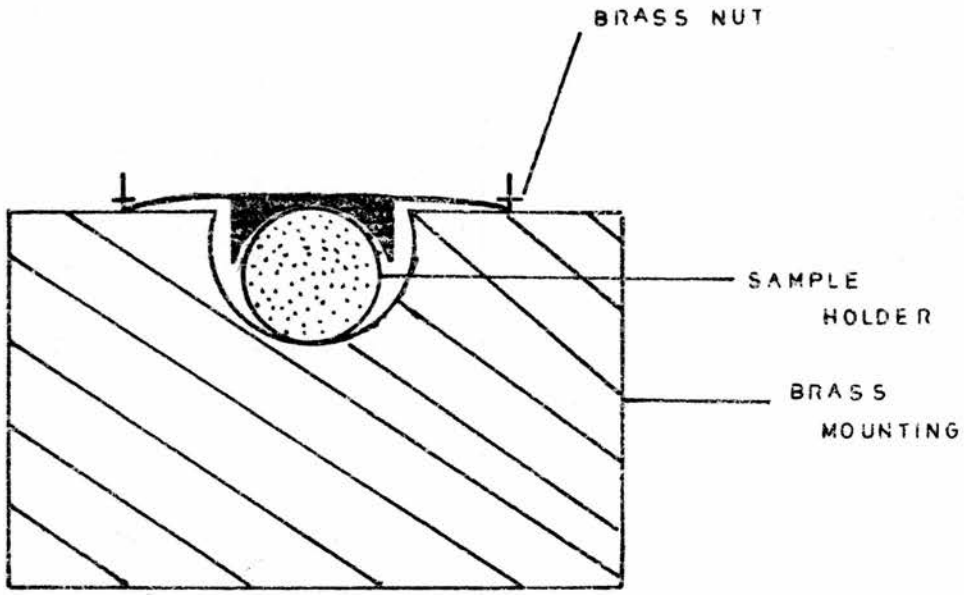

FIGURE 2·3

CROSS -SECTIONAL VIEW OF SAMPLE HOLDER IN BRASS MOUNTING BY ADJUSTING THE BRASS NUTS THE FORCE REQUIRED TO PRODUCE ROTATION MAY BE VARIED

TOP OF INSERT SHOWING HOW ROTATION OF THE SAMPLE WAS ACHIEVED

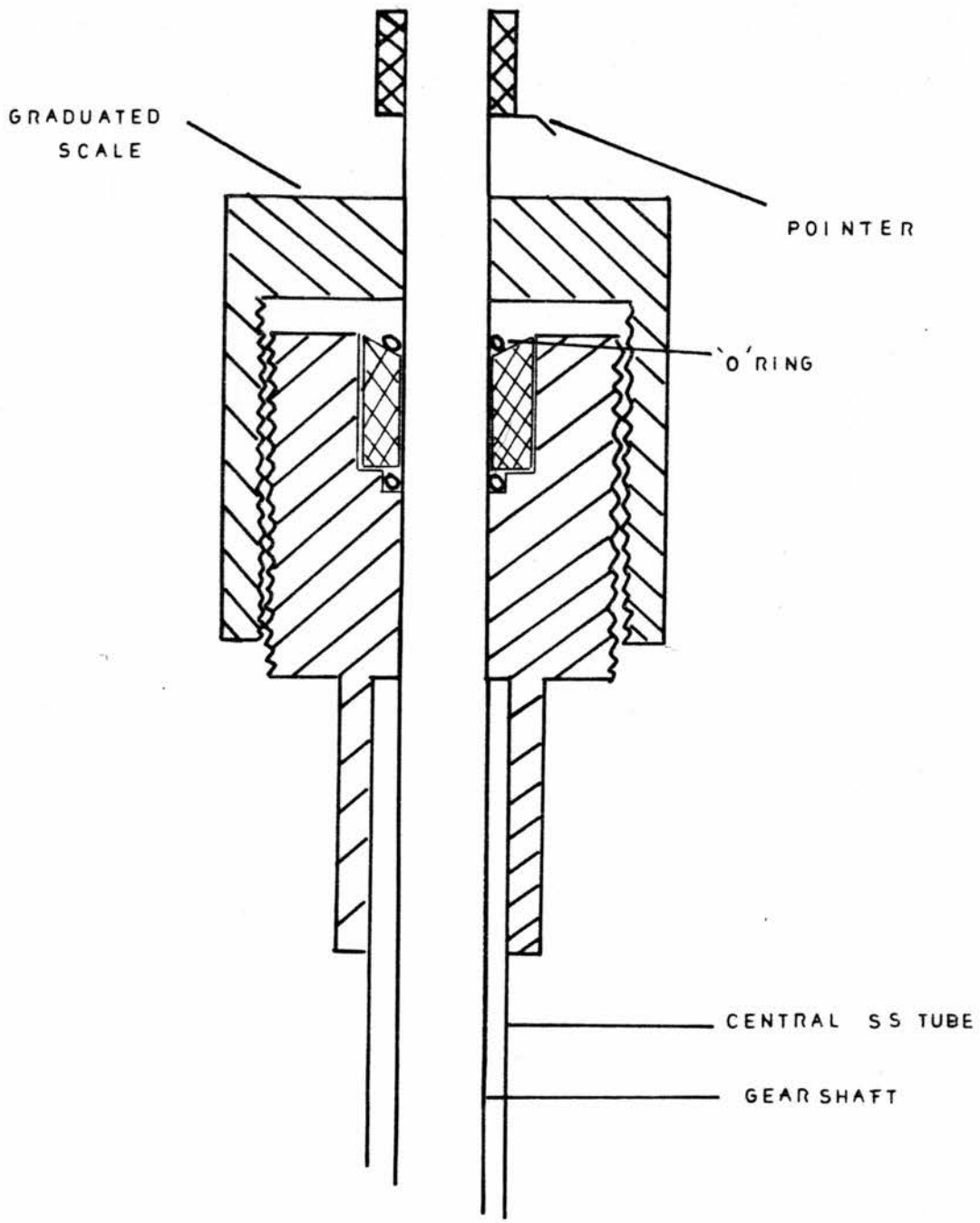

FIGURE 2·4

necessary, which must be evacuated to a pressure of approximately 10^{-4} Torr and then back-filled with a little Helium exchange gas.

For the series of experiments undertaken in this study each sample was mounted on a separate holder in the 3mm wide groove. This groove assisted in orientating the sample parallel to the plane in which rotation took place. It was estimated that with the 2mm - width, and 1cm length of the samples, this placement was never greater than approximately 2 degrees from the true parallel. Each groove carried a double layer of paper tissue impregnated with high vacuum silicon grease which had the effect of anchoring the sample securely without subjecting it to undue mechanical strain during thermal cycling. Samples were initially placed in the insert in the transverse position, (i.e. with their length perpendicular to the central shaft), with estimation of the transverse position being made by eye. They were then rotated to the longtitudinal position (again estimated by eye) and the number of divisions moved through on the calibrated scale noted. This served to confirm that the sample was being rotated smoothly, without slip, as any irregularity was manifested in a large deviation from the 50 unit change for a ninety degree rotation. In practice it was found that the change in units for this operation lay between 48 and 52, this giving an indication of the accuracy to which the angular position of the sample could be measured, (approximately plus or minus 2 degrees), with any error due to backlash eliminated by always rotating in the same direction.

For all experiments the insert performed satisfactorily. Electrical contact was never lost during thermal cycling, and once smooth, trouble-free rotation was attained at room temperature, it continued at 4.2°k. The gears were occasionally cleaned in toluene and then acetone to keep them clear of moisture and grease, which prevented

any 'freezing-up' at low temperatures. As each sample was mounted on a separate sample holder, changing samples merely involved changing sample holders on the insert. This greatly reduced the time taken for the operation which was found to be approximately 1½ hours from the time of removal from the 12.7 Tesla magnet to the start of the next set of experiments.

2.2 MEASUREMENT TECHNIQUES.

Hall and magnetoresistance measurements were performed by passing a constant current (∿5mA) through the sample and feeding the output voltage from the hall contacts (on the sides of the sample), or the potential probes (on the top surface), through a Keithley 149 D.C. amplifier, the output of which was displayed on the y-axis of an X-Y recorder. The x-axis of the chart recorder was driven using an output voltage from the power supply of the 12.7 Tesla magnet. This voltage was not representative of the current through the solenoid, but rather represented the current through the quench protection resistors (which are in parallel with the solenoid inside the cryostat), plus the current in the solenoid. The magnetic field position of any structure was measured using the method now described. The magnetic field was swept at a constant rate and recordings taken for increasing and decreasing magnetic fields. The two recordings obtained were laterally displaced from each other by a constant factor throughout the sweep. The true position of any structure was taken to be the average of the up and down sweeps. The current noted at the end of the field increasing sweep gave the final value of magnetic field, and the field position of any structure (after averaging) was calculated from this value. The validity of this method was tested by increasing the magnetic field by small increments and measuring the magnetoresistance directly, using a Keithley milli-micro-volt meter, at each step. A graph was then plotted of

magnetoresistance versus magnetic field, and was compared to the recording obtained, after averaging, using the field sweep technique. Figure 2.5 shows the two resulting graphs which illustrates the excellent agreement which existed between the results taken by both methods. (Difference in position of last peak 0.8%). The method of sweeping the field was adopted for all magnetoresistance and most Hall measurements.

Errors in the determination of a magnetic field value arose from three sources. Uncertainty in the final magnet current value read out from the power supply (0.1% at a current of 100 Amps), uncertainty in the reading of the peak positions from the chart recordings, and any 'zero error' i.e. any uncertainty in the positions of the start and end of a recording. From the nature of the uncertainties it followed that the percentage error in the middle, or nearing the end of a recording was much less than the percentage error at the beginning. This meant that the percentage error for the low Landau quantum numbers (i.e. p=0, 1, 2) was much less than the percentage error for the high Landau quantum numbers(i.e. p>2). It was estimated that for p<2 the error was typically 1 to 2% whilst for p greater than 2 the error lay between 2 and 6%

2.3 THE METHOD OF DOUBLE DIFFERENTIATION.

The method of double differentiation has, for many years now, been routinely used in magnetophonon experiments[30] where it is employed to extract the very small oscillatory variations from the slowly varying components of the magnetoresistance. It consists of sweeping the magnetic field at a constant rate and passing the time varying signal through the differentiating circuits which reduce any components linear or quadratic in B to a voltage which may be offset on an X-Y recorder. The resulting recordings may be considered to represent

COMPARISON OF PROFILES OBTAINED BY THE FIELD SWEEPING TECHNIQUE TO PROFILES OBTAINED BY MEASURING THE MAGNETORESISTANCE AT VARIOUS VALUES OF STATIC B FIELD

FIGURE 2·5

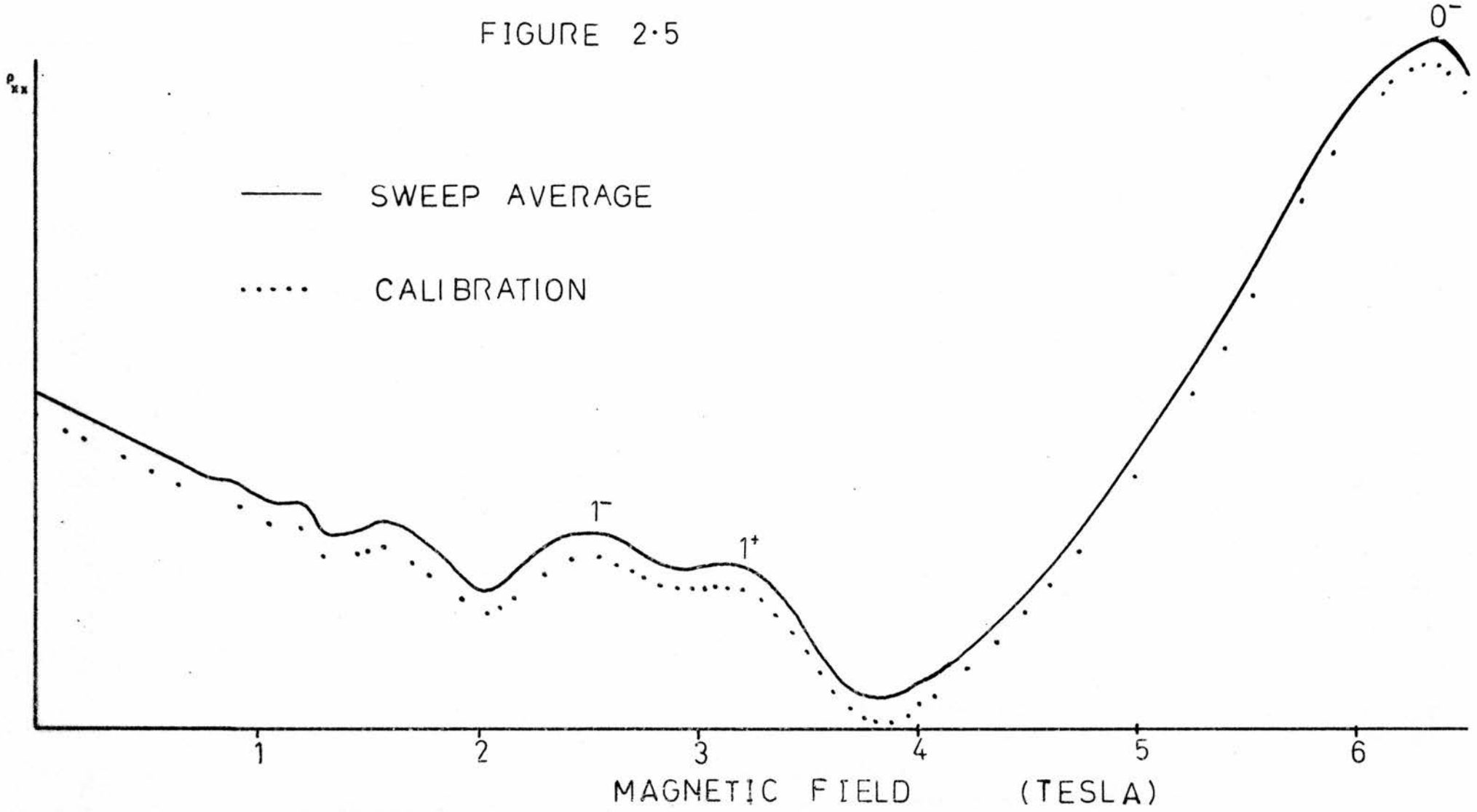

the second derivative of the magnetoresistance with respect to magnetic field, since the field variation is linear in time. Although the oscillatory components in the Shubnikov-de Haas magnetoresistance are pronounced and can be clearly seen, double differentiation of the signal helped to accentuate some of the structure, allowing their field positions to be more accurately measured. This method of double differentiation introduced an experimental time delay in the derivative which appeared as a field displacement on an X-Y recording, the displacement not being constant throughout the sweep. For this reason, complete recordings were taken of the differentiated signal for field-increasing and field-decreasing sweeps, and the average taken as the 'true' position.

The experimental arrangement showing the differentiating circuits is illustrated in figure 2.6. The differentiators employed were simply high-pass, RC filters each having a gain of

$$\frac{j\omega CR}{1+j\omega CR} \qquad 2.1$$

for a sinusoidal signal of angular frequency ω. This reduces to $j\omega CR$ for $\omega CR \ll 1$ and when this condition is fulfilled the filter becomes a crude differentiator. The choice of the time constant CR, was an important factor and was governed by the sweep rate, the particular sample under study and which structure was of interest. This can be explained as follows. The oscillatory component of the Shubnikov-de Haas magnetoresistance is closely periodic in reciprocal magnetic field, meaning that when the magnetic field is swept linearly in time the signal consists of an oscillatory component whose frequency decreases with increasing magnetic field. This may lead to imperfect differentiation of low field components at sweep rates and time constants convenient for observing higher components. An

EXPERIMENTAL SET UP USED TO OBTAIN THE SECOND DIFFERENTIAL OF THE MAGNETORESISTANCE

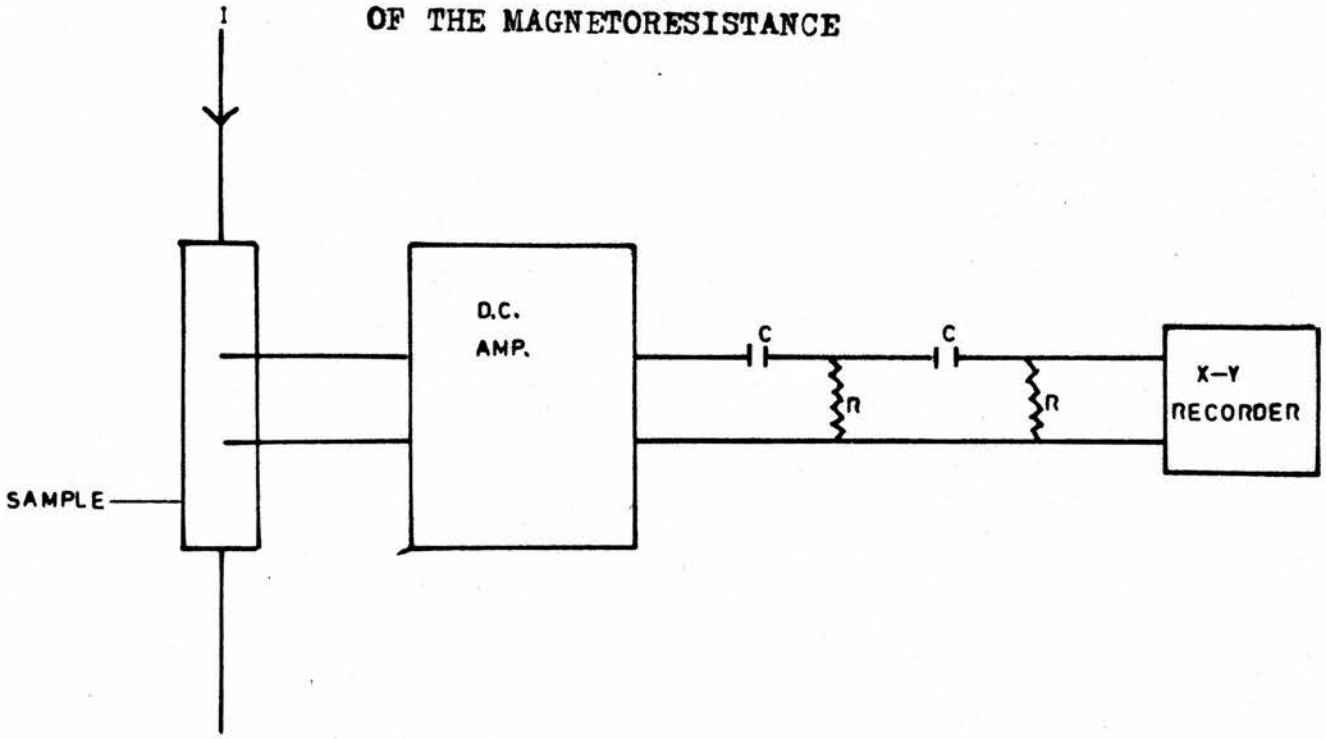

FIGURE 2·6

important feature of this technique is that the gain $-(\omega CR)^2$ of the two filters is proportional to the square of the time constant meaning the smaller the time constant, the much smaller the output signal. Also the gain is proportional to the square of the frequency of the input signal with the result that any higher frequency harmonics of the components are accentuated, this being equivalent to the accentuation of any structure or line shape details which may be present. As in the case of the low field components the sweep rates or the time constants must be small enough to avoid distortion (i.e. imperfect differentiation). In this work different time constants were used for the same sample, each of which extracted different information, the values used varied from 5 seconds down to ½ second. The choice of the time constants is discussed in more detail in chapter 4. The values of C and R are dictated by the need for R to be much greater than the sample resistance and much smaller than the imput impedance of the equipment following the filter. For the time constants used here, the value of R was of the order of tens of kilohms.

The oscillatory components of the magnetoresistance undergo a reversal of polarity on taking the second derivative, to avoid confusion the differentiated signal has been plotted in the positive ordinate and the term 'maxima' or 'peaks' refers to the maxima in the magnetoresistance be it on a differentiated or undifferentiated recording. The term 'differentiation' always refers to the process of taking the second derivative of the signal.

2.4 EXPERIMENTAL PHASE SHIFTS.

Peak positions in the experimental recordings of differentiated and undifferentiated data are phase-shifted with respect to magnetic field from the simple resonance condition of $Bo/B = m$, where $m = ½, 3/2, 5/2,$

etc., and Bo is a magnetic field value determined by the characteristics of the material under study. This phase shift arises from the amplitude variation of the resonance peaks and is greater in the differentiated case. It is not the same as the shifting which was introduced by the current through the quench protection resistors (which produced a constant displacement between the peak positions in the field-increasing and field-decreasing sweeps). Nor is it the same as the shifting caused by passing the time-varying signal through the differentiating circuit (which also produced a relative shifting of the peak positions in the field-increasing and field-decreasing data, with the shift not being the same at all values of magnetic field). Both of these effects were cancelled out by simply averaging the magnetic field values for the sweep up and down cases. The phase-shifting discussed in this section cannot be irradicated in this manner.

The magnetic field values of the magnetoresistance maxima, obtained after averaging, from both the differentiated and undifferentiated data differed by a small amount (the maximum being $\sim$3-4% for m = ½) and was, as previously stated, a direct consequence of the amplitude variation of the resonance peaks. This may be explained as follows:- the simple formula of

$$\rho = -\cos(2\pi Bo/B)$$

giving the field positions of the resonances is pre-multiplied by exponentially decreasing, (with 1/B), factor which describes the amplitudes of the resonance peaks. This has the effect of changing the fields at which the maxima occur in both the differentiated and undifferentiated data, with the magnitude (and in some cases the sign) of the change being different. Hence peak positions given by the two types of data are both different from each other and from the values

predicted by the simple resonance condition.

This phenomenon has been recognised for many years and is discussed in the context of magnetophonon resonance experiments by Wood[31] and in the paper by Blakemore and Kennewell[32], and corrections to results to account for this phase-shifting have regularly been made by workers in the field. Failure to correct for this effect can lead to large errors in the parameters measured by the magnetophonon resonance technique, for example, Blakemore and Kennewell quote an error of 10% in the determination of the effective mass, although it is stressed that a much smaller error results if several extrema are resolved and used in the analysis.

Following the proceedure adopted by previous workers for the phase-shifting in magneto phonon resonance and applying it to the Shubnikov-de Haas effect, a simple functional form which best describes the magnetoresistance variation with magnetic field was chosen and is as follows:-

$$\rho \propto -\exp(-\gamma B_o/B)\cos(2\pi B_o/B) \qquad 2.2$$

Where ρ = Shubnikov-de Haas magnetoresistance.

B = magnetic field.

$\gamma = \beta T_D m'/B_o$

$B_o = m'E_F/(\hbar e)$

This is of the same form (neglecting the negative sign), as the function chosen by Wood and other workers in their treatment of the magnetophonon effect. It is a very simplified version of the true variation of the Shubnikov-de Haas magnetoresistance with magnetic field.

Single differentiation of equation 2.2 gives the field positions of which the maxima (and minima) of ρ occur.

i.e. $$\tan(2\pi B_o/B) = -\gamma/(2\pi) \qquad 2.3$$

from this it follows that for undifferentiated data the percentage shift to higher fields from the fields defined by $B_o = mB$ is given by

$$\frac{100}{2\pi m} \tan^{-1} \gamma/(2\pi) \qquad 2.4$$

Table 2.1 lists (B_o/B) values for m = ½ to m = 9/2 where it can be seen that there is a constant difference between ρ and B_o/B as m is increased.

The second derivative of ρ (i.e. ρ'') is given by

$$(B_o/B)^3\exp(-\gamma B_o/B)\{4\pi(1-\gamma B_o/B)\sin(2\pi B_o/B)$$

$$+[2\gamma+(4\pi^2-\gamma^2)(B_o/B)]\cos(2\pi B_o/B)\} \qquad 2.5$$

which on further differentiation is shown to have magnetoresistance turning points occuring when

$$\tan(2\pi B_o/B) = -\gamma\frac{[(B_o/B)^2(12\pi^2-\gamma^2)-(B_o/B)[24\pi^2/\gamma)-6\gamma]-6]}{2\pi[(B_o/B)^2(4\pi^2-3\gamma^2)+(B_o/B)12\gamma-6]} \qquad 2.6$$

For $\gamma \lesssim 1$ expression 2.6 is well approximated by

$$\tan(2\pi B_o/B) = -\left(\frac{3}{2\pi}\right)(\gamma-2/m) \qquad 2.7$$

this becoming a better approximation as m values increase. This shows

NOMINAL VALUE OF M	BO/B VALUES CALCULATED FROM EQUATION 2.4		
	γ=0.75	γ=1	γ=1.5
0.5	0.48	0.47	0.46
1.5	1.48	1.47	1.46
2.5	2.48	2.47	2.46
3.5	3.48	3.47	3.46
4.5	4.48	4.47	4.46
5.5	5.48	5.47	5.46

TABLE 2.1

that in the experimental recordings obtained by differentiation the magnetoresistance maxima are shifted to higher magnetic fields by a fractional change of

$$1/(2\pi m)\ \tan^{-1}\left(\frac{3}{2\pi}\right)(\gamma-2/m)\ 100\% \qquad 2.8$$

The validity of the approximation in 2.7 is exemplified by table 2.2 where a list of B_o/B values calculated from 2.7 are shown together with B_o/B values taken from the paper by Blakemore and Kennewell who computed the values from equation 2.6 using a computer iteration routine. It whould be noted that the B_o/B values computed by Blakemore and Kennewell correspond to minima in this work. This is because of the minus sign in the expression in equation 2.2 which does not appear in their formula. This is irrelevant as the principle is exactly the same be the analysis for shifting in maxima or minima.

Table 2.1 illustrates that the maxima in ρ are invariably shifted to the low side of the nominal value of m, (corresponding to a shifting to a higher magnetic field), with the shift not being very large. The situation is more complicated in the differentiated case, table 2.2 shows that $\Delta B_o/B$ (i.e. Δm) is negative for low field values but becomes positive as the magnetic field increases (i.e. as $m-\frac{1}{2}$). Two important facts are illustrated by table 2.2, the shifts of the magnetoresistance maxima from the nominal positions given by $B_o/B = m$ are never greater than $\sim$3% for m values greater than 1, also the Δm of ρ'' vary linearly with γ meaning that interpolation can be easily made between the values of γ.

As was previously stressed equation 2.2 is only a very crude approximation to the Shubnikov-de Haas magnetoresistance functional form, a closer approximation is a Fourier series of which equation

NOMINAL VALUE OF M	BO/B VALUES CALCULATED FOR ρ" (EQUATION 2.8)					
	γ=0.75		γ=1		γ=1.5	
0.5	*	+ 0.66	*	+ 0.65	*	+ 0.6
1.0	1.08	1.08	1.06	1.07	1.03	1.04
1.5		1.54		1.52		1.49
2.0	2.02	2.02	2.00	2.00	1.96	1.96
2.5		2.50		2.48		2.45
3.0	2.99	2.99	2.97	2.97	2.94	2.94

* FROM BLAKEMORE AND KENNEWELL.

\+ FROM EQUATION 2.

TABLE 2.2

2.2 is the leading term. The higher Fourier terms become important, in the case of the high magnetic field extrema (i.e. m<5/2), since they increase in strength as the magnetic field increases. In considering the differentiated data the higher harmonics in the Fourier series are paticularly relevant as they are accentuated by differentiation. Failure to correct for phase-shifting in the appropriate manner will lead to errors in the determination of the magnetic field positions of any structure observed in the differentiated recordings. This problem was discussed by Wood and by Blakemore and Kennewell in the context of magnetophonon resonance data, each pointed out that the previously illustrated method of correcting for phase-shifts is not applicable for low-order extrema. Neither suggested any method by which the magnitude of the shifting of the high-magnetic field extrema could be calculated or estimated.

The following equation gives the Fourier series describing the Shubnikov-de Haas effect.

$$\rho \propto \sum_{r=1}^{\infty} (-1)^{r} \exp(-\gamma r B_o/B) \cos(2\pi r B_o/B) \qquad 2.9$$

where r is an integer 1, 2, 3.....

Considering the Fourier component of order r, the turning points occur when

$$\tan (2\pi r B_o/B) = - \gamma/(2\pi) \qquad 2.10$$

i.e. the percentage shift to higher fields away from the resonance condition is

$$\frac{\Delta B}{B}\ 100\% = \frac{1}{2\pi rm}\tan^{-1}\gamma/(2\pi)\ .100\% \qquad 2.11$$

The second deriviative of the Fourier component, order r, is

$$\rho''_r \propto B_o'B^3\exp(-\gamma rB_o'B)\{[4\pi(r-\gamma r^2B_o/B)]\sin(2\pi rB_o/B)$$

$$+[2\gamma r+(4\pi^2r^2-\gamma^2r^2)B_o/B]\cos(2\pi rB_o/B)\} \qquad 2.12$$

Further differentiation of this gives the fields at which the magnetoresistance maxima (and minima) occur for ρ''_r

$$\tan(2\pi rB_o/B)=\frac{\gamma[(B_o/B)^2(12\pi^2-\gamma^2)r^3-(B_o/B)(24\pi^2/\gamma-6\gamma)r^2-6r]}{-2\pi[(B_o/B)^2(4\pi^2-3\gamma^2)r^3+12\gamma rB_o/B\ -6r]} \qquad 2.13$$

This can also be reduced to an analytic expression for $\gamma\nu<1$.

$$\tan(2\pi rB_o/B) = -3/(2\pi)(\gamma - 2/mr) \qquad 2.14$$

i.e. the percentage shift in magnetic field away from the resonance condition is

$$\frac{\Delta B\%}{B} = \frac{1}{2\pi rm}\ \tan-\ \frac{3}{2\pi}\ (\gamma-2/mr)\% \qquad 2.15$$

The conditions for resonance in the Fourier series is given by

$$(-1)^r\cos(2\pi rB_o/B) \qquad 2.16$$

Meaning that for the odd harmonics resonance occurs when rB_o/B, i.e. rxm, = ½, 3/2, 5/2 etc., and that for even harmonics the resonance condition is given by rxm = 1, 2, 3 etc. Tables 2.3 and 2.4 give the

NOMINAL VALUE OF M	BO/B VALUES CALCULATED FOR ρ (EQUATION 2.11)					
	γ=0.75		γ=1.0		γ=1.5	
	r=2	r=3	r=2	r=3	r=2	r=3
0.5	0.490	0.494	0.487	0.491	0.481	0.487
1.5	1.490	1.494	1.487	1.491	1.481	1.487
2.5	2.490	2.494	2.487	2.491	2.481	2.487
3.5	3.490	3.494	3.487	3.491	3.481	3.487
4.5	4.490	4.494	4.487	4.491	4.481	4.487
5.5	5.490	5.494	5.487	5.491	5.481	5.487

TABLE 2.3

NOMINAL VALUE OF M	BO/B VALUES CALCULATED FOR ρ" (EQUATION 2.15)					
	γ=0.75		γ=1.		γ=1.5	
	r=2	r=2	r=2	r=3	r=2	r=3
0.5	0.54	0.51	0.53	0.51	0.52	0.5
1.5	1.5	1.49	1.49	1.49	1.47	1.47
2.5	2.49	2.49	2.48	2.48	2.46	2.47
3.5	3.48	3.49	3.47	3.48	3.46	3.47
4.5	4.48	4.48	4.47	4.48	4.46	4.47
5.5	5.48	5.48	5.47	5.48	5.45	5.47

TABLE 2.4

values of B_o/B in the undifferentiated and differentiated data for the r^{th} harmonic in the Fourier series, calculated using equations 2.10 and 2.14. As in the case of the first harmonic, table 2.3 shows that the values of ρ are invariably shifted to the low side of nominal value m. The shift is again constant and small, and is, in fact, equal to the shift in the leading term divided by the harmonic number r. As it was for the leading term in the Fourier series, the situation is more complicated for the differentiated data in the higher harmonic case. Table 2.4 shows that for certain values of γ and r, the values of Δm are positive for low values of m and become negative as m increases. For other values of γ and r the B_o/B values are always shifted to the low side of the nominal value m with the change (Δm) increasing as m increases.

Values of γ may be obtained from the experimental recordings by use of the equation.

$$\gamma = \ln \frac{A''(m)}{A''(m+1)} \left(\frac{(m+1)}{m}\right)^4 \qquad 2.17$$

where A" (m) is the amplitude of the m^{th} order magnetoresistance maximum in the differentiated signal, where $m<5/2$ since only maxima which show no sign of sharpening may be used in the calculation. Equation 2.17 is derived from the expression for ρ'' (equation 2.5) which may also be expressed in the following form.

$$\rho'' \propto (B_o/B)^4 \exp(-\gamma B_o/B)\cos(2\pi B_o/B + \Phi) \qquad 2.18$$

$$\text{where } \Phi = \tan^{-1} \frac{4\pi(\gamma - B/B_o)}{(4\pi^2 - \gamma^2 + 2\gamma B/B_o)} \qquad 2.19$$

A typical γ value for the samples used in this work was 1.2. The magnitude of the shifts expected with this value are tabulated in table 2.5. This shows that for low field extrema, (i.e. m>1.5), the percentage shifts in the leading term of the Fourier series are of the order of 1-2% for both the differentiated and undifferentiated signals, which is well within experimental error for the results obtained by both methods. The shift for the m = 1.5 extrema (i.e. $1^{\pm}$ peaks) lies just on or just within the experimental error. For the higher harmonics the percentage shifts for all extrema, except the m = ½, (i.e. 0^{+} peak), are approximately equal to 1% and therefore is also within the experimental error. The above statements are supported by the fact that for the magnetoresistance maxima occuring at low fields (i.e. $2^{\pm}$, $3^{\pm}$ and also, in the most cases the $1^{\pm}$ peaks) there was good agreement (to within 1-2%) between the values obtained from ρ and ρ''.

This chapter has essentially been devoted to the discussion of magnetoresistance measurement techniques and the phase shifting (different for each method) introduced by those techniques. The phenomenon of phase shifting is an important factor when detailed accurate measurement of peak positions in magnetic field is desired as was the case in this work. Formulae allowing the calculation of the magnitude of the shifts have been derived from a simple starting formula. By comparing this formula with those given in chapter 1, which describe the variation of ρ_{zz} and ρ_{xx} with magnetic field, it is seen that starting formula given by equation 2.9 is a better approximation to the expresssion describing the longitudinal magnetoresistance than that describing the transverse (ρ_{xx}) magnetoresistance. This is because ρ_{xx} has an additional term R, which describes the scattering within the Landau level. This term becomes more important as the magnetic field increases, implying that

NOMINAL VALUE OF M	BO/B VALUES CALCULATED FOR A γ VALUE OF 1.2					
	r=1		r=2		r=3	
	ρ	ρ''	ρ	ρ''	ρ	ρ''
0.5	0.47	0.65	0.48	0.53	0.49	0.5-
1.5	1.47	1.51	1.48	1.48	1.49	1.48
2.5	2.47	2.47	2.48	2.47	2.49	2.48
3.5	3.47	3.45	3.48	3.47	3.49	3.47
4.5	4.47	4.44	4.48	4.47	4.49	4.48
5.5	5.47	5.44	5.48	5.46	5.49	5.48

TABLE 2.5

the formula in equation 2.9 becomes a less good approximation as the magnetic field is increased. This problem becomes particularly relevant when the magnetic field positions of low order maxima are being compared for different sample orientations, with any difference seen not automatically being attributable to a genuine change in magnetic field position, but may be due to different phase shifting in each orientation if the magnetoresistance variation with magnetic field has a different functional form for each orientation.

The problem of phase shifting, its effects and how it was corrected for in this work is discussed in the context of the experimental results in chapter 4. This may be quickly summarised as follows. For low field maxima which were used to calculate the carrier concentrations of the samples (chapter 3) no correction was made since the experimental error was greater than the shifting. For high field maxima (i.e $1^{\pm}$ and $0^{\pm}$ peaks) like was always compared with like from orientation to orientation eg. differentiated data in one orientation was always compared with differentiated data in another orientation. To a certain extent this assured that the phase shifting was the same for each set of data and that any change in field position observed was genuine.

CHAPTER 3

NEUTRON DOPING/SAMPLE PREPARATION.

3.1 INTRODUCTION.

Neutron transmutation doping (N.T.D.) is one of the most successful methods of producing controlled, homogeneous doping in certain semi-conductors such as silicon,[33] germanium and indium antimonide.[34, 35] The method was first used by Lark Horovitz[36] for the nuclear doping of germanium and today virtually all high-power silicon devices have been doped using N.T.D. Neutron transmutation doping is the result of host lattice atoms capturing thermal neutrons and being transformed by the (n,γ) reaction to a stable isotope of the elements occuping nearby positions in the periodic table. In the case of silicon the transmutation product is phosphorus (31), which is a donor, for germanium the products are Ga(71) and As(75) in a ratio of 3 to 1, thus making the Ge p-type, and in InSb the main product is tin (116), which is also a donor. The amount of doping is proportional to the capture cross-section of the host atoms, the intensity of the thermal neutron flux, and the time that the semi-conductor is exposed to the radiation. Control over the amount of doping is therefore achieved by varying the intensity of the neutron flux, the irradiation time, or both. Since the transmutation of elements by thermal neutron capture is a random process, it follows that the end products will be located randomly at lattice or interstitial sites in the host material leading to an induced concentration that is extremely uniform on a macroscopic scale.

The one major problem connected with N.T.D. is that of radiation

damage to the lattice. There are two sources of this damage one is associated with the recoiling atom in the (n,γ) reaction and the other is the damage caused by other forms of radiation (e.g. fast neutrons, electrons, gamma rays) present in the reactor environment interacting with the lattice atoms. This damage and its effects have been studied in detail for silicon[33], germanium[33] and indium antimonide[34,35,37-42] using electron microscopy[43], x-ray[44], optical, ESR[45,46], and electrical techniques[38-42]. In general it was found that the damage was of a complicated nature, consisting of vacancy complexes, divacacies and interstitials with the extent of the damage depending on the character of the incident radiation and the temperature of the material during irradiation. This means that the damage incurred by any one sample during irradiation is dependent upon the reactor locale in which bombardment takes place. The lattice defects caused by irradiation have a marked effect on the electrical properties of the semi-conductor. They act in part as donors or acceptors and also as additional scattering or capture centres which reduces the mobility of the charge carriers. They are not always stable with respect to temperature and can be partially annealed away thus changing the electrical properties. For this reason neutron doped samples are usually annealed after irradiation, with the annealing temperature being decided by the nature of the damage and the particular material under study.

3.2 N.T.D. IN InSb.

The thermal neutron transmutations relevant to InSb, along with the radioactive by-products of the (n,γ) reaction and the half-lives are shown in tables 3.1 and 3.2. These illustrate several facts. A) 97.9% of the end products are Tin (a donor), 2.1% are Tellurium (a donor), and 0.05% are cadmium (an acceptor). Hence the overall effect is to produce an increase in the donor concentration and therefore at the temperatures at which the donors are ionised, an increase in the

ISOTOPE	THERMAL CAPTURE. CROSS-SECTION (BARNS)	DECAY PRODUCTS.
In(113)	56	0.955 Sn 0.045 Cd
	2	0.99 Sn 0.01 Cd
In(115)	145	1.00 Sn
	52	1.00 Sn
Sb(121)	5.3	0.03 Sn 0.97 Te
Sb(123)	2.5	1.00 Te
	0.03	1.00 Te
	0.03	1.00 Te

TABLE 3.1

NEUTRON IRRADIATED InSb

ISOTOPE	% ABUNDANCE	REACTION	HALF LIFE	RADIATION
In^{113}	4.2	(n,γ)	72 secs	98% β^- 1.988 MeV; β^+;γ
			50.0 days	17% γ 0.192 MeV; 3.5% γ 0.724 MeV, 0.558
In^{115}	95.8	(n,γ)	14 secs	β^- 3.3
			54 mins	β^- 1.0 MeV 80% γ 1.293 MeV 53% γ 1.09 MeV 36% γ 0.417 MeV
Sb^{121}	57.2	(n,γ)	2.8 days	97% β^- 1.97 MeV; β^+ 0.56 MeV 66% γ 0.564 MeV 3.4% γ 0.686 MeV
Sb^{123}	42.8	(n,γ)	60 days	β^- 2.31 MeV 50% γ 1.692 MeV 97% γ 0.603 MeV 14% γ 0.72 MeV
Sb^{123}	42.8	(n,γ)	93 secs	β^- 1.19 MeV 20% γ 0.644 MeV 0.603 MeV 0.505 MeV
			24 min	γ

TABLE 3.2

electron concentration. B) High energy x-rays and electrons are emitted and appropriate safety precautions have to be taken when handling the doped samples. (Precautions taken during this work are discussed later in this chapter). C) 97% of all transmutations have a half-life of 54 minutes or less, meaning that after several hours the sample will have reached 97% of the final induced donor concentration. D) A combination of a large natural abundance and capture cross-section results in In(115) transmutating to Tin being the reaction responsible for the large majority of the end products. This leads to a problem known as self-shielding; the intensity of a beam of thermal neutrons is attenuated by a factor of e^{-1} over a path of 3.3mm in InSb. Therefore in order to produce doped samples with a high homogeneity it is necessary that at least one of the sample dimensions be small. It has been estimated[35] that with a sample thickness of 1mm the donor concentration would be uniform to 3% with even greater uniformity being achieved with thickness of less than 1mm.

A problem related to that of self-shielding is caused by the huge resonant capture cross-section ($\sigma = 2.2 \times 10^{4}$b) of In at 1.46ev (Figure 3.1). A beam of neutrons having this energy will be attenuated by a factor of e^{-1} over a path length of 0.03mm in InSb Thus if any neutrons of this energy are present in the neutron beam it will result in a much higher doping density at the surface of the sample than in the bulk, hence destroying homogeneity. The solution to this phenomenon is to wrap the crystal in 0.25mm - thick Indium foil, which absorbs the resonance neutrons before they can reach the sample.

Much work has been carried out on the irradiation of InSb, ranging from

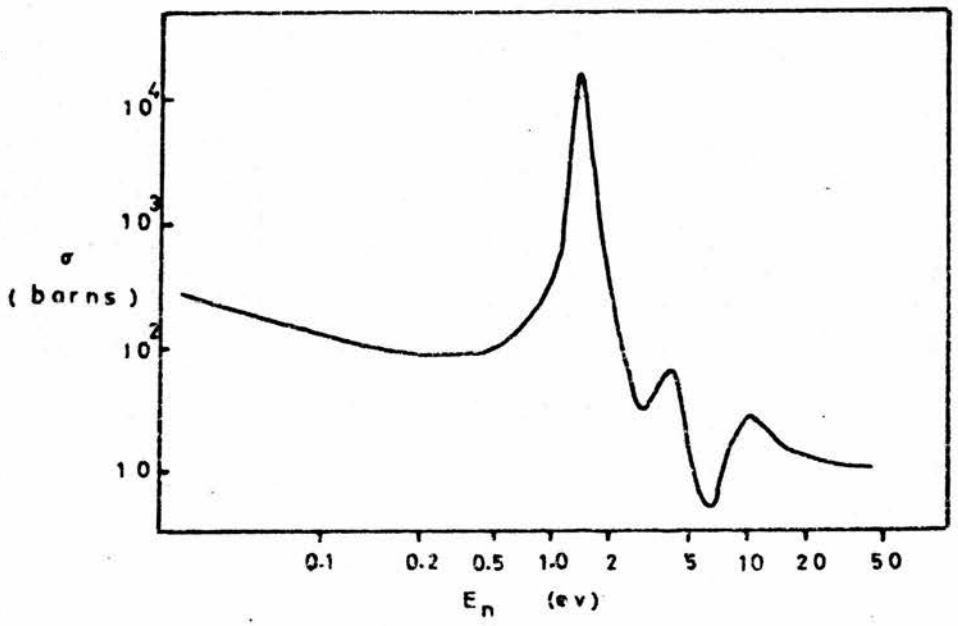

FIGURE 3·1

THERMAL NEUTRON CAPTURE CROSS-SECTION VERSUS NEUTRON ENERGY FOR INDIUM

N.T.D.[34,35] to the study of damage caused by γ-rays[41], fast neutrons[40] and high-energy electrons[42]. The controlled doping by thermal neutron irradiation has been documented in detail by several works. Kuchar[34] et al doped samples in the donor concentration range of 0.6 -> 5×10^{14} cm^{-3} using a well-thermalised neutron beam. They found excellent agreement between the theoretically predicted induced donor concentration calculated from the values of capture cross-sections and neutron flux, and the experimentally measured values after annealing. They did not compare sample characteristics before and after annealing. Clark and Isaacson[35] produced n-type InSb with carrier concentrations varying from 10^{14} ->10^{17} cm^{-3}. The neutron beam was not well thermalised and consequently the crystals were wrapped in Indium foil to eliminate the resonant neutrons. Measurement of carrier concentration and mobility at 77°K before annealing showed that the carrier concentraction (n) fell below the predicted values, with the degree of control over the amount of doping being ±6%, and that for low doping densities the mobility was approximately equal to predicted values, falling below these values for higher induced donor concentrations. Annealing of the samples at various temperatures produced the following results:- the predominant behaviour of n was a slow increase up to 400°C followed by a sharp decrease at 450°C with the discrepancy between predicted and annealed experimental values being 16%. The mobility increased very slightly up to 400°C and then also decreased sharply. The increase in carrier concentration and mobility up to 400°C was attributed to the annealing away of radiation damage acting as electron traps and scattering centres, and the sharp decrease in both was thought to be due to the diffusing in of p-type impurities. An interesting phenomenon observed by Clark and Isaacson[35] was that after irradiation and before annealing, the nuclear spin-lattice relaxation rate of In(115), Sb(121), and Sb(123), in the temperature range 1.3 - 4.2°K was greatly increased (by a factor of 30 for

doping density of $10^{16}cm^{-3}$). Annealing to a temperature of 350°C . reduced the relaxation rate by a factor of four. They attributed the increased relaxation rate to the presence of paramagnetic centres caused by radiation damage.

The damaging effect of fast neutrons on semiconductors and particularly InSb has now been well established. As a high energy recoil from the collision of a fast neutron nears the end of its range, the rate of energy loss to the lattice becomes so large that a region estimated to contain approximately 10^4-10^5 atoms is heated to a very high temperature ($\sim 10^4$°K) and rapidly quenched ($\sim 10^{-11}$ s). : This thermal spike, as it is called, permits rearrangement or interchange of atoms which may then be quenched into their new positions, thus generating a disordered region of a size estimated to be 150 - 200 Angstroms in radius. This has been supported by direct electron-microscopic examinations.[43]

The influence of this damage on the electrical properties of the material was shown to be significant. With prolonged exposure to fast neutrons p-type InSb was converted to n-type and the carrier concentration, n, approached a saturation value nl, n-type InSb decreased in conductivity towards a limiting value close to that of the p-type limiting value of nl. Vitovskii et al[39] found that for n-type InSb the initial conductivity of 70 $ohms^{-1}\ cm^{-1}$ at 4.2°K, reduced to $\sim 4\times10^{-3}\ ohm^{-1}\ cm^{-1}$ after a neutron dose of $3.2\times10^{14}\ cm^{-2}$. For p-type material they found that the initial conductivity of approximately $4\times10^{-5}\ ohms^{-1}\ cm^{-1}$ at 4.2°K reduced to $\sim 2\times10^{-6}\ ohms^{-1}\ cm^{-1}$ (before p-n conversion) after a dose of $3.6\times10^{13}cm^{-2}$ and finally increased to $3\times10^{-3}\ ohms^{-1}\ cm^{-1}$ on receiving a total neutron dose of $3.2\times10^{14}\ cm^{-2}$. The same authors and others found that the mobilities of both electrons and holes decreased monotonically with increased exposure

to the radiation. They also observed that the temperature of the sample during irradiation had no effect on the production of disordered regions but did alter the rate of production of Frenkel defects. Annealing experiments carried out by most workers were in agreement; a temperature of approximately 30°C removed the Frenkel defects whilst a temperature of 350°C was required to remove, or partially remove the disordered regions. Heating to 350°C restored the carrier mobility and concentration to their initial values.

Studies on x-ray and high-energy electron damage have shown that the character, effects and annealing properties of the damage are essentially the same as that for fast neutrons.

3.3 SAMPLE PREPARATION.

Starting material for this work was two single crystals (IS563) and (IS544) of high purity, uncompensated InSb, orientation (111), supplied by Mining and Chemical Products Ltd. The ingot characteristics were:- IS563, mobility at 77°K - 5.66×10^{5} cm^{2}/voltsec, carrier concentration at 77°K - 8.3×10^{13} cm^{-3}. IS544, mobility at 77°K- 4.3×10^{5} cm^{2}/voltsec, carrier concentration at 77°K - 4.22×10^{14} cm^{-3}. The choice of sample dimensions was governed by two factors, the need for a long, narrow sample for Shubnikov-de Haas measurements and the necessity for the sample thickness to be 1mm or less in order to obtain high uniformity of doping. The first stage of sample fabrication was performed using a sliding-table, tungsten wire saw, with a cutting medium of carborundum powder suspended in water plus detergent. Rectangular shapes of approximately 1cm length and 2mm width were cut out using this assembly. The required thickness was achieved by polishing down both faces of each sample manually, using a lapping jig, with carborundum powder plus analar proponal on a glass plate. The crystals were then washed in proponal followed by acetone

to remove the carbon, and their dimensions accurately measured using a travelling microscope and chemical balance. Light polishing of the surfaces was attained by gently rubbing with Jewellers Rouge on filter paper, with any rouge being subsequently removed by soaking the crystals in acetone overnight.

Samples from the IS544 ingot were orientated by the following proceedure; the crystal was cleaved along the (110) plane, the direction perpendicular to this plane being the (110) direction. Some samples were cut with their length parallel to the (110) direction (plus or minus approximately 3 degrees) and some were cut with their length in the (221) direction. Samples from the IS563 ingot were not orientated in any particular crystallographic direction.

The last stage of sample preparation was to wrap the crystals in Indium foil as the reactor locale in which the material was irradiated contained a significant number of neutrons at 1.4ev. The foil thickness was nominally 0.25mm which was calculated to have the result of reducing the intensity of the resonant neutrons by a factor of 10^{-9} and the thermal neutron flux by a factor of 0.87. One problem which was considered was that of what tolerance was acceptable on the thickness of the Indium foil. If the thickness varied over the length of a sample then different areas of the crystal would be subjected to different neutron intensities and homogeneity along its length would be destroyed. Also control over the doping density would decrease with increasing variance of foil thickness from sample to sample and reproducibility of results would disappear. Calculations on this aspect were performed using the following equation:-

$$I = I_o e^{-n\sigma t} \qquad 3.1$$

I_o = Initial intensity.

I = Final intensity.

N = Number of atoms per unit volume in absorber.

σ = Neutron capture cross-section of atoms in absorber.

t = Thickness of absorber.

This illustrated that with a variation in thickness of ±0.05mm the resonant neutron intensity is different by a factor of 10^3 with the thermal neutron intensity differing by 6%. A difference of 0.01mm results in a thermal neutron variation of approximately 1% and a factor of ten difference for the resonant neutrons. Measurements of foil thickness showed that the deviation from 0.25mm was equal to, or less than 0.01mm which was judged to be within acceptable limits for this work. The calculated factor of ten deviation in the resonant neutron intensity was thought to be irrelevant since the number of neutrons with this energy reaching the sample was negligible. Great care was taken when wrapping the samples not to cause any 'stretching' or overlapping of the Indium foil.

For irradiation purposes samples were placed in a polythene vial which had a lining of paper tissue to absorb any mechanical shocks. As far as it was possible to judge the lining of paper tissue was kept the same from crystal to crystal.

Irradiation was carried out at SURRC, NEL., East Kilbride, where samples from the ingot IS563 were placed in position 1 (figure 3.2) and received a mixed dose of

SURRC REACTOR PROFILE

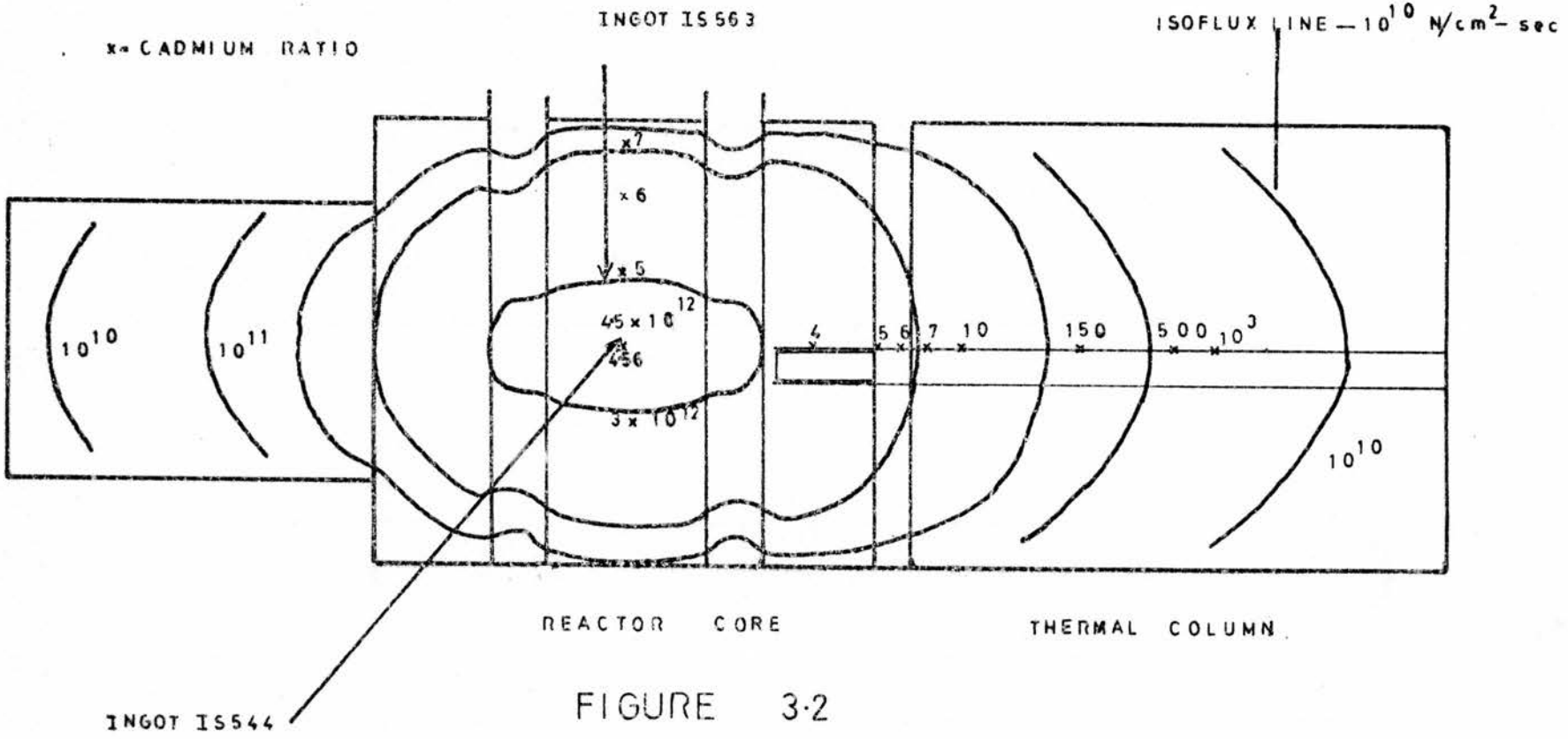

FIGURE 3·2

3×10^{12} thermal neutrons $cm^{-2} sec^{-1}$

3×10^{12} fast neutrons $cm^{-2}sec^{-1}$

1.5×10^{7} rads/hr gamma rays

at 300kw reactor power. Samples cut from IS544 were irradiated at a different reactor locale (figure 3.2) and they received

$4\ 5 \times 10^{12}$ thermal neutrons $cm^{-2}sec^{-1}$

$> 4.5 \times 10^{12}$ fast neutrons $cm^{-2}sec^{-1}$

$> 1.5 \times 10^{7}$ rads/hr gamma rays.

The ambient temperature at any particular point in the reactor was strongly dependent upon what particular point in time was being considered, and varied from as low as 25°C at start up on a Monday to almost 100°C at shut down after several days operation. The induced activity after irradiation was of the order of 1 Curie which was much too high to handle without special precautions and so the samples were placed in the reactor for the requisite time immediately before shutdown and were left there until the next day. During this time the fission product rate was 10^{6} Rad/hour following shutdown, falling exponentially to $< 10^{3}$ Rad/hour. The neutron level was negligible.

The required irradiation time for a certain doping density was calculated using equation 3.2.

$$\Delta N_D = n\sigma F t \qquad 3.2$$

where

$$n\sigma = \sum_i n_i \sigma_i$$

The sum being taken over the different isotopes with concentration n_i and capture cross-section σ_I, F is the thermal neutron flux in $cm^{-2}sec^{-1}$ and t is the irradiation time. This equation does not take account of the In foil or the packaging of the sample and hence only gave an indication of the appropriate irradiation times. equation 3.2 is amended to

$$\Delta N_D = pn\sigma Ft \qquad 3.3$$

which corrects for the foil plus packaging where p is a constant of proportionality (less than 1) to be determined experimentally. In this study, crystals having a doping density ranging from 5×10^{15} to $5 \times 10^{16} cm^{-3}$ were desirable and on substituting the value of flux into equation 3.2 yielded times varying from 20 minutes to 5 hours. (Table 3.3)

Handling of the samples was delayed for approximately 2 months after doping by which time the radio-activity had decreased to a manageable level. After removal from the In foil the crystals were etched to clean the surfaces prior to contacting. The etch choosen was 10% Bromine-Methanol rather than the more established CP4. This decision was taken for several reasons. Bromine-Methanol is less dangerous than CP4 and is consequently more convenient to work with. The etching rate of CP4 on InSb greatly exceeds that of Bromine-Methanol, with the etching time required to polish the surfaces of InSb using CP4 being of the order of seconds, whereas for Bromine-Methanol the etching time is of the order of minutes. Thus the use of Bromine-Methanol allowed greater control over the degree of etching. Samples were etched for ½ - 1 minutes and it was estimated that the etching rate of this solution was 0.7 $mg/cm^2/sec$.CP4 degrades with time and therefore the action from sample to sample may differ, whereas

Bromine-Methanol was very simply made up fresh for each etching operation, ensuring equivalent conditions from sample to sample.

For measurements of carrier concentration (n) and mobility, end contacts, potential probes on the top surfaces of the sample, and Hall contacts on the sides were made. The end contacts were pure Indium directly soldered onto the sample, and the potential probes and Hall contacts were made from Silver Preparation MH140, supplied by Johnson-Mathey Chemicals Ltd., which had a high surface tension thus enabling the contact area to be kept to a minimum. Contacts using Indium were ohmic with a contact resistance of 1 ohm or less at $77^{\circ}K$, the silver epoxy contacts occasionally turned out to be rectifying and had a contact resistance between 100 and 1,000 ohms at $4.2^{\circ}K$.

During handling precautions were taken to avoid radio-active contamination of working surfaces. Etching was performed inside a moulded metal tray having no seams or welds and this served to contain any spillage of radio-active fluid during contacting etc., samples were never allowed to come into direct contact with the working surface but were placed on a perspex sheet. In addition, all work benches used, the etching tray and perspex sheet were intermittently monitored for contamination. Personal safety was ensured by always manipulating the crystals with tweezers and by wearing glasses which absorbed the harmful beta particles before they could reach the eyes.

3.4 EXPERIMENTAL MEASUREMENTS AND RESULTS.

Values of carrier concentration(n) were obtained by Hall and Shubnikov-de Haas measurements at $4.2^{\circ}K$ and values for the mobility by D.C., conductivity also at $4.2^{\circ}K$. D.C. conductivity was carried out using the standard method of passing a constant current through the sample and measuring the voltage across the potential probes with a high

impedance voltmeter, which in this work was Keithley 155 microvoltmeter. Shubnikov-de Haas measurements were taken as described in section 2.2 of chapter two. The free electron density was obtained from the equations describing the peak positions which are periodic with reciprocal magnetic field. For spherical energy surfaces we have

$$1/Bp = (2\pi e/\hbar)\ 1/S_F(p+\tfrac{1}{2}) \qquad 3.4$$

S_F = Fermi surface cross-sectional area.

Bp=value of magnetic field at which p^{th} Landau level crosses. Fermi surface.

p = Quantum number.

$$S_F = (3n\pi^2)^{\frac{2}{3}} \qquad 3.5$$

where n = carrier concentration.

Peak quantum number values of differentiated and undifferentiated data for all sample orientations were plotted against reciprocal magnetic field, the gradient calculated in each case by a least squares fit and the respective values of n obtained by use of equation 3.5. The mean of the carrier concentration values was calculated and taken as the 'true' value with the standard deviation being quoted as the error. Equation 3.4 does not include the effects of spin and the shifting of the Fermi energy with magnetic field and for these reasons, only low field, unsplit maxima were used in the calculations. For concentrations of the order of $n>1x10^{16}cm^{-3}$ the p values plotted ranged from p = 3 up to p = 9, for $n<1x10^{16}cm^{-3}$ the p values lay between 2 and 4.

The Hall measurements taken merely acted as a rough check on the Shubnikov-de Haas method. They carry a large error ($\sim$10%). This is

because the shape of the samples was not conducive to accurate Hall measurements. With a rectangular shape the contacts introduce several sources of inaccuracy. For example, if the current contacts cover the ends of the sample they will short out the Hall voltage at that point, conversely if they are point contacts the current paths in the sample will not be parallel. The error due to this may be reduced by having a length to width ratio of 3 to 1 (as was the case in this work). There remains however the inaccuracies resulting from the misalignment of the Hall probes on the sides of the sample and their finite contact area. The former introduces an extra potential difference into the measured Hall voltage and the latter causes circulating currents. The most accurate method for measuring the Hall coefficient - (and hence n) is the Van der Paul method where the sample has a 4-leaf clover shape. The measurement of the carrier concentration in rectangular samples is intrinsically more accurate by the Shubnikov-de Haas method which avoids all the above mentioned problems and only involves measurement of the magnetic field positions of the magnetoresistance maxima. For this reason, in this work, the value of n obtained from the magnetoresistance data were taken to be the values best representing the true carrier concentrations.

The results are listed in table 3.3. Figure 3.3 illustrates graphically the relationship between the carrier concentration and the integrated thermal neutron flux (Ft). (In this work the carrier concentration was equal to the induced donor concentration, since the samples were essentially uncompensated, and at 4.2°K all the donors were ionised). This shows that for all but the lowest and highest donor concentation, the induced doping density was directly proportional to the integrated thermal neutron flux (Ft). The solid line drawn in was for $\Delta N_D = 0.7$ Ft. Five of the points lie within ±7% of this line which gives an indication of the degree of control of doping that can

SAMPLE	TIME IRRADIATED	INTEGRATED NEUTRON FLUX cm^{-2}	B.A. n (S-D-HAAS) $X10^{-16}cm^{+3}$	B.A. n(HALL) $x10^{-16}cm^{-3}$	MOBILITY B.A. $X10^{+4}$ cm^2/voltsec	A.A. n(S-D-H) $x10^{-16}cm^{-3}$	MOBILITY A.A. $x10^{+4}$ cm^2/voltsec
A[IS544(110)]	3hrs 20mins	$5.4x10^{16}$	4.6±3%	3.9	3.6	5.6	4.14
B[IS544(221)]	3hrs 20mins	$5.4x10^{16}$	4.1±3%	3.8	3.2	4.9	3.67
C[IS563]	5 hours	$5.4x10^{16}$	3.6±3%	3.4	3.74	4.67	4.21
D[IS544(110)]	2hrs 40mins	$4.32x10^{16}$	2.72±3%		4.12	3.55	4.84
E[IS563]	3 hours	$3.24x10^{16}$	1.99±3%	1.4	4.8	2.38	6.06
F[IS544(110)]	1hr 20mins	$2.16x10^{16}$	1.47±3%	0.99	5.37	1.79	5.64
G[IS544(221)]	4 mins	$1.08x10^{16}$	0.76±4%		5.67	1.06	6.06
H[IS544(221)]	20 mins	$5.4x10^{15}$	0.53±4%	0.50	6.39	0.6 34	6.07

TABLE 3.3

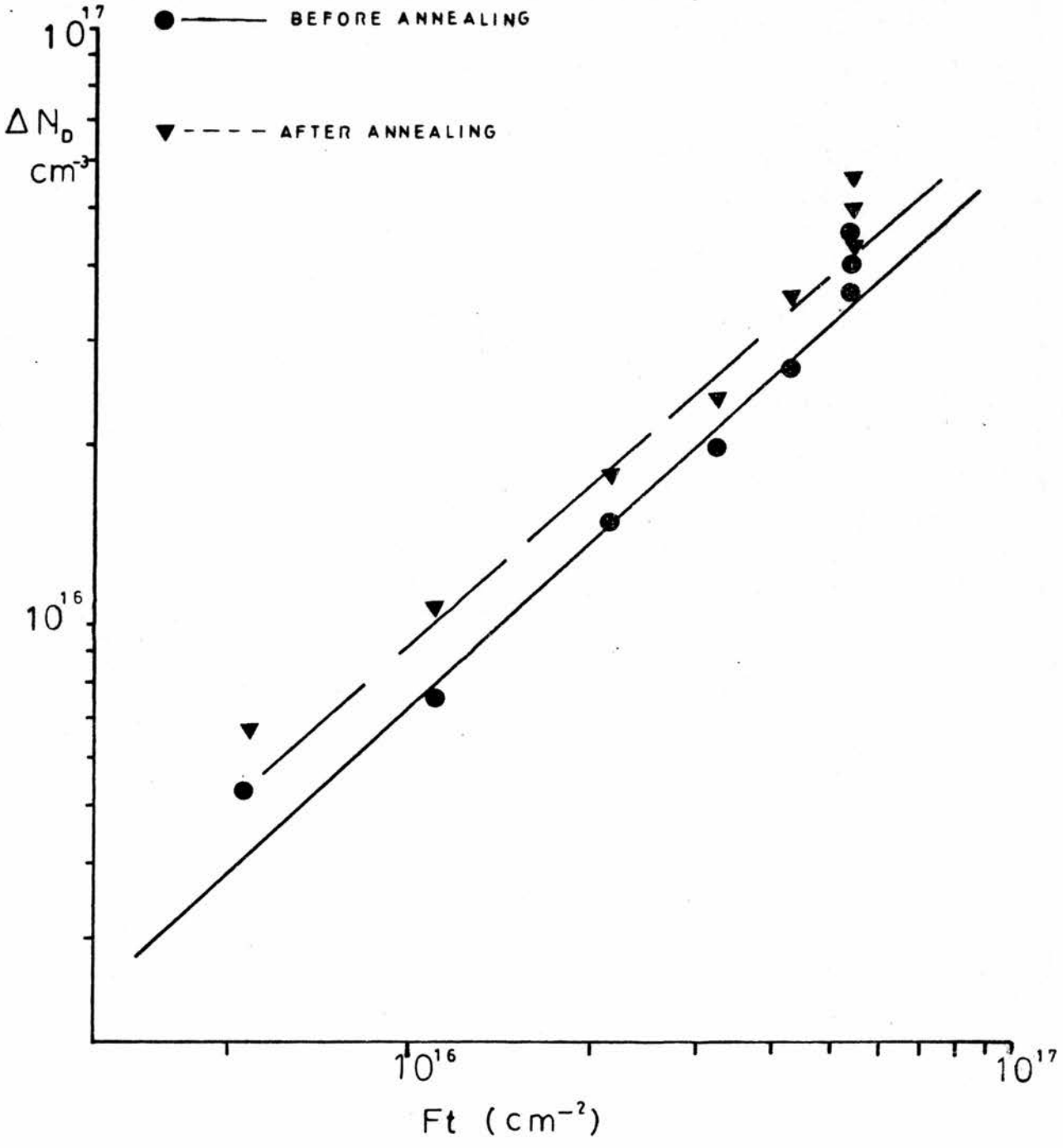

FIGURE 3·3

MEASURED INDUCED DONOR CONCENTRATION VERSUS INTEGRATED THERMAL NEUTRON FLUX

be expected with this method.

A check on the homogeneity along the crystals' length was carried out using the apparatus shown in figure 3.4. This gave a resistivity profile, at 77°K of the sample, the principle being that any inhomogeneity would be manifested by a varying resistance (assuming that the sample dimensions were constant throughout its length). A current was passed through the sample and the voltage measured by top surface pressure contacts which were moved along the sample thus allowing different regions to be probed. The potential probes were two stainless steel 10 B.A. screws whose ends had been sharpened to a point. These were lowered onto the crystals, to make pressure contacts, by a micromanipulator which also provided movement in the direction of the long axis of the crystal. The separation of the probes (i.e. distance from point to point) was 3mm and the contact resistance approximately 10^3 ohms. Electrical contact was made to the screws by soldering copper wire to the solder tag held between the two brass nuts. This copper wire led back to a Keithley digital multimeter where the voltage was measured. The probes were screwed into a perspex plate which allowed them to be independently moved in a vertical plane and hence enabled both to make contact to the sample should the surface not have been exactly horizontal.

The end contacts were made from silver epoxy as it was judged that the crystals were too brittle to withstand any pressure applied along their length. The samples were mounted on the P.T.F.E. block using paper tissue impregnated with silicon grease, which on cooling to 77°K anchored them securely in place. The P.T.F.E. block was in turn fixed to the polystyrene basin using superglue. The basin was filled with liquid nitrogen to a level well above that of the sample.

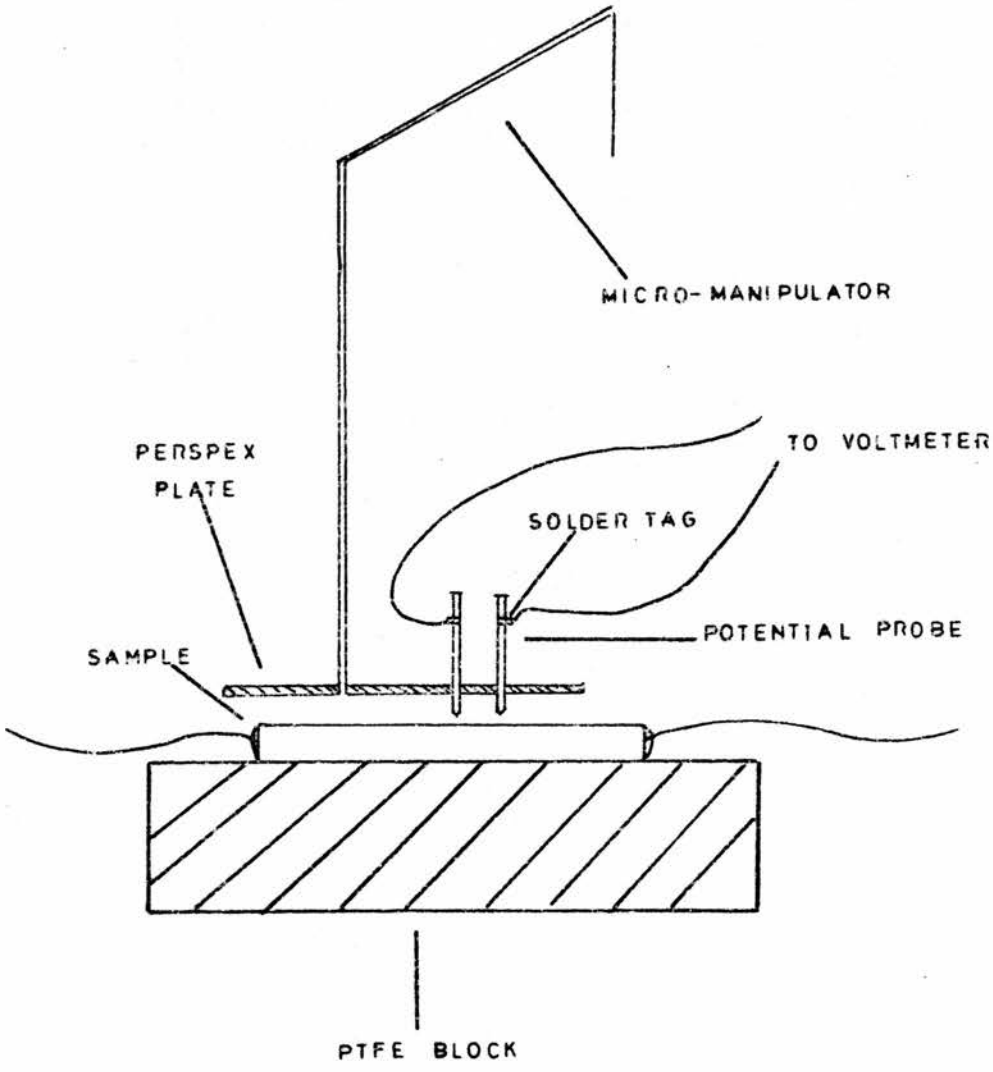

FIGURE 34

EXPT. SET UP USED TO OBTAIN RESISTANCE PROFILES OF SAMPLES

The resistance was measured at 1mm intervals along the sample. Measurements were taken for both directions of current which would have shown up any spurious effects due to thermal emfs. The results obtained for sample E are presented in figure 3.5. The x-axis represents the distance along the length of the crystal, with the y-axis representing the resistance. The horizontal bars drawn in illustrate which part of the crystal was probed and what value of resistance (R) was found for that particular region. The interpretation of the results was not simply a matter of comparing values of resistance obtained for each region. If two regions which did not overlap had a percentage difference in R then this also represented the percentage difference in doping density. For two neighbouring regions the analysis was as follows:-

Region 1, resistance $R_1 = r_1+r_2+r_3$

where r_1, r_2 and r_3 represent the resistances of each 1mm sub-region

Region 2, resistance $R_2 = r_2+r_3+r_4$

Since regions 1 and 2 overlapped by 2mm.

Let $$\frac{R_1 - R_2}{\frac{1}{2}(R_1+R_2)} \times 100 = \gamma\%$$

then $$\frac{(r_1-r_4)}{\frac{1}{2}(R_1+R_2)} \times 100 = \gamma\%$$

$$= \frac{(r_1-r_4)\times 100}{\frac{1}{2}(3(r_1+r_4))} = \gamma\% = \frac{(r_1-r_4)}{\frac{1}{2}(r_1+r_4)} \times 100 = 3\gamma\%$$

RESISTANCE PROFILE OF A NEUTRON DOPED SAMPLE

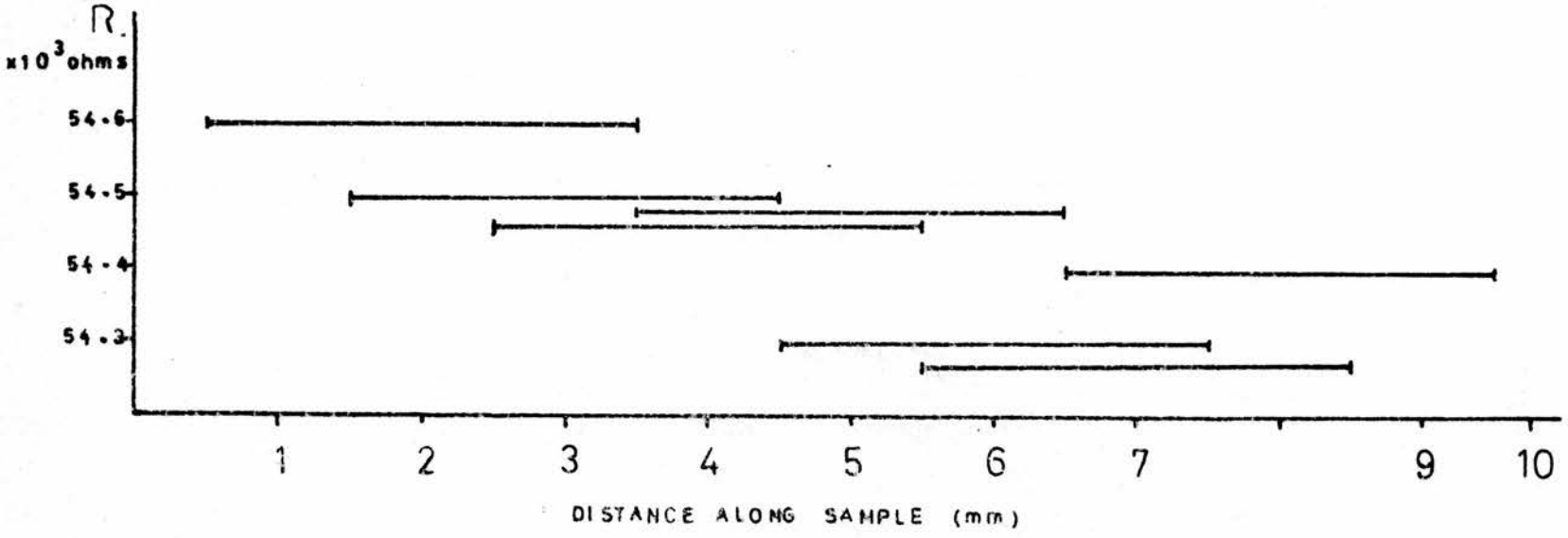

FIGURE 3·5

Since $r_1 = r_2 = r_3 = r_4$

Hence for two neighbouring regions a percentage difference in R of $\gamma\%$ meant a $3\gamma\%$ difference in the doping density. A similar analysis was employed for regions overlapping by 1mm. Four samples were measured and the results analysed in this manner. For all it was found that the measured percentage variance in the doping density was never greater than 1%. In reality the homogeneity was probably better than this with the change in resistance merely reflecting irregularities in the thickness and width of the sample.

The resistance profiles only gave information on the homogeneity in one plane, they gave no indication of the uniformity of doping throughout the thickness of the sample. Shubnikov-de Haas recordings displayed oscillation amplitudes indicative of samples with a high uniformity of doping. It has been shown that the presence of inhomogeneities is equivalent to a high Dingle temperature and that their effect on the Shubnikov-de Haas magnetoresistance is to greatly reduce the amplitudes of the maxima and to broaden the peaks out, such that few oscillations are seen and spin-splitting is not observed. The samples used in this work produced profiles where several ($\sim$5) maxima were observed and for carrier concentrations greater than $1 \times 10^{16} cm^{-3}$ spin-splitting in the $1\pm$ doublet was present in ρ_{xx}.

3.5 ANNEALING.

Samples were annealed under vacuum (pressure $\sim 10^{-4}$Torr), for six hours at a temperature of $350^{\circ}C$, so chosen because it was the temperature which previous workers quoted as being adequate for reducing the damage due to fast neutrons etc., without introducing impurities into the material. Figure 3.6 is a schematic diagram of the annealing system. The samples were housed inside the graphite vial inside the quartz tube

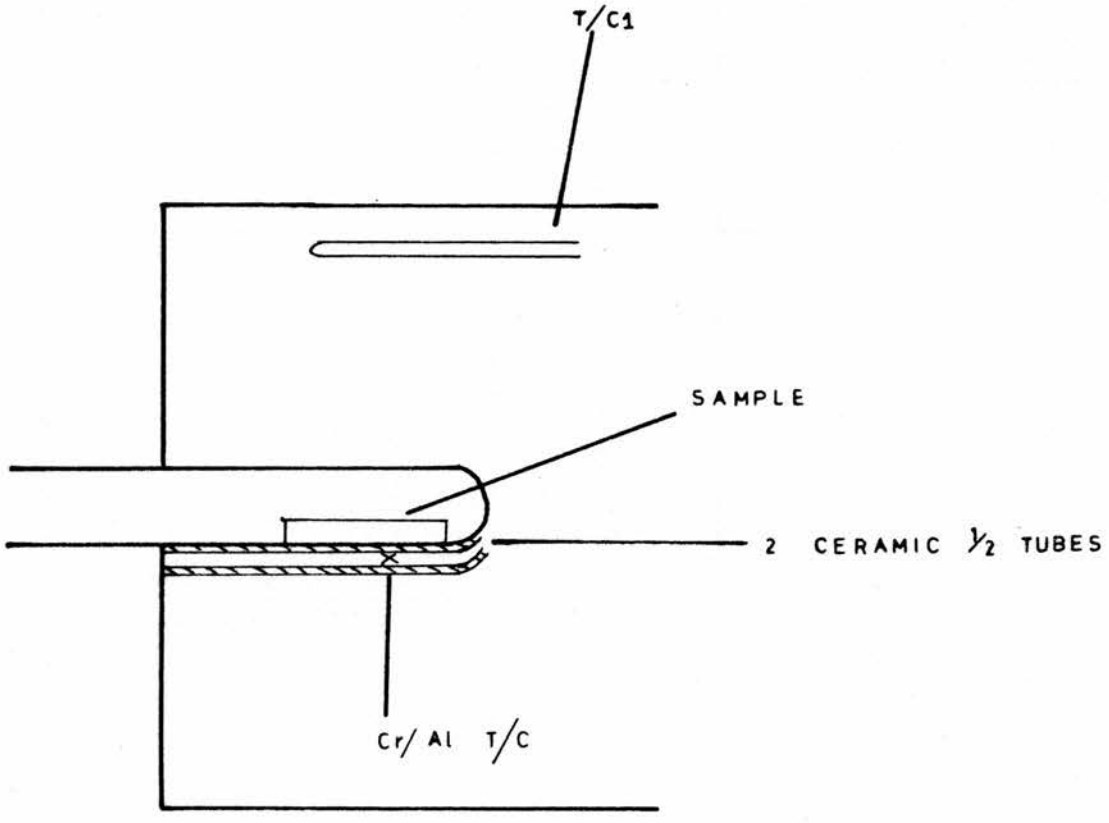

FIGURE 3·6

DIAGRAM OF THERMAL ANNEALING ARRANGEMENT

of ordinary purity Vitreosil. This quartz tube, in turn, rested in two ceramic half-tubes sandwiched between which was a Cr/Al thermocouple so placed to avoid disturbing its position when the quartz tube was inserted and withdrawn from the furnace. This thermocouple was connected to a Comark digital thermometer which displayed the temperature in degrees centigrade . Thermocouple 1 was connected to a temperature controller in the furnace which kept the temperature at that particular location at a pre-set value. This set value was very different from the temperature at the Cr/Al thermocouple which was fixed at approximately 350^{o}C by a method of trial and error. The accuracy to which the temperature registered by the Cr/Al thermocouple represented the temperature of the sample was determined by measuring the temperature gradient across ceramic plus quartz. (It was assumed that the temperature gradient across the thickness of the graphite was small and that the sample attained the same temperature as the graphite). The difference in temperature between two points was found to be approximately six degrees centigrade once the temperature inside the furnace had stabilised.

The furnace had always been on for at least 24 hours prior to the annealing of any sample, by which time the temperature had fully stabilised. The Vitreosil tube was continuously evacuated by diffusion pump throughout the annealing process and after removal from furnace when it was allowed to cool to room temperature naturally. The temperature registered by the Cr/Al thermocouple was monitored throughout each heat treatment and the temperature was never found to deviate from 350^{o}C by more than ±5^{o}C. Care was taken to always insert the quartz tube to the same depth for each anneal so that the samples were in equivalent conditions during heat treamtment. With the described annealing system it was estimated that the temperature of the samples was known to within 10 degrees i.e. 350^{o}C±10^{o}C.

The danger of contamination from impurities during heat treatment was great and special precautions were taken to avoid this. One of the main possible contaminants was Copper (an acceptor in InSb) which has a high diffusion coefficient in InSb($\sim 10^{-8} cm^{-2} sec^{-1}$). Copper is present in small quantities in Vitreosil and this can lead to the kind of effects discussed in the paper Heat Treatment of GaAs by J. T. Edmond.[47] This compared the effects of using two grades purity quartz, (high purity Sectrosil and ordinary purity Vitreosil) for heat treatments of GaAs to 1000°C. It was found that n-type GaAs became p-type or less strongly n-type with the magnitude of the changes being much less for the high purity quartz. It was also noted that for Vitreosil the magnitude of the effects found in GaAs were $\Delta n \tilde{=} 7 \times 10^{17} cm^{-3}$ at 1000°C; in InAs, $1 \times 10^{17} cm^{-3}$ at 850°C and in InSb $\Delta n \approx 3 \times 10^{15} cm^{-3}$ at 500°C all for 60 hours treatment. These changes were all attributed to the diffusion of copper into the materials.

In this work, although ordinary purity quartz was used, copper contamination from the Vitreosil was avoided by placing the samples in a high purity graphite vial. Steps taken to have a 'clean' system were extensive. Samples were cleaned with acetone then etched with Bromine-Methanol before annealing. The graphite was washed in toluene and then heated under vacuum (presssure 10^{-4} Torr), in an rf heater for 10 minutes at a temperature of approximately 500°C. This drove off any impurities which were likely to be given off during the anneal. The quartz tube was etched in Aqua Regia for 12 hours, after which it was washed out in acetone followed by propanol, allowed to dry and lastly was flamed.

After annealing the samples were re-contacted and their characteristics measured using the same techniques as before. The results are presented in table 3.3 where it can be seen that the carrier concentration

increased by between 20-25% and that the mobility increased by approximately 15% for $n \geq 10^{16} cm^{-3}$ and by ~5% for $n \leq 1 \times 10^{16} cm^{-3}$

3.6 DISCUSSION OF RESULTS.

In agreement with other workers it was found that in general, before annealing, the induced donor concentration was directly proportional to the integrated thermal neutron flux, with the constant of proportionality in this case being ~0.7. This is much lower than the value found by Kuchar et al and is about half the value found by Clark and Isaacson. This can be explained by the packaging of the samples which modifies the neutron flux in an uncontrollable manner, with prediction of the induced donor concentration only possible once several samples have been doped in a calibration run. In the former case samples were irradiated bare, no modification of the flux was introduced, and accordingly the proportionality constant was in good agreement with $\Sigma_i n_i \sigma_i$. The difference in values found between this work and that of Clark and Isaacson may be attributed to different packaging geometry or different packaging materials.

Examination of figure 3.3 reveals that two points (samples A & H) lie well away from the solid line prediciting the doping densities. For sample H the deviation is probably due to an inaccuracy in the estimated integrated thermal neutron flux arising from an error in the irradiation time. Since the total irradiation time for this sample was only 20 minutes, a few minutes inaccuracy in the timing would have resulted in a large percentage deviation in the induced donor concentration. It is unlikely that the deviation in the donor density of sample A is a manifestation of error in irradiation time alone, as the percentage difference is so large and an error in timing of nearly 50 minutes would have been necessary to produce such a differnce. A combination of bad timing, a different thermal neutron flux and different packaging

could have produced this effect, with one other possible influencing factor discussed in the next paragraph.

The large fast neutron flux ($\gtrsim 3\times10^{12}/cm^2/sec$) which the samples were subjected to is an important consideration in this work as it has been shown that in n-type InSb the induced damage from fast neutrons is great and that the damage centres act as electron traps, (hence reducing the carrier concentration by which the donor concentration is measured), and additional scattering centres (hence reducing the mobility). This damage and its effects is not accurately predictable in magnitude but it has been shown that the density of electron traps produced is not linear with the integrated fast neutron flux and that a saturation value is reached at a total of greater than $10^{18}cm^{-2}$neutrons. It is possible therefore that the fast neutron bombardment also contributed toward any deviation from reproducibility.

The annealing results supported past work. Heat treatment to 350°C for 6 hours was found to increase the carrier concentration by 20-25% (in agreement with Clark and Isaacson) and the mobility by approximately 15% for high concentrations – these two facts indicating that the damage sustained was completely, or partially annealed away. It is difficult to compare the observed change in mobility in this work and that seen by Clark and Isaacson, since in the former case the mobility was measured at 4.2°K (where ionised impurity scattering dominates) and the latter was measured at 77°K (where the scattering by phonons is dominant). The change in mobility does however, give an indication of the importance of the scattering by the damage centres at that particular temperature. It should also be noted from figure 3.3 that although the carrier concentration of each sample has increased, the scatter of points about the solid line predicting the donor densities has not decreased but rather increased, apparantly reducing the reproducibility of the results.

The method of N.T.D. outlined in this chapter was not one of the better methods of utilising a very elegant technique. This is so for several reasons. The irradiation times used to obtain the smaller donor concentrations were too small (20 and 40 mins.), requiring very accurate measurement, (to within one minute), in order to have a high degree of control over the induced donor concentration. A reduced neutron flux and increased irradiation time would have been much more preferable. The high fast neutron intensity which the crystals were subjected to was undesirable due to the amount of lattice damage incurred from this source. An important effect from this is that since the induced donor concentration was evaluated by measurement of the free electron density, the estimated value of the density of transmutated atoms was affected by the fast neutron flux damage which in part acts as electron traps. Finally, wrapping of the samples with In foil was yet another possible source of error where the variation of foil thickness could have caused inhomogeneities, irreproducibility of results, or both.

In conclusion therefore, although this work was moderately successful with very homogeneously doped samples being produced, much better control over the doping and much less damage sustained by the crystals could have been attained if irradiation had been performed in a different reactor locale where the neutron flux was well thermalised and much lower than $4.5 \times 10^{12} cm^{-2} sec^{-1}$. For example instead of placing samples in the core of the reactor (figure 3.3) much more satisfactory results could be obtained by placing the samples in a thermal column where the thermal neutron/fast neutron ratio is much higher.

CHAPTER FOUR.

SPIN SPLITTING IN SHUBNIKOV-DE HAAS OSCILLATIONS.

4.1 INTRODUCTION.

The influence of the electron spin on the quantum oscillatory effects, first investigated Gurevich and Efros[49], at low temperatures and sufficiently high magnetic fields leads to the splitting of the Landau levels, which in turn produces spin-split peaks in the magnetoresistance oscillations. Experimentally such factors as electron scattering, finite temperature and inhomogeneous impurity concentration cause broadening of the extrema so that for $p>2$ the double peaks are unresolved. The observation of well defined spin-split peaks for $p<2$ requires large magnetic fields, however under such conditions the Fermi energy E_F has in general a complicated magnetic field dependence and the location of the extrema is shifted from the exact 1/B periodicity. The spin splitting in the Shubnikov-de Haas oscillations has been much used in the past to deduce the effective g factor of the electrons in several materials[10,12,13], such as Grey Tin[12] and Mercury Selenide[48] (HgSe), where, in both cases, the g factor was determined as a function of carrier concentration and crystallographic orientation, thus reflecting the shape of the Fermi surface. Indium Antimonide in particular has been a great source of interest, initial investigations by Amirkhanov et al[50] used the positions of the the 0^- peaks to find a g factor of between 64-70, later work allowed calculation of the g factor from the 0^- and the $1^\pm$ spin-split peaks. Antcliffe and Stradling[51] determined the spin-splitting of the ρ_{xx} maxima for several samples with carrier concentrations $4\text{-}11\times10^{16}cm^{-3}$. The value of g was calculated from the positions of the first ($1^\pm$) and second ($2^\pm$) doublets. Good agreement was found between the theoretical values (calculated on a 3-band model) and the experimental values obtained from both doublets for the higher

concentration samples. Similar experiments were performed by Bliek[16] et al who calculated g from the splitting of the p=1 peak in the transverse magnetoresistance. They also found good agreement between experiment and theory. Gluzman et al[52] analysed other workers data in terms of the 3-band model and found good agreement, although their measurements of g from the 1± maxima in ρ_{xx} produced values which fell 20-30% below the values predicted by the model.

Other properties also exhibit oscillatory behaviour and spin-splitting such as the thermo-power as seen in HgSe by Dietl etal[53], and the magnetic susceptibility[16, 48] (de Haas Van Alphen effect), both of which have been used to determine the g factor. It is also worth noting that the determination of g has been carried out using the unsplit maxima by the direct curve fitting of the Shubnikov-de Haas theory to the experimental magneto-conductivity oscillations[54]. The values obtained were in good agreement with the values obtained from spin resonance experiments.

Comparison of spin-splitting characteristics in the longitudinal (ρ_{zz}) and transverse (ρ_{xx}) magnetoresistance reveals striking differences in contradiction to theory. Firstly, in the longitudinal configuration the 0^- maximum is very weak, which according to Efros[55] can be explained by a very small probability for spin-flip scattering. Since momentum relaxation in the z-direction within the 0^- level is impossible, the only contribution to ρ_{zz} is from scattering between 0^+ and 0^- levels. Hence if the probability of spin-flip scattering is small then the 0^- peak will be missing from the longitudinal magnetoresistance Conflicting results have been observed for the splitting of the higher order (ie. p=1, 2, etc.) Landau levels in ρ_{zz}. In Indium Antimonide Amirkhanov and Bashirov[50] found spin-splitting of the p=1 peak, similarly Gluzman etal found spin-splitting in ρ_{zz} although the amplitude

of the 1^+ peak (ie. the maxima falling at higher magnetic fields) was much reduced. In contrast to this, Bliek et al[16] observed results which were dependent on the type of contacting and size of sample. They found that with small samples and soldered potential probes spin-splitting was present, whereas with large samples and spot welded contacts spin-splitting in the longitudinal configuration was absent. In cases where spin-splitting was observed in ρ_{zz} it was found that the value of $B_1^+ - B_1$ was larger than that seen in ρ_{xx}. The magnitude of this difference was reported to be between 40-50% by Gluzman et al[52] and was found to be due to a shift in the 1^+ peak to stronger magnetic fields.

Similar phenomena have been found in other materials. In n-type HgSe[56] spin-splitting was absent in ρ_{zz} although it was present in ρ_{xx}. Investigations of the Shubnikov-de Haas effect in Sb-doped gray tin[12] samples having low electron concentrations ($8\times10^{15}cm^{-3}$) and also those having a high carrier concentration (10^{18}-$10^{19}cm^{-3}$) revealed that the high concentration samples showed splitting for both ρ_{zz} and ρ_{xx}, with the low concentration samples showing splitting in the transverse orientation alone. Apart from the normal magnetoresistance maxima, additional peaks in the recordings, not predicted by theory, were observed by several workers[56,10] in HgSe and HgCdTe. The origin of these peaks is not understood although it has been suggested by Galazka[56] et al that they may be caused by the coincidence of the Fermi level and impurity levels.

Several attempts have been made to explain the behaviour of the longitudinal magnetoresistance. Earlier workers[57] postulated a different scattering rate for spin-up and spin-down electrons to account for the smaller amplitude of the 1^+ peak in ρ_{zz} for InSb. Narita and Suizu[10] produced a set of selection rules to describe the transverse and longitudinal magnetoresistance. In the transverse case the selection

rules describing electron transitions between Landau levels are as follows:-

1. $P\uparrow \not\rightarrow (P-1)\uparrow$

ie. transitions between the spin-down P^{th} Landau level and the spin-down $(P-1)^{th}$ Landau level are allowed.

2. $P\uparrow \not\rightarrow (P-1)\uparrow$

3. $P\uparrow \not\rightarrow P\uparrow$

and for the longitudinal magnetoresistance:-

$P\uparrow \not\rightarrow (P-1)\uparrow$

Gluzman etal[52] tried to explain the observed behaviour of the longitudinal magnetoresistance within the frame-work of the accepted theory of the Shubnikov-de Haas effect. They made computer calculations and produced the oscillation profiles of ρ_{xx} and ρ_{zz} predicted by the theoretical formulae (chapter 1 equations 1.12 to 1.17). The following points were made:- the relative amplitudes of the peaks in each doublet of ρ_{xx} and ρ_{zz} depend on the values of T_D/B and R (where T_D = Dingle temperature, R = term describing scattering within a particular Landau level, only present in ρ_{xx}), with an increase in T_D/B resulting in the higher magnetic field peak of the doublets becoming smaller than the low magnetic field peaks. An increase in R, which is greater at higher magnetic fields results in the high field peak becoming larger than the low field one. The conclusion arrived at was that the observed smaller amplitude of the 1^+ peak in ρ_{zz} was a consequence of the factor R appearing in ρ_{xx} but not ρ_{zz}.

Investigation of the dependence of the oscillation profile on the spin-splitting parameter $\nu(=\frac{1}{2}gm^*/m)$ produced plots which suggested that with a value of $\nu = 0.25$, (Where the second, and other even harmonics for which r/2 equals an odd number, disappear), and at a Dingle temperature of 4^oK the spin-splitting in the ρ_{xx} and ρ_{zz} maxima disappears, whereas for a T_D of 1^oK, spin-splitting is present. They attributed the difference to the fact that at a T_D of 1^oK the contribution from the higher harmonics in the series is significant whereas for a T_D of 4^oK the contribution from the higher harmonics is negligible. The above results were used to conclude that for a ν close to 0.25 and a Dingle temperature of $\approx 4^oK$ the maxima of ρ_{zz} may not be split when those in ρ_{xx} should be split, the difference again being due to the term R appearing in the expression for ρ_{xx}. No computer plots where shown to substantiate this. They did however, consider results which reported the absence of splitting in ρ_{zz} and found that in most cases the experimental value of ν was 0.25.

4.2 EXPERIMENTAL DETAILS.

Magnetoresistance measurements were carried out, at a temperature of 4.2^oK, on eight samples (samples A-H), having carrier concentrations ranging from $\sim 5\times10^{15} cm^{-3}$ to $5\times10^{16} cm^{-3}$. The measurement technique employed was the standard method of sweeping the magnetic field, passing a D.C. constant current through the sample, feeding the voltage developed across the potential probes through a D.C. amplifier and displaying the resulting signal on the y-axis of an X-Y recorder with the X-axis recording the magnetic field. Measurement of the magnetic field was as described in chapter 2. Possible spurious effects resulting from hot electrons were avoided by limiting the electric field developed across the sample to much less than 1 volt/cm. also, additional checks were made by ensuring that the I-V characteristics were linear for all values of magnetic field. Typical sample dimensions

were 1cmx2mmx0.5mm. Some were orientated with their lengths parallel to the (110) direction (A,D and F), other with their lengths parallel to the (221) direction (B,G and H), and for samples C and E the crystallographic orientation was unknown.

Recordings were taken for longitudinal (magnetic and electric fields parallel), transverse (magnetic and electric fields perpendicular), and intermediate orientations. Double differentiation of the signal was carried out using the system described in chapter two. Careful choice of the time constant and sweep rate allowed certain structure to be accentuated thus allowing easier measurement of the magnetic field position. For example in sample B, having carrier concentration $4.1x10^{16}cm^{-3}$ it can be seen (figure 4.1a) that in the longitudinal configuration the $1^{\pm}$ doublet was not fully resolved in the undifferentiated recording, but rather the 1^{+} maximum appeared as an almost discernable shoulder on the 1^{-} maximum. Accurate measurement of the magnetic field position of the 1^{+} peak was impossible from this recording. Higher order doublets (ie. $p>1$) showed no signs of spin-splitting. Double differentiation of the signal with a time constant of 5 seconds and sweep rate of ~130G/s (figure 4.1B) resolved the 1^{+} and 1^{-} maxima into two well defined peaks. With these values of time constant and sweep rate the $p=2^{\pm}$ doublet was just beginning to show spin-splitting but not enough to allow accurate measurement of the position of the 2^{+} maximum. A shorter time constant of ½ second reduced the gain of the system but did fully resolve the p=2 doublet into the two spin-split maxima, (figure 4.1c)

This gives an excellent illustration of the advantages of the differentiation technique, not only does it help to resolve peaks in the undifferentiated data but also reveals any structure not seen in these recordings. Values of time constant and sweep rate which show

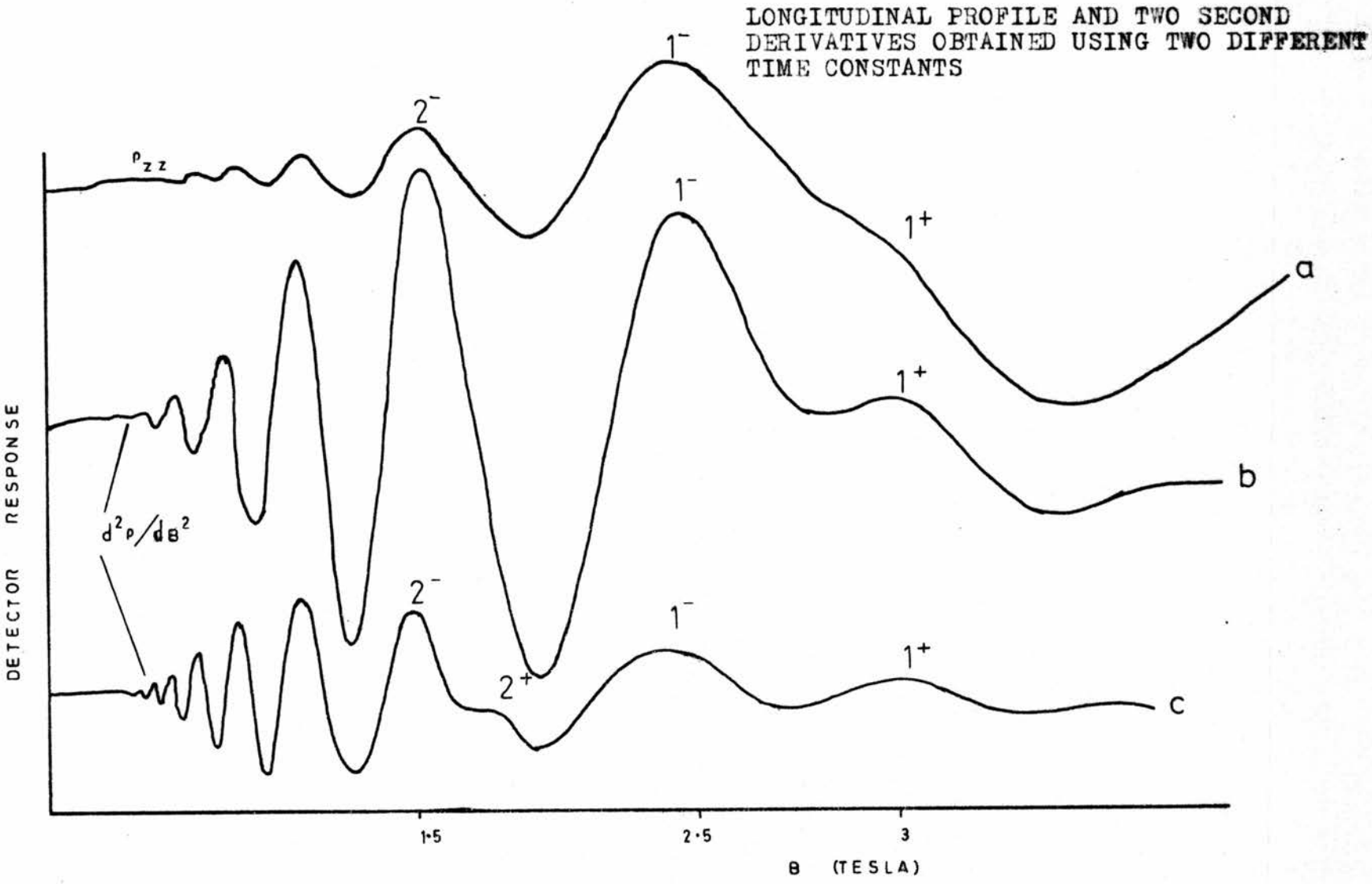

FIGURE 4·1 a,b,c

spin-splitting in one sample do not necessarily have the same effect in other samples, but rather depend on the carrier concentrations of the samples. This is because the magnitude of the spin-splitting is proportional to the magnetic field at which the doublet falls (increasing with carrier concentration), and hence since the time constant must be smaller than the period of the oscillations, which is proportional to B and (sweep rate)$^{-1}$, it follows that the smaller the carrier concentration, the smaller must be the time constant and/or sweep rate required to resolve the same doublet. Figure 4.2 illustrates how a time constant of 5 seconds resolved the 1± maxima for a carrier concentration of $4.1 \times 10^{16} cm^{-3}$ whereas it failed to resolve the same maxima for a sample having a carrier concentration of $5 \times 10^{15} cm^{-3}$ (both recordings taken at same sweep rate).

The phenomenon of experimental phase-shifting was previously discussed in chapter 2 where it was concluded that for low-field maxima (ie. $P > 1$) the shifting in both the differentiated and undifferentiated data was within experimental error and consequently no phase-shift corrections were made to these peaks. The situation for the high field maxima was complicated. At high fields the contribution from the higher harmonics in the Fourier series is more significant - this being particularly relevant in the case of the differentiated signal which accentuates the higher frequency components, making the calculation of the phase-shifts more difficult. Calculations on the shifting for a γ value of 1.2 (which was a typical value for the samples under study) estimated the shifting in the fundamental term of the 1± maxima in the undifferentiated recordings to be approximately 2%. This was on the limit of experimental error (taken to be between 1 and 2%), with the magnitude of the shifting for the higher harmonics being well within the experimental error, for both the differentiated and undifferentiated data. Again no phase-shift corrections were made since

SECOND DERIVATIVE PROFILES OF TWO SAMPLES HAVING DIFFERENT CARRIER CONCENTRATIONS. THE TIME CONSTANT IS THE SAME IN BOTH CASES.

FIGURE 4·2

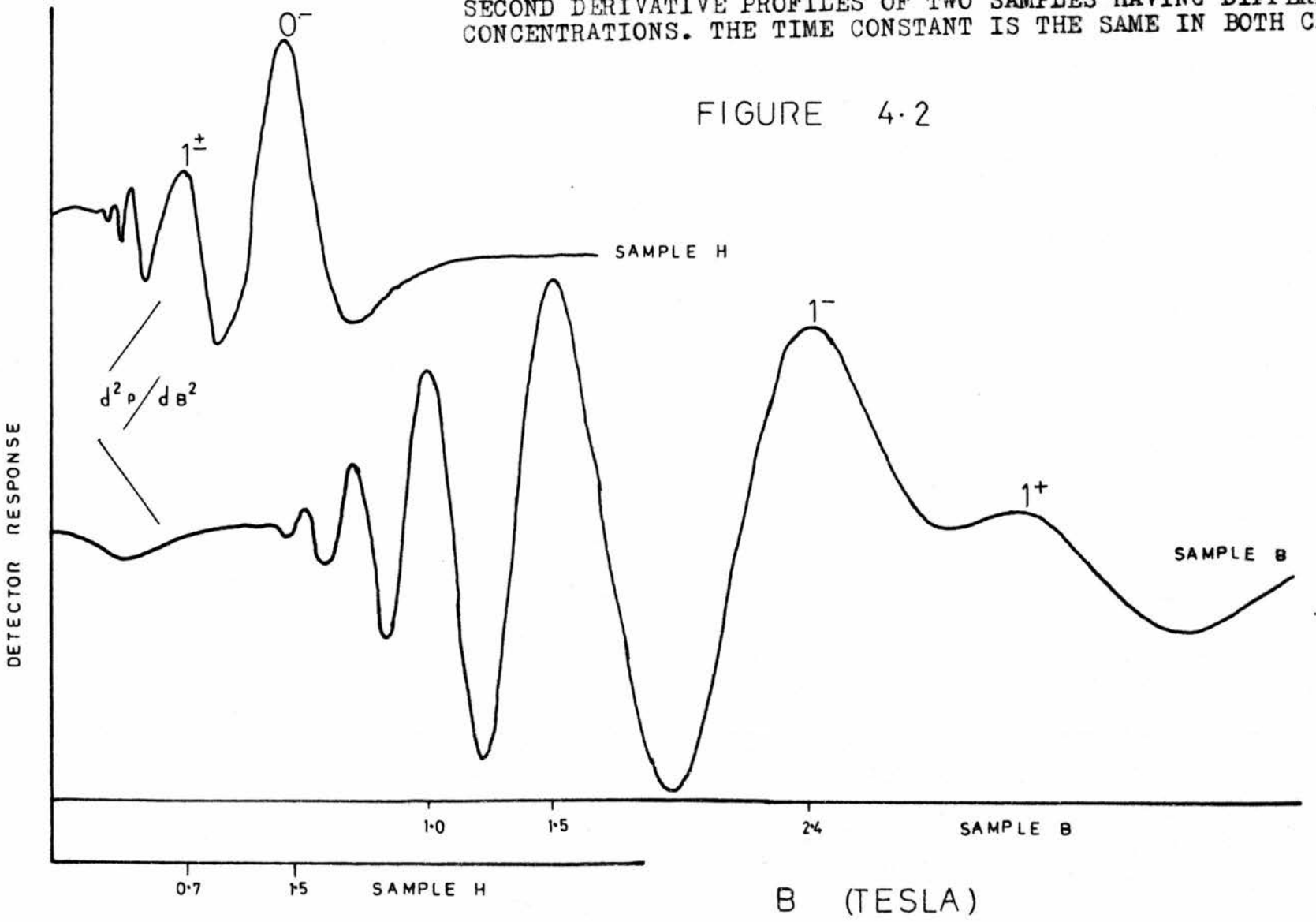

the contributions from the higher harmonics was significant at these fields and the calculated shifts for these harmonics were within the experimental error. The field positions of the $1^{\pm}$ peaks, were, when possible taken from the differentiated recordings, the reason being that these peaks were much sharper hence allowing greater accuracy in the determination of the positions of the turning points. This was particularly true in the case of the 1^{+} peak in the longitudinal orientation.

Calculated phase-shifts for the 0^{-} peak for both types of data far exceeded the estimated experimental error. This is confirmed by the experimental measurements where it was found that the values obtained from both sets of data for the magnetic field positionof the 0^{-} maximum differed by a substantial amount (up to 4%). It was found that the magnitude of the calculated shifts varied significantly from harmonic to harmonic and since it was not known which, if any, harmonics dominated the series it was impossible to make any exact estimation of the shift in the 0^{-} peak.

Another important effect which moves the maxima away from the normal resonance condition of Bo/B = ½, 3/2, etc., is the magnetic field dependence of the Fermi level. This is only important at high magnetic fields and hence only affects the low order (p = 0, 1) maxima, especially the 0^{-} peak. Finally, another form of shifting, again at high magnetic fields, was first discussed by Antcliffe and Stradling[51]. It has been shown by Adams and Holstein[7] that the contribution from many filled states below the Fermi level sum to produce a phase shift ϕ in the magnetoresistance. This phase may be defined by

$$\frac{1}{Bp}\ \frac{1}{\Delta(1/B)} = p+\tfrac{1}{2}+\phi/2\pi \qquad 4.1$$

where p = Landau index

and $\Delta(1/B) = e\hbar/m^*E_F$ = period of unsplit oscillations.

when only a few levels remain occupied the phase factor is different and consequently the peaks are shifted. Again, this effect is particularly important for the 0^- peak.

Due to the various shifts away from resonance suffered by the 0^- peak any parameter (eg. carrier concentration or g value) obtained using its magnetic field position would be subject to large errors. For this reason any parameter values were calculated from the higher order peak positions. Also, when comparing the 0^- peak positions for different orientations like data was always compared with like, the assumption being that the experimental phase-shifting discussed in chapter 2 was the same for each orientation.

4.3 THE g-FACTOR IN InSb..

The very large and negative magnetic moment of conduction electrons in InSb is a consequence of the interaction between the conduction and valence bands. Formula linking the g-factor with the effective mass m^* the spin orbit splitting of the valence band, λ, and the energy gap Eg, for a parabolic band structure was first derived by Roth[58] etal. Bowers and Yafet[59] obtained equations for the energy eigenvalues in the presence of a magnetic field for a Kane-type[60] band structure. Zawadski[61] used the results of these workers and extended them to produce an equation describing the variation of the g factor as a function of position in the band.

i.e. $$g(k) = 2\left[1-\left[\frac{m}{m''(k)}-1\right]\frac{\lambda}{3(E^1+Eg)+2\lambda}\right] \qquad 4.2$$

where λ = spin orbit splitting

Eg = band gap energy

E' = energy of electrons

k = wave vector

m* = effective mass of electron

m = electron free mass.

This leads to the equation giving the dependence of the g factor on the electron density

$$g = 2\left[1-\left[\frac{m}{m^*} -1\right]\frac{\lambda}{3(E_f+Eg)+2\lambda}\right] \qquad 4.3$$

where E_F is the Fermi energy.

which may then be approximated to

$$|g| = 2m/m^*\left(\frac{\lambda}{3(Eg+E_f)+2\lambda}\right) \qquad 4.4$$

The values of E g and λ were taken to be 0.235 ev, (in agreement with Zwerdling[62] etal), and 0.9ev, (from Pidgeon and[63] Brown), respectively. Evaluation of g at the bottom of the conduction band reduces the expression in equations 4.2 and 4.3 to that given by Roth[58] etal

ie. $$g = 2\left[1-\left[\frac{m}{m^*} -1\right]\frac{\lambda}{3Eg+2\lambda}\right] \qquad 4.5$$

Values of the effective mass and Fermi energy are given by Zawadzki and Szymanska[64] who derived analytical equations describing the variation of both parameters with electron concentration in the extreme degenerate limit. The effective mass is given by

$$m_0^* = m^*\sqrt{\Delta_0} \qquad 4.6$$

$$E_F = \tfrac{1}{2}Eg(\sqrt{\Delta_0} - 1) \qquad 4.7$$

where m^*_0 is the electron effective mass at the bottom of the conduction band having the value 0.0139m and

$$\Delta_0 = 1+2\pi^2(3/\pi)^{2/3}(\hbar^2/em^*Eg))n^{2/3} \qquad 4.8$$

n being the electron density.

The equation given by Zawadzki[61] for the g factor dependence does not take into account the influence of the conduction band anisotropy. Detailed calculations[65, 66] have indicated the existence of an anisotropy in the conduction band g-value due to higher band interactions near $k_z=0$. This anisotropy was shown to be directly proportional to the magnetic field B and $(p+\tfrac{1}{2})$. The maximum variation in g is predicted to occur when the applied magnetic field is rotated from the (100) to the (111) crystallographic direction with the g-value being smallest for B parallel to the (111) direction. The magnitude of the maximum anisotropy was predicted to be about 3% in g within the first Landau level for a magnetic field of 10 Tesla and approximately 10% for the p=1 level, also at 10 Tesla. The calculations were shown to be valid for electron concentrations less than $10^{17}cm^{-3}$. The maximum fractional anisotropy is given by the expression

$$\frac{4\gamma_0}{3g}(eB/\hbar)(p+\tfrac{1}{2}-k^2_H)$$

where $$\gamma_0 = \frac{4\hbar^2|P|^2|Q|^2}{m^3E^2_gE'_g}$$

In this expression P is the conduction - valence band momentum matrix element; Q is the valence band - higher band momentum matrix element; Eg and E'g are the conduction - valence band and conduction - higher

band energy separations, respectively; g is the conduction band - edge g value and k_H is the component of the wave vector along the magnetic field divided by $(eB/\hbar)^{\frac{1}{2}}$.

Combined resonance measurements[67,68] involving both a change in the Landau (p) and spin (S) quantum numbers, ($\Delta p=1$ and $\Delta S = -1$) verified the theoretical predictions of Ogg[65] and Pidgeon[66] etal. Estimates of the expected maximum anisotropy in this work were made from the observed magnetic field positions of the $1^{\pm}$ maxima and the linear magnetic field dependence of the anisotropy. Percentage maximum changes (ie. on rotating from (100) to (111)) were calculated to be of the order of 2-4% which was within the experimental error of 5%. Hence it was not expected that the anisotropy would be observed and that the Zawadzki formula would be sufficient to describe the g-factor dependence. This is supported by the work of Gluzman etal. The magnetic field dependence of the g-factor, including band warping was calculated for n-type InSb by Pidgeon etal.[66] Gluzman etal[52] used the relation.

$$(3\pi^2 n)^{\frac{2}{3}} = (p+\tfrac{1}{2})eB/\hbar$$

to calculate g(n) from g(B) and found excellent agreement with the results obtained using the 3-band model of Zawadzki, this indicating that the influence of the higher bands on the g value is small.

Experimental values of the effective g value may be determined by the measurement of the magnitude of the spin-splitting of the magnetoresistance maxima. The energy of a free electron in a magnetic field, B, is given by (chapter 1)

$$\epsilon = (p+\tfrac{1}{2})\hbar\omega + \frac{\hbar^2 K_z^2}{2m^*} \pm \tfrac{1}{2} g \mu_B B. \qquad 4.10$$

ω = cyclotron frequency = eB/m^*

μ_B = Bohr magneton = $e\hbar/2m$

which may be rewritten as

$$E_f = (p+\tfrac{1}{2}\pm\tfrac{1}{2}\nu)\hbar\omega \qquad 4.11$$

where $\nu = \tfrac{1}{2}gm^*/m$ 4.11a

rearranging this gives

$$1/B_p^{\pm} = (p+\tfrac{1}{2}\pm\tfrac{1}{2}\nu)\Delta(1/B) \qquad 4.12$$

$B_p^{\pm}$ = magnetic field position of spin split maxima.

The g value may then be obtained from the equation

$$\nu = 1/\Delta(1/B)\left[\frac{1}{B_p^+} - \frac{1}{B_p^-}\right] \qquad 4.13$$

These equations essentially assume that $E_F(B_p^+) = E_F(B_p^-) = E_F(0)$ where $E_F(0)$ is the value of the Fermi energy in zero magnetic field and also that the period of the oscillations is independent of magnetic field. Both of these assumptions are false at high fields, where the Fermi energy increases with increasing magnetic field and the periodicity is destroyed both by this, and the changing of the phase factor ϕ (equation 4.1). This numerical phase factor may be included in equation 4.13 in the form

$$p = \frac{1}{B_p^{\pm}}\frac{1}{\Delta(1/B)} - \phi + \tfrac{1}{2}\nu - \tfrac{1}{2} \qquad 4.14$$

$$= \frac{1}{B_p} \frac{1}{\Delta(1/B)} - \phi - \tfrac{1}{2}\nu - \tfrac{1}{2} \qquad 4.15$$

The subtraction of the two equations 4.14 and 4.15 again gives equaton 4.13. This shows that the evaluation of the Lande g factor by measurement of spin-splitting is intrinsically more accurate since to first order it does not require any knowledge of the phase factor ϕ. Unfortunately, as previously mentioned, measurement of the spin-splitting is only possible at high magnetic fields since only low order ($1^{\pm}$) doublets are resolved, meaning that inaccuracies due to the changing of the Fermi energy and phase factor, (which affect the periodicity), are present in any derived g value.

The spin-splitting of the $1^{\pm}$ doublet in the transverse magnetoresistance was measured for all samples except that having the lowest carrier concentration (sample H). All values were derived from double differentiated data, where the time constants ranged from 5 seconds to ½ second, depending on sample carrier concentration and sweep rate. Resolution of the $1^{\pm}$ doublet for sample H required a time constant of less than ½ second. This greatly reduced the signal to noise ratio, making determination of the turning points of $1^{\pm}$ maxima very difficult and consequently no values of the spin-splitting were taken for this sample. The spin-splitting factor ν was calculated using the expression given in equation 4.13 with the Lande g factor subsequently obtained through equation 4.11a. The effective mass and Fermi energy used in equations 4.13 and 4.11a were evaluated from the Zawadski and Szmanska expressions (equations 4.6 to 4.8). Percentage errors in the value of ν (and hence g) were computed from the error in the magnetic field positions of the maxima ($\sim$1-2%), and the error in the period of the oscillations ($\sim$2-3%), giving a final value of $\sim$5%. The g factors expected for Indium Antimonide at the relevant carrier concentrations were obtained with the use of equations

4.2 to 4.8. It should be noted that the value of E_F inserted in equation 4.2 does not reflect the magnetic field dependence of the Fermi energy and is therefore not strictly accurate. However it was estimated that since the Fermi energy was only approximately 3% of the total denominator at most, (equation 4.2), the effect of this dependence on the final expected value of g was insignificant.

Measurements were taken on the samples both before, and after annealing. The results are tabulated in tables 4.1 and 4.2 along with calculated effective mass values and theoretical values of ν and g. The information is also represented graphically in figure 4.3. The g values obtained on unannealed samples fell below the expected values calculated from the three-band model of Zawadzki. Subsequent heat treatment to 350° produced an increase in the spin-splitting which brought the experimental g values into close agreement, (within experimental error), with the theoretical values. This proved to be true for all, except one, sample (sample D). It is worth comparing these results with Gurevich and Efros[49] who derived a rather involved formula giving the positions of the $1\pm$ maxima, taking into account the dependence of the Fermi energy on magnetic field.

$$(B^-/B^+)^{3/2} = \frac{1+\sqrt{\nu}+\sqrt{(1+\nu)}}{1+\sqrt{(1+\nu)}} \qquad 4.16$$

Substituting into this expression the theoretical value of g obtained from the Zawadzki formula, and the theoretical values of the effective mass yielded values of B^-/B^+ equal to 0.75 for a g value of 44 and 0.756 for a g value of 40. Comparing these two values to the experimental values of 0.77 and 0.75 respectively, it is seen that fairly good agreement existed between the experimental results and the Gurevich and Efros theory.

SAMPLE	n $x10^{16}cm^{-3}$	m^*/m	lgl (THEORY)	lgl (EXPERIMENT)
G	0.76		47.4	42.
F	1.47	0.0156	45.2	40.2
E	1.99	0.016	44	40.4
D	2.72	0.0164	42.7	47.0
C	3.60	0.0169	41.2	35.6
B	4.10	0.0172	40.5	37.0
A	4.60	0.0174	40	38.0

TABLE 4.1 (-g factors obtained before annealing).

SAMPLE	n x10^{16} cm^{-3}	m*/m	lgl (THEORY)	lgl(EXPERIMENT)
G	1.06	0.0153	46.3	45.0
F	1.79	0.0158	44.6	43.7
E	2.38	0.0162	43.2	45.6
D	3.55	0.0169	41.26	45.0
C	4.67	0.0174	39.8	38.8
B	4.90	0.0175	39.6	40.9
A	5.60	0.0178	38.8	38.1

TABLE 4.2 (-g factors after annealing).

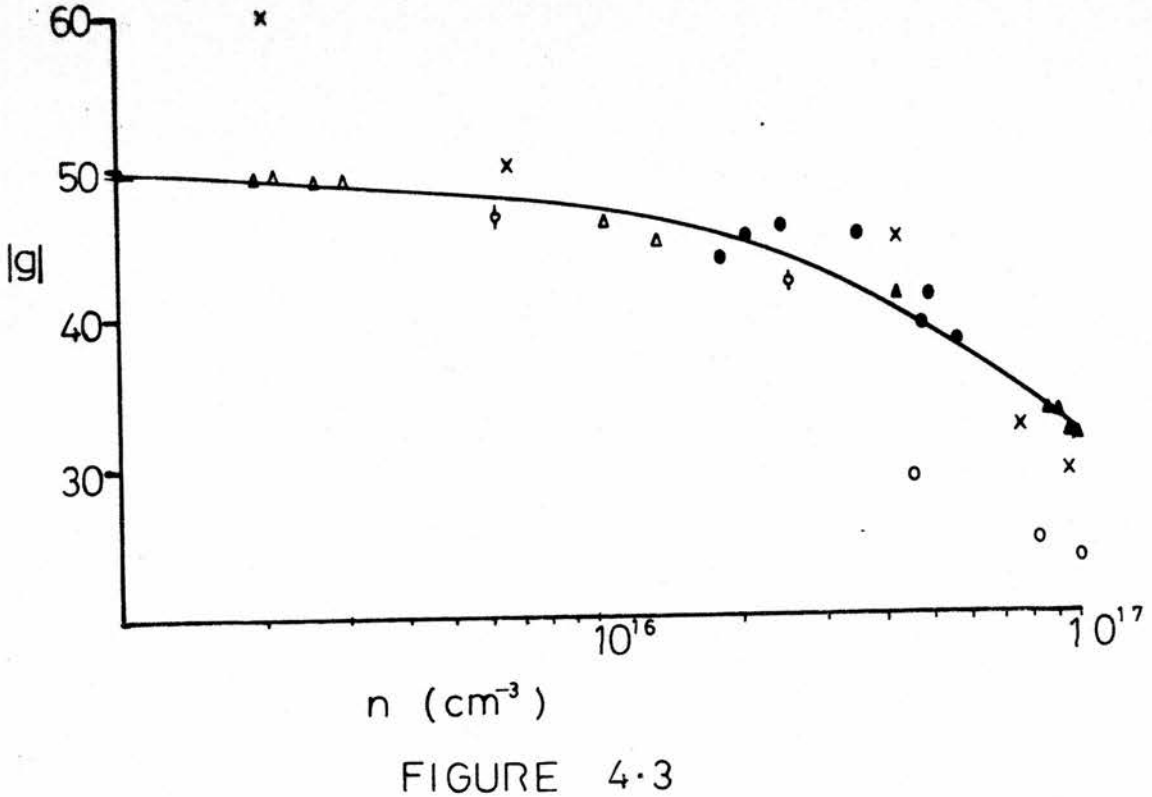

FIGURE 4·3

- △ SPIN RESONANCE
- ▲ COMBINED RESONANCE
- ◇ UNSPLIT SHUBNIKOV-DE-HASS DATA
- o SEPARATION OF $1^{\pm}$ DOUBLET
- ● THIS WORK
- x POSITION OF 0^{-} MAXIMUM

g-FACTOR AS A FUNCTION OF FREE CARRIER DENSITY

The above experimental findings indicate that the three-band approximation well describes the variation of g with sample carrier concentration. This is in agreement with other spin-splitting[57] measurements, spin resonance[69-71] data, combined resonance[68] data, and with the results obtained from the direct curve fitting of the unsplit magneto-conductivity maxima to theory.[54] In addition, it is also indicated that the determination of the spin-splitting from well resolved 1± maxima and the use of equation 4.13 leads to accurate experimental values of g. This in turn suggests that the corrections to the magnetic field positions of the 1± maxima arising from the field dependence of the Fermi energy and phase factor ϕ, are small and within experimental error. This was also postulated by Antcliffe and Stradling[51] who found that values of the spin-splitting factor ν ($=\frac{1}{2}gm^*/m$) derived from both the 1± and 2± doublets were not significantly different. The findings of this work were at variance with the results of Gluzman[52] etal who calculated g from equation 4.16 and the spin splitting of the 1± doublet in samples having carrier concentrations between $1\times10^{16}cm^{-3}$ and $5\times10^{18}cm^{-3}$. They found that the experimentally deduced values of g were always 20-30% smaller than the theoretical values. They noted that all the samples were characterised by Dingle temperatures greater than $8^{o}K$ and concluded that in cases when the Dingle temperature, T_D, is greater than the sample temperature, T, the determination of the Lande g factor from the Shubnikov-de Haas oscillations becomes unreliable. Computer calculations of the oscillation profiles showed that an increase in T_D brings closer the 1^+ and 1^- peaks and the authors estimated that an increase in T_D from $1^{o}K$ to $8^{o}K$ results in the g factor being reduced by a factor of approximately 12%. The latter observation was, in part, supported by this work. Annealing studies (chapter 3) have shown that heat treatment reduced the radiation damage, (and hence the density of scattering centres and electron traps), thus producing an increase in the carrier mobility with a corresponding

decrease in T_D. Examination of figure 4.3 and/or tables 4.2/4.2 shows that unannealed samples (which had a lower mobility) gave values of g smaller than those obtained on the same sample after heat treatment. The increase seen in g after annealing may also be due to two other factors. Increased resolution of the spin-split peaks in the $1^{\pm}$ doublet or annealing away of paramagnetic centres caused by radiation damage (chapter 3, section 3.2). The production of these centres and their subsequent disappearance after heat treatment was postulated by Clark and Isaacson who observed a pronounced increase in the nuclear spin-lattice relaxation rate in In(115), Sb(121) caused by neutron doping.

Increased resolution is the least likely explanation for the observed change, since for most samples it was possible to completely resolve the $1^{\pm}$ doublet by double differentiation both before and after annealing. The simple picture $T_D \propto (\text{mobility})^{-1}$ is not entirely accurate, especially as a level is about to empty and resonant scattering occurs, hence it is not possible to state, with confidence, that the increased mobility is solely responsible for the increase in the g-values. In this case, the change is probably due to a combination of a decrease in the density of paramagnetic centres and an increase in the mobility.

Until now, apart from the direct curve fitting of magnetoresistance data to theory which is rather involved, the determination of the Lande g factor from Shubnikov-de Haas experiments on samples having moderate carrier concentrations, (5×10^{15} to $5\times10^{16}cm^{-3}$), has resulted in large experimental errors. This is because the doublets having a Landau index of greater than 1 show no signs of spin-splitting and the $1^{\pm}$ doublet is incompletely resolved, meaning that determination of the field positions of the $1^{\pm}$ maxima is difficult and inaccurate. Attempts

to determine g from the position of the 0^- maximum have yielded values which were much different from those predicted by theory. Again this was due to the inaccuracy of the method where the source of error lay in the various shifts away from resonance suffered by the 0^- maximum.

This work has achieved, by the method of double differentiation, the accurate (to within 1-2%) measurement of the magnetic field positions of the $1^\pm$ maxima in samples with moderate carrier concentrations, and hence has led to more accurate values of g. It is a technique which has the potential of allowing measurement of the spin-splitting in the higher order doublets, ($2^\pm$ and even $3^\pm$), which eliminates any possible error arising from the magnetic field dependence of the Fermi energy or phase factor ϕ. (The resolution of the $2^\pm$ doublet has been attained in this work in the longitudinal and intermediate orientations although, unfortunately, not in the transverse configuration from which the g factor is traditionally determined.) The technique may be applied to high carrier concentration samples to obtain the g factor from the higher order doublets, this being particularly useful since ESR measurements fail at high concentrations due to the broadening of the resonance. Conversely, it may also be applied to low electron density samples ($\sim 10^{15} cm^{-3}$) to derive the g value from the spin-splitting of the first doublet. It should be noted that Shubnikov-de Haas measurements do not give the sign of the g factor, only the magnitude. The convention adopted here was that B^- refers to the higher energy spin state ie. the peak falling at the lower magnetic field. This is because the material under study was n-type Indium Antimonide which has been shown by Roth et al[58] to have a negative g factor, meaning the electrons with spin in the direction of the magnetic field have a lower energy than those with spin directed against the field.

4.4 SPIN-SPLITTING CHARACTERISTICS OF InSb.

As was previously pointed out, there is still much controversy over the spin-splitting characteristics of ρ_{zz}. Measurements were carried out on eight samples (A-H) having carrier concentrations ranging from $\sim 5 \times 10^{15} cm^{-3}$ to $5 \times 10^{16} cm^{-3}$. Recordings of the magnetoresistance were taken for longitudinal, transverse and intermediate orientations. The effect of sample orientation on the oscillation profiles is illustrated in figure 4.4. In agreement with past workers, it was found that on rotation from a transverse to a longitudinal configuration the 0^- amplitude approached zero and the amplitudes of the higher field components (p^+) of the doublets were much reduced. The amplitude of the 0^- maximum showed itself to be very sensitive to the angular position of the sample with respect to magnetic field. At $\theta = 0^\circ$, ie. sample length, electric and magnetic fields all parallel, (longitudinal configuration), the 0^- peak was absent, with a displacement of 15°-20° from the longitudinal producing a profile where the 0^- peak was easily distinguishable, and a displacement of greater than 20° producing a profile where the 0^- peak was well resolved. In contrast to this the amplitude of the 1^+ peak was not found to vary significantly about the longitudinal configuration and not much change was observable between $\theta = 0^\circ$ and $\theta = 15^\circ$. This proved to be true for all eight samples investigated, regardless of crystallographic orientation.

Some preliminary conclusions may be made at this point. The existence of the p^+ maxima in the ρ_{zz} doublets are not a consequence of contributions from ρ_{xx} resulting from poor orientation but are genuine artefacts of the longitudinal magnetoresistance. This may be concluded from the behaviour of the p^+ amplitudes on rotation about the longitudinal configuration. If the p^+ peaks observed in ρ_{zz} arose from poor orientation then it would be expected than on an increase in displacement to 15° from the longitudinal the amplitudes of the p^+ maxima in the

ORIENTATION DEPENDENCE OF THE OSCILLATION PROFILES

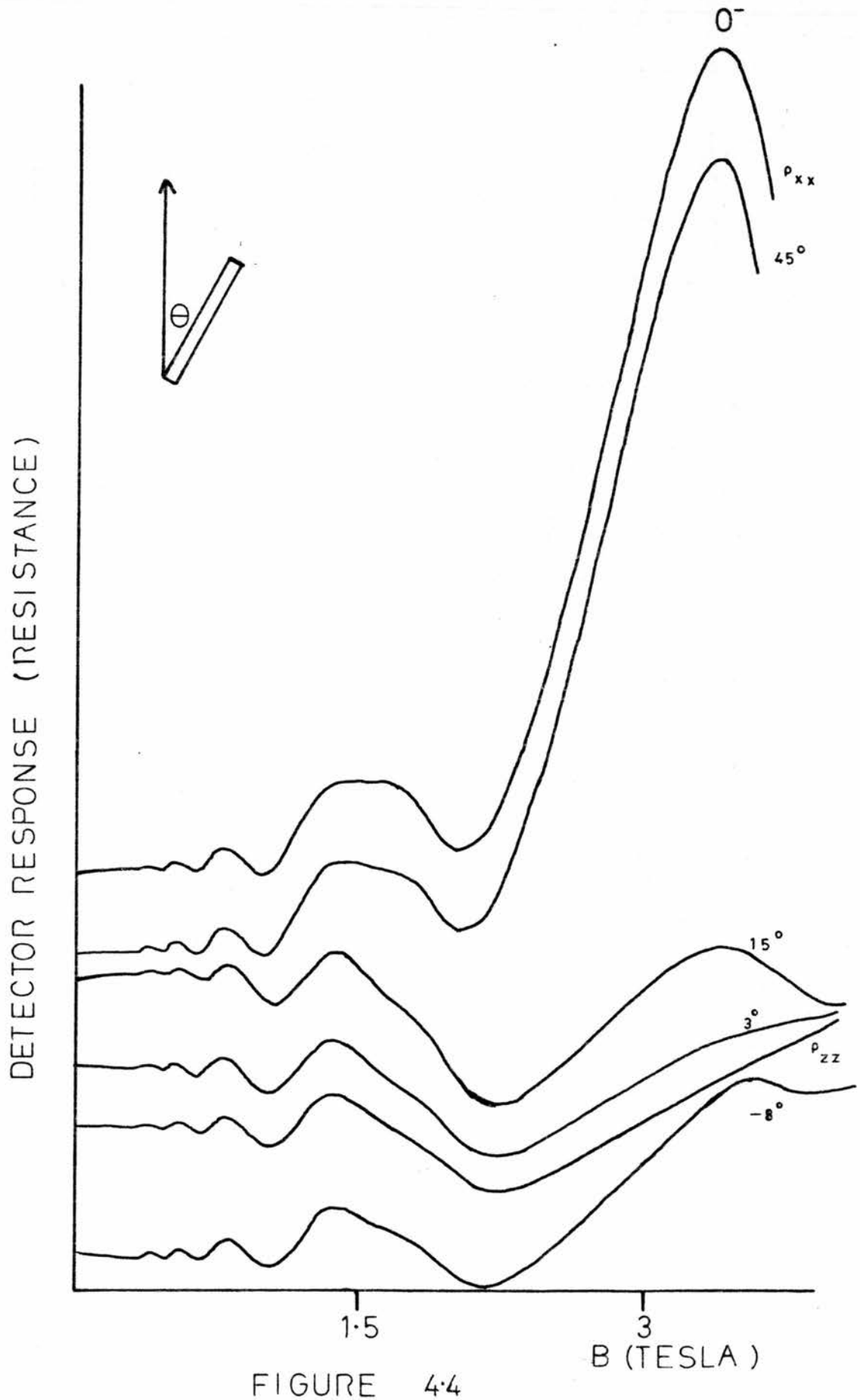

FIGURE 4·4

doublets would have increased markedly. 'This was not found to be the' case. Secondly, in contrast to the results of Bliek etal it was concluded that the existence of the p^+ maxima was not a consequence of bad sample geometry or surface effects due to contacting. The samples used in this investigation were long and narrow (1cmx2mm), the current contacts covered the ends of the samples to encourage parallel current paths and the potential probes were fabricated from Silver epoxy which minimised the interference with the sample surface.

Double differentiation of the data allowed a more complete analysis of the results and revealed some interesting facts. In the unannealed samples comparison of the magnitude of the spin-splitting in ρ_{xx} and ρ_{zz} showed that the spin-splitting of the $1^{\pm}$ doublet was greater by approximately 20-30% in ρ_{zz}, and that this was solely due to the shift of the 1^+ maximum in the direction of higher magnetic fields. This is similar to the Gluzman[52] results who found a 40-50% increase in the spin-splitting factor, ν. The discrepancy in the magnitude of the shifting may be due to the fact that the measurement of the turning point of the 1^+ maximum was more accurate with the use of the double differentiation technique. For two samples (A and B) it was also possible to measure ν from the $2^{\pm}$ doublet in ρ_{zz}. The results are presented in table 4.3 and suggest that the increased spin-splitting is true for all doublets in ρ_{zz}, which tends to discount any argument that the shifting is a high magnetic field phenomenon. At an angular displacement of approximately 10° either side of longitudinal it was found that the spin-splitting was the same as for the longitudinal with a noticeable difference occurring at around 15°, when the 1^+ and 1^- peaks started moving closer together. Similarly it was found that to within approximately ± 10 degrees of the transverse orientation the magnitude of the splitting remained unchanged and equal to the value obtained from ρ_{xx}. This shows that in the measurement of g from

SAMPLE	n $\times 10^{16} cm^{-3}$	$\nu 1^{\pm}$(long.)	$\nu 2^{\pm}$(long.)	$\nu 1^{\pm}$(trans.)
F	1.47	0.379	-	0.313
E	1.99	0.347	-	0.326
D	2.72	0.346	-	-
C	3.61	0.365	-	0.301
B	4.1	0.418	0.409	0.318
A	4.6	0 .410	0.392	0.331

TABLE 4.3 (-spin-splitting from ρ_{zz} and ρ_{xx} before annealing.)

ρ_{xx} the alignment of the sample is not absolutely crucial for obtaining accurate g values.

On performing identical experiments on the same sample after heat treatment, the spin-splitting characteristics were found to be different. Although the behaviour of the amplitudes was similar, it was found that, unlike the characteristics of the samples before annealing the 1^- maxima were shifted in addition to the 1^+ maxima. Measurements of ν and g in both orientations (table 4.4) revealed that, after heat treatment, the Lande g factor was independent of sample orientation and was in good agreement with the values predicted by the three-band Zawadzki model. Again measurements of g from the $2^{\pm}$ doublets proved to give values which were in agreement, (within experimental error), with the values deduced from the $1^{\pm}$ doublets. It was impossible to observe any orientation dependent shifting which may have been present in the higher order maxima (ie. ($p>1$). This was because the experimental error in the peak positions at these fields is 6%, a value greater than the magnitude of the shifting observed for the $1^{\pm}$ maxima.

By the technique of double differentiation it was possible to show the existence of the 0^- maximum in data, (close to, or actually on the longitudinal position), where it was not at all obvious in the undifferentiated recordings (figure 4.5) Measurement of the 0^- maximum field position as a function of sample orientation gave the results illustrated in table 4.5 and may be summarised as follows. Before annealing the peak position in all orientations was the same, (within experimental error), whereas, after annealing, the magnetic field position of the 0^- maximum was found to be higher in the longitudinal configuration. Expressing the shifts in the form

SAMPLE	n $x10^{+16}cm^{-3}$	$\nu 1\pm$(long.)	$\nu 1\pm$(trans.)	ν(THEORY)
F	1.79	0.340	0.345	0.352
E	2.38	0.362	0.369	0.350
D	3.55	0.372	0.380	0.348
C	4.67	0.340	0.337	0.346
B	4.90	0.346	0.358	0.346
A	5.60	0.358	0.339	0.345

TABLE 4.4 (-spin-splitting from ρ_{zz} and ρ_{xx} after annealing.)

LONGITUDINAL MAGNETORESISTANCE PROFILE AND ITS DOUBLE DERIVATIVE

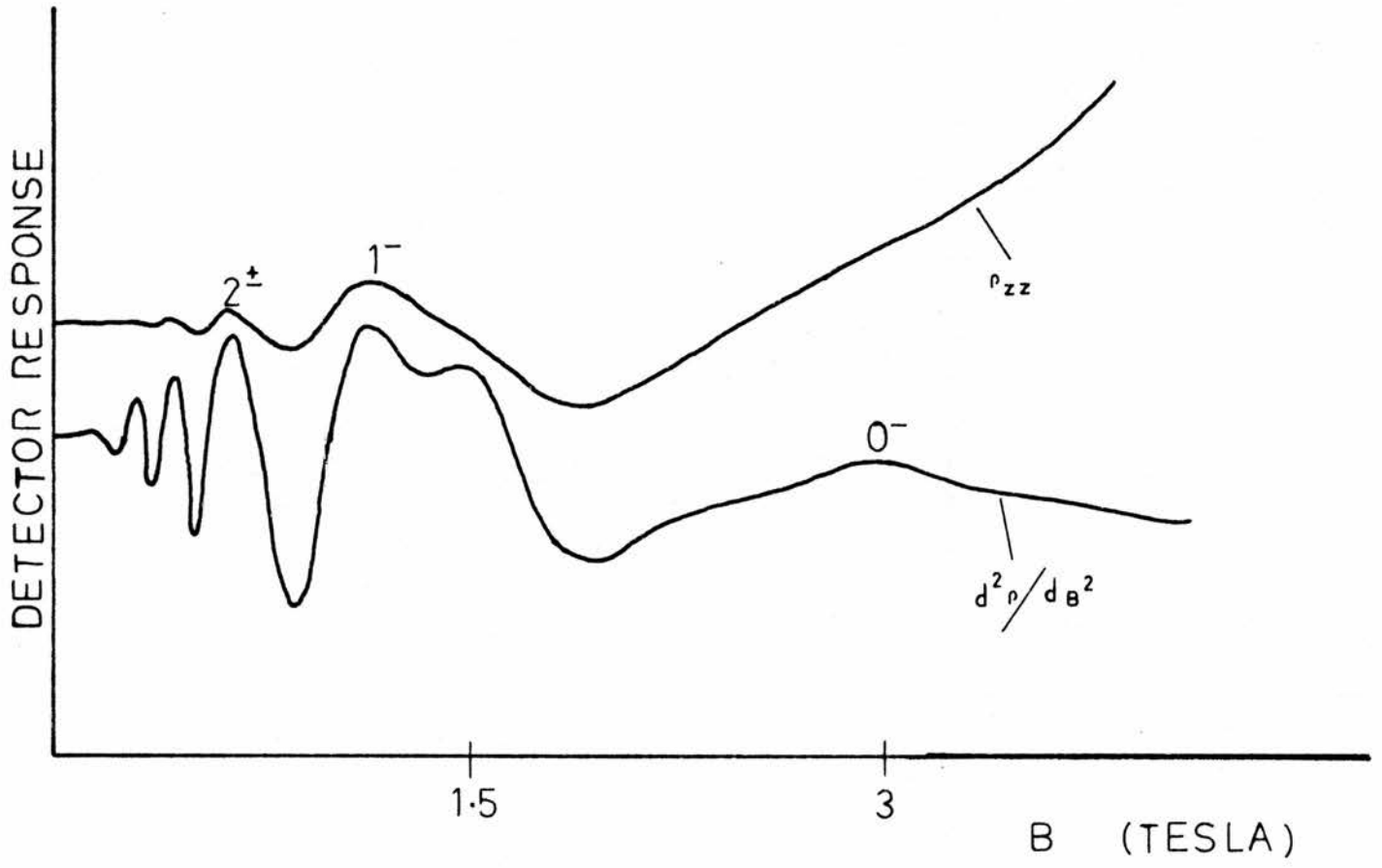

FIGURE 4·5

SAMPLE	$\phi_T - \phi_L$
G	0.015
F	0.027
E	0.021
D	0.024
C	0.033
B	0.019
A	0.023

TABLE 4.5

$$(1/B_T - 1/B_L)\left(\Delta(1/B)\right)^{-1} \qquad 4.17$$

where B_T and B_L represent the magnetic field positions of the 0^- peak in ρ_{xx} and ρ_{zz}, respectively

By the use of equations 4.14 to 4.16 it follows

$$(1/B_T - 1/B_L)\left(\Delta(1/B)\right)^{-1} = \phi_T - \phi_L \qquad 4.18$$

where ϕ_T = phase factor in ρ_{xx}

and ϕ_L = phase factor in ρ_{zz}

i.e. equation 4.17 gives the difference in phase between ρ_{xx} and ρ_{zz} Table 4.5 gives the values of $\phi_T - \phi_L$ for seven samples, where it can be seen that the values lay between 0.015 and 0.033. There was no observed correlation between carrier concentration and the phase difference.

As was previously mentioned, several attempts have been made to explain the spin-splitting behaviour of InSb. Gluzman[52] etal performed computer calculations to determine the oscillation profiles of ρ_{xx} and ρ_{zz} based on the equations from the review of Roth and Argyres[72].

$$\rho_{zz}/\rho_o = 1+\sum_{r=1}^{\infty} b_r \cos(2\pi rF/B - \pi/4) \qquad 4.19$$

$$\rho_{xx}/\rho_o = 1+5/2\sum_{r=1}^{\infty} b_r \cos(2\pi rF/B - \pi/4) + R \qquad 4.20$$

where

$$b_r=(-1)^r (r/2FB)^{1/2} \frac{\beta Tm'\cos(\pi\nu r)}{\sinh(r\beta Tm'/B)} \exp -(r\beta T_D m'/B)$$

$$R = 3/4(B/2F)\left[\sum_{r=1}^{\infty} b_r [A_r \cos(2\pi rF/B) + C_r \sin(2\pi rF/B)]\right.$$

$$\left. -\ln(1-\exp(-\beta T_D m'/B))\right.$$

$$A_r = 2r^{\frac{1}{2}} \sum_{s=1}^{\infty} [s(r+s)]^{-\frac{1}{2}} \exp-(2\beta T_D m's/B)$$

$$C_r = r^{\frac{1}{2}} \sum_{s=1}^{r-1} (s(r-s))^{-\frac{1}{2}}$$

$$\beta = 2\pi^2 km/\hbar e$$

$$F = E_F m^*/\hbar e$$

$$m' = m^*/m$$

The sum on the RHS of equation 4.20 represents the contributions made to ρ_{xx} by transitions involving change in quantum number p and the quantity R describes the contribution to ρ_{xx} from transitions inside one Landau sub-band. The authors tried, through the computer calculations, to explain the smaller amplitude of the 1^+ maximum by postulating that the effect was merely due to a combination of certain values of parameters appearing in the theoretical equations 4.19 and 4.20. Substituting in values of F=6.75, m^1=0.019 (both of which correspond to a carrier concentration of $1x10^{17}cm^{-3}$), and values of T=4.2°K, with T_D = 1, 8, or 20°K, they found that for a Dingle temperature >1°K, the higher field peak in the ρ_{zz} $1^{\pm}$ doublet was smaller than the lower field peak, whereas for ρ_{xx} which has the additional term R, the 1^+ peak was found to be greater than the 1^+ peak for T_D up to ~8°K. The calculations also revealed that for a Dingle temperature approaching 20°K the influence of R was small and qualitative difference betwen ρ_{xx} and ρ_{zz} disappeared. Basing their argument on the above findings they concluded that the very much smaller 1^+ amplitude observed in ρ_{zz} was a consequence of the Dingle temperature being greater than 1°K and the reason for the difference

in ρ_{xx} was the term R which helped to increase the amplitude of the 1^+ peak. There are several points to be made about these conclusions. Firstly, although the computer profiles predicted a smaller 1^+ peak, the difference in magnitude between the 1^- and 1^+ peaks was not great, whereas experimentally the amplitude of the 1^- maximum greatly exceeded that of the 1^+ maximum. Secondly, although R does increase ρ_{xx} in comparison to ρ_{zz} it does not have such a strong magnetic field dependence that it would have a much greater effect on the 1^+ than the 1^- peak, as would have to be the case if the qualitative difference between ρ_{xx} and ρ_{zz} was solely due to the presence of R in ρ_{xx}. Thirdly, an experimental curve was obtained by the authors which was estimated to have a Dingle temperature of nearly $20^{\circ}K$. As pointed out above, the prediction from the theoretical profiles was that no qualitative difference should exist between ρ_{xx} and ρ_{zz} at this T_D. The experimental curve was not in agreement with this, but rather exhibited the familiar behaviour of the 1^+ maximum in having a much smaller amplitude than the 1^- maximum. Fourthly, this argument could only be valid at high magnetic fields where R makes a significant contribution to ρ_{xx}. It would therefore be expected that for the higher order doublets, (p>1), the ρ_{xx} and ρ_{zz} profiles would be the same, except for the absolute amplitude which is different due to the factor 5/2 appearing in front of the sum in equation 4.20. This is borne out by the computer profiles. Careful examination of the experimental curves, both in this work, and those obtained on sample 6 by Gluzman etal, reveals that the shapes of the higher order doublets (which are not resolved), differ between ρ_{xx} and ρ_{zz}, with ρ_{zz} doublets appearing much sharper than ρ_{xx} doublets (figure 4.6). This may be attributed to the larger amplitude of the p^+ peaks in the doublets 'broadening' out the maximum. The final point to be made, is that although this theory attempts to explain the smaller amplitude of the

1^+ peak it does not offer any suggestion as to why the peak falls at a higher magnetic field than its ρ_{xx} counterpart.

The same authors adopted a similar approach to account for the apparent complete absence of the higher field peaks from the ρ_{zz} doublets in such materials as HgCdTe. By investigating the dependence of the oscillation profile on the spin-splitting parameter ν they produced some very interesting magnetoresistance curves. For a value of $\nu=0.25$ and $T_D = 4^oK$ they found that the spin-splitting in both ρ_{xx} and ρ_{zz} disappeared, whereas, for the same value of ν and a T_D of 1^oK spin-splitting was present. The difference was attributed to the fact at 1^oK the contribution from the higher harmonics (which are responsible for spin-splitting) is significant, even although the second, and other even harmonics for which r/2 is odd, are missing, whereas for $T_D=4^oK$ the contribution from the higher harmonics is negligible and hence the spin-splitting is absent. They extended this to explain the absence of spin-splitting ρ_{zz} by predicting that for ν close to 0.25 the maxima of ρ_{zz} may not be split whereas those of ρ_{xx} should be split, with the factor R again being responsible for the difference. The final conclusion reached by the authors was that in all cases, absence of spin-splitting was a consequence of the disappearance of the second harmonic in the sum 4.19.

Again some points have to be made about the above findings and conclusions. Firstly assuming that for the said value of ν and T_D the spin-splitting in ρ_{zz} did disappear, then this would be because there were not enough higher harmonics present to sharpen up the $1^\pm$ peaks sufficiently to produce splitting, and hence the doublet would appear as a broad maximum. This means that the turning point would fall at a magnetic field which was approximately half-way between the positions of the $1^\pm$ maxima. However all workers have observed experimentally that the ρ_{zz} peak is sharp and falls at the lower-field-maximum position,

leading them to the conclusion that the spin-splitting was not necessarily absent but that the higher-field-maximum was.

Computer calculations carried out during the course of this work and based on the same equations 4.19 and 4.20 were found, in part to agree with the results of Gluzman et al. The values of parameters chosen were based on a sample of n-type InSb having a carrier concentration of $10^{17}cm^{-3}$, this giving the values

$F = 6.75$

$m' = 0.019$

$\nu = 0.33$

The value of temperature was $4.2^{o}K$ with the Dingle temperature being varied between $15^{o}K$ and $25^{o}K$. Figure 4.6 shows the profiles obtained for the transverse magnetoresistance. The Dingle temperature dependence of the profiles was found to be similar to the Gluzman results, i.e. the higher the value of Dingle temperature, the less clear are the oscillations, the smaller are their amplitudes and the less well resolved are the doublets. However it proved impossible to reproduce the Gluzman results for a spin-splitting value of o.25.

The exact parameters quoted by Gluzman were substituted into two independently written programs[73] which were run on two different computer systems. Both of these produced identical results (figure 4.7) and both were at variance with the Gluzman profiles. They showed no evidence of the disappearance of spin-splitting for $\nu = 0.25$ and $T_D = 4^{o}K$, and in fact very little difference in the profiles was observed between $\nu=0.27$ and 0.25 ($T_D=4^{o}K$), this being in complete contrast to the striking difference found by Gluzman et al (figure 4.8)

THE INFLUENCE OF DINGLE TEMPERATURE ON THE OSCILLATION PROFILES
-A COMPUTER SIMULATION

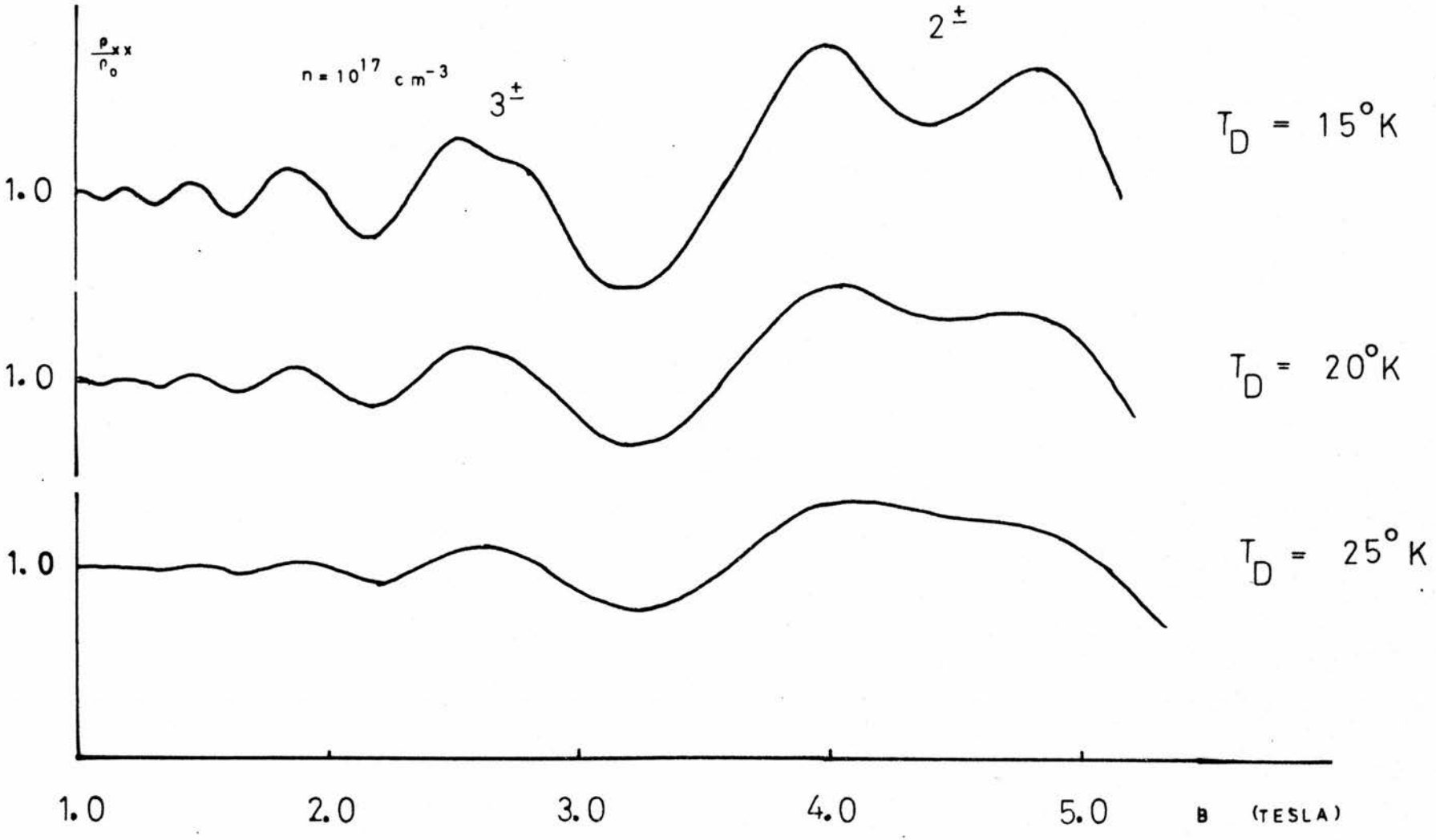

FIGURE 4·6

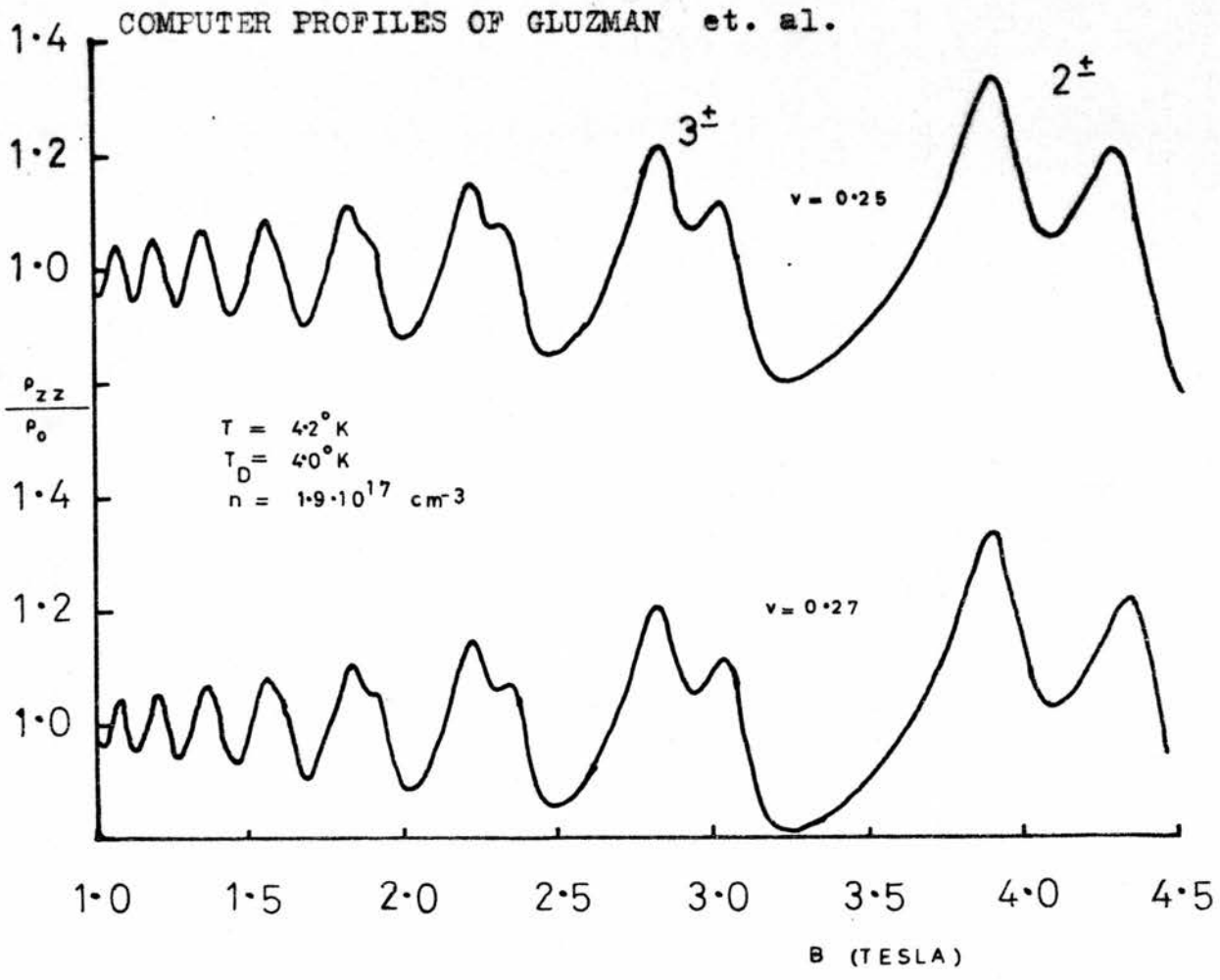

FIGURE 4·7

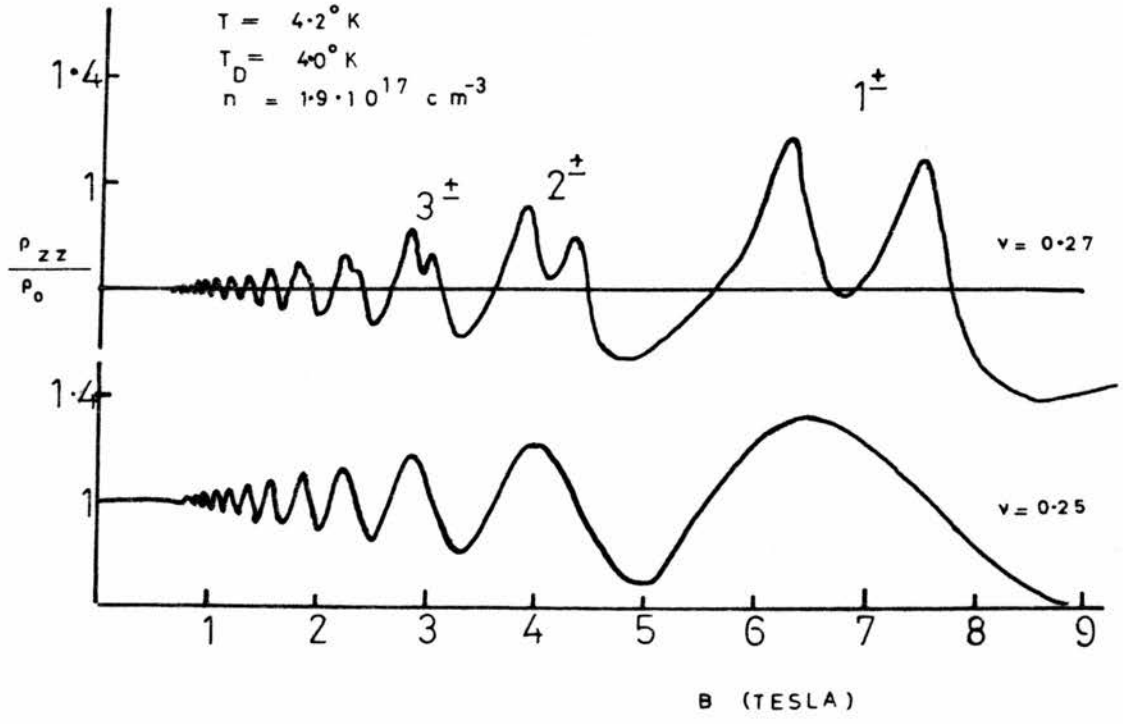

FIGURE 4·8

There still remains the two other previously mentioned theories:-

The selection rules produced by Narita and Suiza[10] are founded on a theory which has some basic and important mistakes[74] such as a divergent expression for part of the conductivity, and several equations representing the same quantity but having different units. The remaining explanation of differing scattering rates for spin-up and spin-down electrons to account for the much smaller p^+ amplitude seems to be the most probable. A reason for differing scattering rates has been suggested by Stradling[75] and is based on the angular dependence of ionised impurity scattering, (small angle events predominate in ionised impurity scattering). This may be understood qualitatively by examining figure 4.9 and the following equations, where it can be seen that the angle scattered through depends upon the particular transition (+ or -) being considered, ie electrons scattered from the $(p-1)^+$ level to the p^+ level as it is about to empty are scattered through a larger angle than the electrons going from the $(p-1)^-$ to p^- as the p^- level is about to empty.

$$E_F = \epsilon_{p\pm} + \epsilon_z \qquad 4.21$$

$$= \hbar\omega(p+\tfrac{1}{2}\pm\tfrac{1}{2}\nu) + \hbar^2 k_z^2/2m^* \qquad 4.22$$

$$= \hbar^2 k_{p\pm}^2/2m^* + \hbar^2 k_z^2/2m^* \qquad 4.23$$

where

E_F = Fermi energy.

ϵ_z = energy in direction of magnetic field (z-direction) = $\hbar^2 k_z^2/2m^*$

$\epsilon_{p\pm}$ = energy in plane perpendicular to magnetic field (x-y plane)

In dimensionless units (i.e. dividing throughout by $\hbar\omega$)

$$R_0^2 = R_{p\pm}^2 + R_z^2 = (p+\tfrac{1}{2}\pm\tfrac{1}{2}\nu) + R_z^2 \qquad 4.24$$

where the variables R_0 and R_z are shown in figure 4.9

For the p^{th} level emptying $R_0^2 = (p+\tfrac{1}{2}\pm\tfrac{1}{2}\nu)$ and the energy of the $(p-1)^{th}$ level is given by

$$((p-1+\tfrac{1}{2}\pm\tfrac{1}{2}\nu) + R_z^2 = R_0^2 \qquad 4.25$$

which on subtraction, (and considering levels having the same spin), gives

$$R_z^2 = 1 \qquad 4.26$$

Comparing the specific cases of the transitions $0^+ — 1^+$ and $0^- — 1^-$

$$0^+ — 1^+ : 3/2+\tfrac{1}{2}\nu = R_0^2 \text{ and } R_z^2 = 1$$

$$\Rightarrow R_z^2/R_0^2 = \tfrac{3}{4} \Rightarrow \delta = 30^0$$

since $\tfrac{1}{2}\nu = -1/6$ (the minus sign is due to the negative g-value)

$$0^- — 1^- : 3/2-\tfrac{1}{2}\nu = R_0^2 \text{ and } R_z^2 = 1$$

$$R_z^2/R_0^2 = 1/(3/2+1/6) = 3/5$$

$$\delta = 39.2^o$$

The above calculations show that the 0^- to 1^- transition is a smaller

angle and therefore more probable event than the 0^+ to 1^+ transition (where θ = angle scattered through = $(\pi/2 - \delta)$. This then could be a contributory factor to the much smaller amplitude of the 1^+ peak compared to the 1^- peak in ρ_{zz}. Applying the above to the higher order doublet p=3 gives

$$3^+ \; 2^+ : \; R_z^2/R_0^2 = 1/(7/2-1/6) = 3/10$$

$$\delta = 56.8^0$$

and $$3^- \; 2^- : R_z^2/R_0^2 = 1/(7/2+1/6) = 3/11$$

$$\delta = 58.5^\circ$$

Hence it can be seen that for p=3 the difference in scattering angle is only approximately 2°. This exhibits the general trend of the higher the quantum number p, the smaller is the difference in the scattering angle θ (figure 4.9). This in turn suggeststhat if the differing amplitudes of the $p^\pm$ peaks is solely due to the difference in the scattering angles then the difference in amplitudes should become less as p is increased unless the function describing the probability of scattering (as a function of θ) is much more rapidly varying at $\theta = (\pi/2-56)=34^\circ$ than at $\theta = (\pi/2-30)^\circ = 60^\circ$

The difference in the scattering angle between spin-up and spin-down electrons is also a function of the magnitude of the splitting, ν. On experimenting with Gray Tin, Booth and Ewald[12] found that for a value of $\nu/2=0.129$ (which corresponded to a carrier concentration of $7.6\times10^{18}cm^{-3}$) spin-splitting was completely absent in ρ_{zz} whereas for a value of $\nu/2=0.105$($n=2.5\times10^{18}cm^{-3}$) the higher field peak of the doublet appeared as a shoulder on the lower field peak. Applying the above to

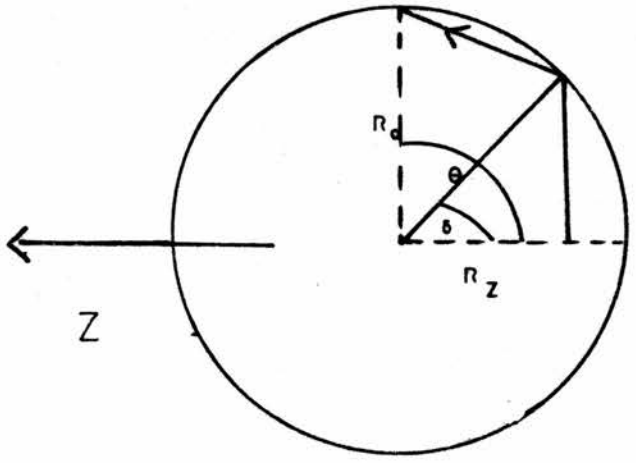

FIGURE 4·9

DIAGRAM RELATING SCATTERING ANGLE TO A PARTICULAR TRANSITION

the p=1± maxima for both values of ν/2 (and adopting the authors sign convention) we have

For $\nu/2 = 0.129$

$0^+ 1^+$: $R_z^2/R_0^2 = 1/(1.5+0.129) = \delta = 38.4^\circ$

$0^- 1^-$: $R_z^2/R_0^2 = 1/(1.5-0.129) = \delta = 31.3^\circ$

Hence for a value of ν=0.129, the difference in the scattering angles for spin-up and spin-down electrons is 7°. Similarly on substituting in a ν/2 value of 0.105 it is found that the difference in scattering angle is equal to 6°. This shows that the appearance of the higher field component of the doublets may not be attributed to a smaller difference in the scattering angle between the spin-up and spin-down electrons for ν/2=0.105 compared to the difference in angle for ν/2=0.129. In the case of the Booth and Ewald results the observation of the higher-field peak in the doublets at high carrier concentration is probably due to increased resolution of the doublets.

Although much attention has been focused on the spin-splitting characteristics of the Shubnikov-de Haas effect, no satisfactory model has yet been proposed to explain the much smaller amplitude of the higher-field maxima of the doublets in ρ_{zz} compared to the corresponding maxima on ρ_{xx}. The various shifting of the peaks observed on rotation from a transverse to a longitudinal configuration maybe explained within the framework of the existing theory. For convenience the findings of this work will now be restated. Before annealing the lower-field maxima of the 1± doublet fell at the same magnetic field in both ρ_{xx} and ρ_{zz}, in contrast to this the higher field maxima in the 1± doublet in ρ_{zz} occured at higher magnetic fields than the corresponding maximum in

ρ_{xx}. The magnitude of the spin-splitting in the transverse magnetoresistance was found to be less than the theoretical values (table 4.1) whereas the spin-splitting values, ν, obtained from the longitudinal data were in general found to be larger than the theoretical values (table 4.3). After annealing both the maxima in the $1^{\pm}$ doublets in ρ_{zz} fell at higher magnetic fields than the corresponding ρ_{xx} maxima, however it was found that the spin-splitting values obtained from both sets of data were in close agreement with each other and also with the theoretical values.

The results obtained with the annealed samples may simply be explained in terms of the phase factor ϕ (Chapter 4, section 4.4). It has been shown that the cosine term describing the scattering between Landau levels has a phase factor $\phi 1$ and that the term R describing scattering within one Landau level has a different phase factor associated with it. It follows that ρ_{xx} and ρ_{zz} which are represented by the cosine term +R and the cosine term alone, respectively, have different phase factors associated with them and this is manifested by equivalent peaks in ρ_{xx} and ρ_{zz} occurring at different magnetic fields. The observed behaviour of the unannealed samples i.e. the shifting of the 1^{+} peak to higher magnetic fields in the longitudinal magnetoresistance is more difficult to explain. It maybe that there is a large change in the phase factorbetween the 1^{-} and 1^{+} maxima or that any influencing effect of the paramagnetic centres is orientation dependent.

4.5 THE 0^{-} PEAK IN ρ_{zz}

It is now accepted that the 0^{-} maximum does not appear in the longitudinal magnetoresistance in the case of ionised impurity scattering for a perfect crystal. However, it has been found in this work, through the method of double differentiation, that a very small amplitude 0^{-} maximum does exist in the longitudinal magnetoresistance

(figure 4.5). It is not thought that this is due to components of the transverse magnetoresistance appearing in ρ_{zz} due to poor sample orientation and/or non-parallel current paths. The experimental findings indicate that the existence of the 0^- peak in ρ_{zz} is a true artefact of the longitudinal magnetoresistance. For example the positional behaviour of the 0^- peak in ρ_{zz} followed the behaviour of the other p^- peaks in ρ_{zz}; i.e. before annealing the 0^- maximum did not change position on rotation from the transverse to the longitudinal configuration, whereas after annealing it did change position. Were the 0^- in ρ_{zz} a consequence of transverse components then it would be expected that the position would not change on rotation. This is illustrated by sample A, which on annealing exhibited a very strong 0^- maximum in ρ_{zz} (figure 4.10). This behaviour was probably due to the diffusion of impurities into the sample during heat treatment which subsequently caused non-parallel current paths. Examination of figure 4.10 will show that the 0^- maximum fell at the same magnetic field in both ρ_{xx} and ρ_{zz}.

Raymond[76] et al obtained longitudinal magnetoresistance profiles for three samples two of which did exhibit the 0^- maximum and one which did not. They interpreted the data in terms of a model of medium range fluctuations of potential (which were assumed to appear during the growth of the crystal) and concluded that the appearance of the peak in ρ_{zz} was caused when these fluctuations were large. The given explanation of the phenomenon is that spin-flip transitions become possible in the case of ionised impurity scattering when the density of states is broadened and shifted beyond $k_z=0$. Amirkhanov and Bashirov[50] obtained ρ_{xx} and ρ_{zz} profiles at 77^oK and observed extrema in ρ_{zz} which were absent at 4.2^o. They did not specifically identify the peak in ρ_{zz} as being the 0^-. (In fact from their experimental recordings the

TRANSVERSE AND LONGITUDINAL MAGNETORESISTANCE PROFILES OF SAMPLE A

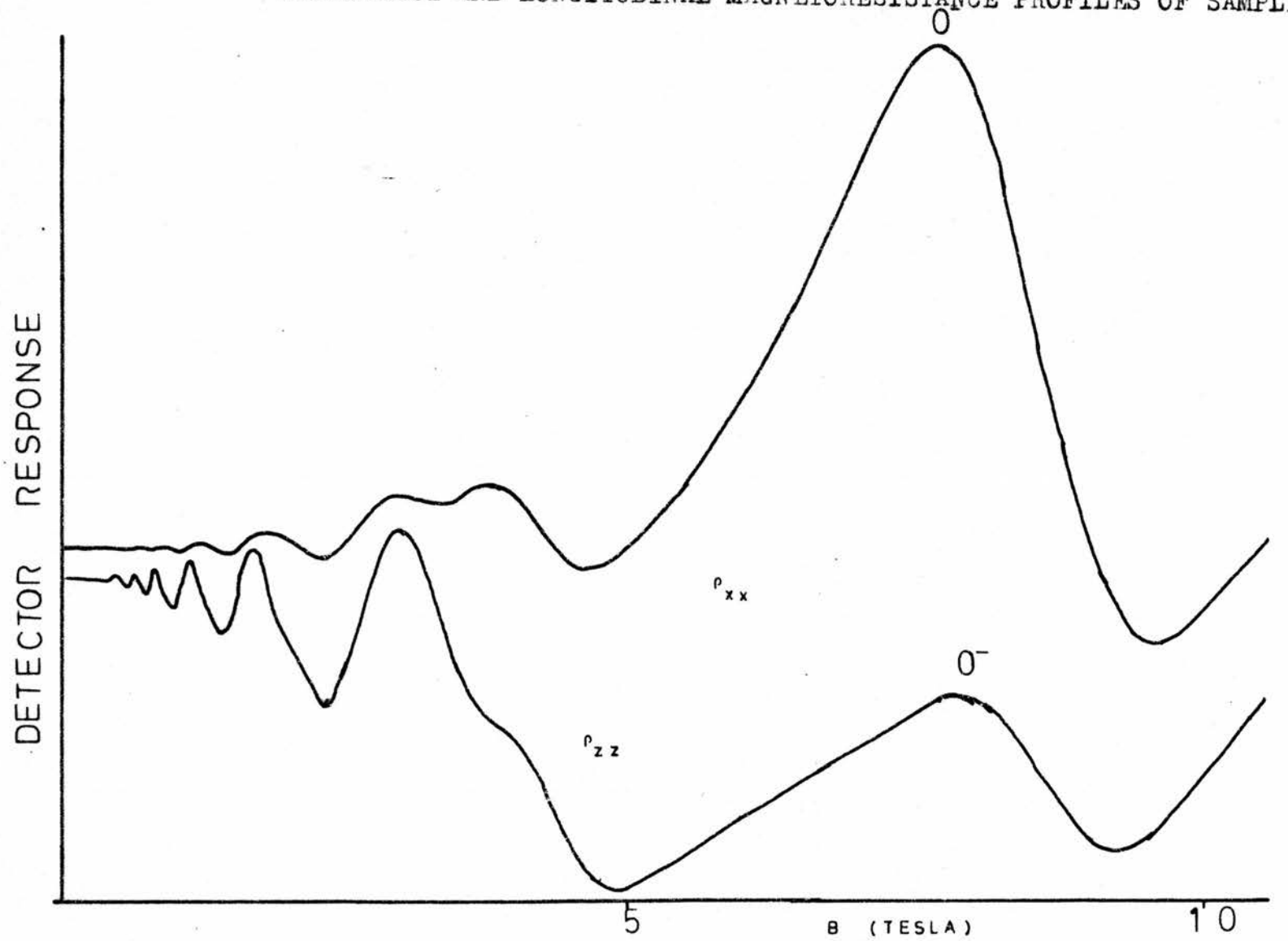

FIGURE 4·10

peak appeared to fall at a field which was approximately 10% below the 0^- in ρ_{xx}). They postulated that the extremum occurred as a result of a fairly large number of phonon-induced spin-flip transitions between the zeroth Landau sublevels. In this work it is possible that the 0^- peak in ρ_{zz} was a consequence of two effects - one being a remnant from the process occurring at $77^{o}K$ and one being due to the effect described by Raymond et al, although the latter is thought to be a verysmall effect since the samples were neutron doped and were therefore very homogeneous.

4.6 DINGLE TEMPERATURE IN THE SHUBNIKOV-DE HAAS EFFECT.

The Dingle temperature of the samples was calculated by two methods. The first method used the measured mobility of the samples and the equations

$$\Gamma = \hbar/2\tau \qquad 4.27$$

and

$$\Gamma = \pi k T_D \qquad 4.28$$

where

Γ = width of the level

τ = $e\mu/m''$, μ=mobility

T_D = Dingle temperature.

The second method compared computer profiles of ρ_{xx}/ρ_0 with the corresponding experimental data. The theoretical graphs were obtained for three samples (figure 4.11) using equations 4.27 and 4.28 and the appropriate values of T, ν, m* and F. The value of Dingle temperature was varied until the resolution of the spin-splitting in the $1^{\pm}$ doublet matched that observed experimentally. The value of T_D obtained by both

methods are shown in table 4.6 where it can be seen that the Dingle temperatures calculated from the mobility fell far below those predicted by the resolution of the spin-splitting in the $1^{\pm}$ doublet. A possible reason for this may be as follows; the Dingle temperature is proportional to the level width, Γ, which in turn is proportional to the amount of scattering into that level. As the level is about to pass through the Fermi surface, the density of states becomes very large and resonant scattering takes place, this greatly increases the level width which results in a much larger Dingle temperature and less well resolved doublets than expected.

4.7 ANOMALOUS PEAKS IN THE SHUBNIKOV-DE HAAS DATA

Some interesting additional maxima, not predicted by theory have been observed in some Shubnikov-de Haas data. Narita and Suizu[10] found additional peaks in the longitudinal magnetoresistance of HgCdTe. These peaks fell between the p=1 and p=0 peaks and also between the p=2 and p=1 peaks. No detailed experimental study was carried out to determine the behaviour of these maxima with temperature, crystallographic orientation etc., and no attempt was made to explain their existence. Galazka et al[56] observed additional maxima but this time in the transverse magnetoresistance of HgSe. They found that the appearance of these maxima was orientation dependent, with the peaks being absent when B was parallel to the <110> and <100> directions, and present when B was parallel to the <111> direction (figure 4.12a and 4.12b). They postulated that the additional maxima resulted from the coincidence of the Fermi level and impurity levels which are degenerated with the conduction band.

In this work no additional maxima were observed in the undifferentiated recordings. However on double differentiation there was some evidence of extra structure being present between the p=1 and p=0 maxima

n $10^{16}cm^{-3}$	T_D(comp) ^oK	μ $cm^2/volt\ s$	$T_D(\mu)$ ^oK	$m^*/m.$
1.47	>6	5.37	2.54	.0156
4.6	∿15	3.6	3.40	.0174
2.72	∿/0	4.12	3.23	.0164

TABLE 4.6

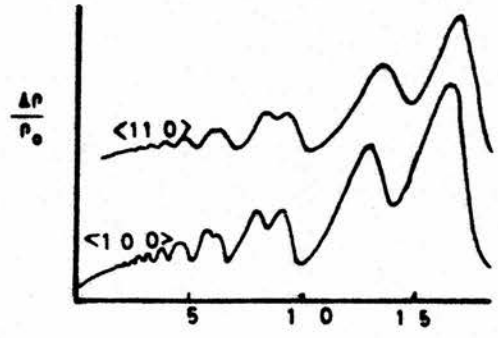

FIGURE 4·12a

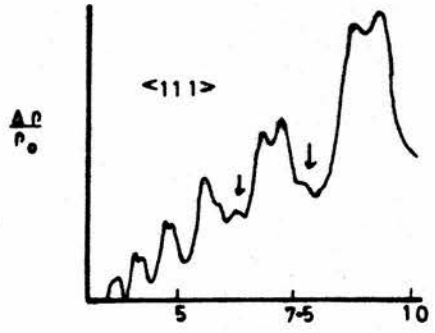

FIGURE 4·12 b

TRANSVERSE MAGNETORESISTANCE OF MERCURY SELENIDE AS FOUND BY GALAZKA et. al.

SECOND DERIVATIVE OF OSCILLATION PROFILE - ARROW INDICATES POSITION OF "ANOMALOUS PEAK"

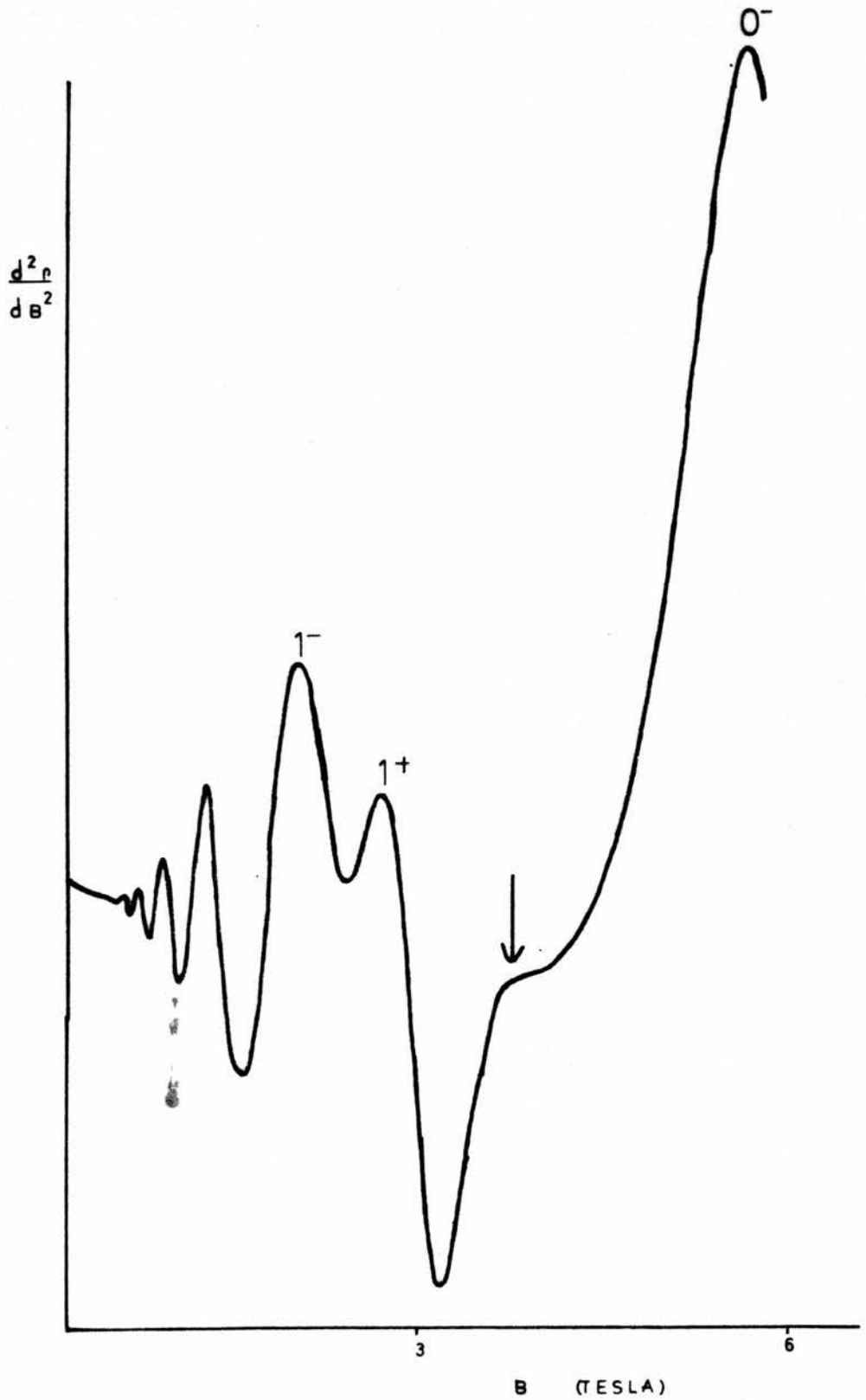

FIGURE 4·13 a

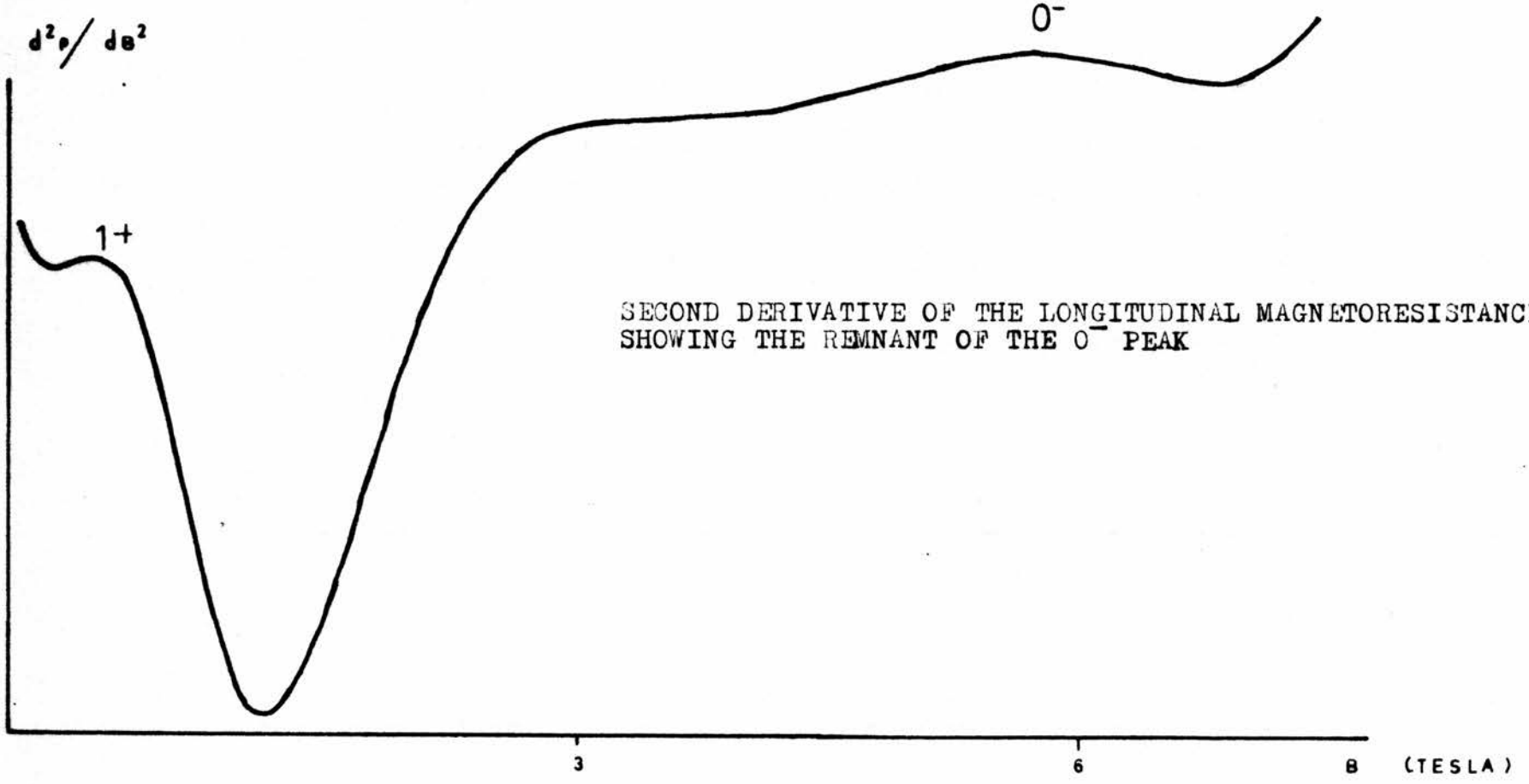

SECOND DERIVATIVE OF THE LONGITUDINAL MAGNETORESISTANCE SHOWING THE REMNANT OF THE 0^- PEAK

FIGURE 4·13b

(figure 4.13a,b). The structure was found to be present in the transverse (figure 4.13a) data of all samples, both before and after annealing, this indicating that the existence was independent of crystallographic orientation, and was not a consequence of radiation damage. This phenomenon may be impurity related as suggested by Galazka, or may be due to large inhomogeneities in the samples. The latter was suggested by Gluzman[52] et al, who produced computer profiles of the magnetoresistance as a function of doping fluctuations which indicated that these additional maxima were caused by spatial inhomogeneities. This explanation seems unlikely since it was thought that the spacial distribution of the donors in the InSb was very uniform. It was also found that this 'anomalous peak' was very much weaker in the longitudinal orientation (figure 4.13b) this suggesting that the peak was a transverse phenomenon.

CHAPTER 5

MAGNETIC FREEZE-OUT InSb

5.1 INTRODUCTION.

The behaviour of the magnetoresistance and Hall effect in the ultra quantum limit region (i.e. $\hbar\omega > E_F$) has been a source of great interest over many years. In 1956 Keyes and Sladek[77] observed experimentally that at 4.2K the Hall effect in Indium Antimonide increases in strong magnetic fields. This phenomenon was interpreted, by the workers, as a decrease in the free carrier concentration, caused by an increase in the binding energy of the shallow donor states by the magnetic field. Yafet et al[78] derived equations, based on a hydrogenic model, giving the variation of the donor binding energy with magnetic field and showed that the ionisation energy of the impurity levels increases when the energy difference between the Landau levels of a free electron becomes comparable with the Rydberg ionisation energy.

The experimental determination of the binding energy has been carried out by many workers using various techniques, such as investigation of the transport properties[79-83] and optical measurements.[84-85] Transport experiments give the values of the binding energy via the measurement of the free electron density which is given by the well known relation of

$$\frac{N_A+n}{N_D-N_A-n} = \frac{N_c}{n} \exp(-E_D/kT) \qquad 5.1$$

where N_A and N_D are the concentrations of the acceptors and donors respectively, n equals the free electron density, E_D equals the binding energy of the donors and

$$N_c = (2\pi m^* kT)^{1/2} eB/\hbar^2 \qquad 5.2$$

The measurement of n, the free electron concentration is not a trivial task but rather is complicated by the effect of conduction occurring by transfer of electrons among the impurities. Several workers have used a two-band model to interpret the Hall coefficient and transverse resistivity, treating conduction among the impurities as though they formed a band. This treatment was criticised by Mansfield and Ahmad[79] who suggested than in the doping concentration under study (10^{14}-10^{15} cm^{-3}) a hopping process was more likely. They adopted the method of measuring the longitudinal magentoresistance, where the assumptions were made that only the electrons in the conduction band contributed to the conductivity and that the mobility in the conduction band was independent of magnetic field as was predicted by Adams and Holstein[7] and Kubo[8] et al. The value of E_D was then obtained through the equation

$$ne\mu = \sigma_{zz} = \frac{1}{\rho_{zz}} = \frac{(N_D-N_A)N_C}{N_A} \exp(-E_D/kT)e \qquad 5.3$$

Where it is taken that $n<(N_D-N_A)$ and $n<N_A$. By assuming that any change in magnetoresistance was due only to a change in the carrier concentration, the dependence $E_D(B)$ was measured. They tested this hypothesis by re-populating the conduction band by avalanche ionisation and found good agreement between the theoretical and experimental behaviour of $E_D(B)$ and the electric field required to produce the avalanche ionisation. Mansfield and Kustzelan[82] measured the Hall coefficient and transverse magnetoresistance as a function of both magnetic field and temperature. They used the conductivity tensor $\sigma=\sigma_c+\sigma_i$ where σ_c is the conduction due to the electrons in the conduction band and σ_i is the conduction due to electrons hopping between donor centres ie

$$\sigma_{xx} = (\sigma_{xx})_c + (\sigma_{xx}) = \rho_{xx}^{-1}[1-(R(H)B\rho_{xx}^{-1})^2]^{-1} \qquad 5.4$$

$$\sigma_{xy} \tilde{=} (\sigma_{xy})_c = -RB\rho_{xx}^{-1}[1+(RB\rho_{xx}^{-1})^2]^{-1} \qquad 5.5$$

The assumption being made that the contribution to σ_{xy} from the impurity conduction was negligible. This was based on the evidence from other materials that the Hall effect due to hopping is very much less than the Hall effect from a band process. From the above equations the value of n, the free carrier concentration was deduced i.e.,

$$\frac{ne}{B} = R(H)B\rho_{xx}^{-1}[1+(R(H)B\rho_{xx}^{-1})^2]^{-1} \qquad 5.6$$

where R(H) is the Hall coefficient

B is the magnetic field

ρ_{xx} is the transverse resistivity.

Hence by measuring the Hall coefficient and transverse resistivity as a function of magnetic field and temperature, and by using equations 5.1 and 5.6 they found the magnetic field dependence of the binding energy. Robert[81] et al performed similar experiments to find n and by plotting $\ln(nT^{-\frac{1}{2}})$ versus T^{-1} for various magnetic field values the binding energy dependence $E_D(B)$ was found. Robert[86] et al again used the same method for determining n, but the donor activation energy was deduced not from 5.1 but by use of the approximation

$$E_D(B) = bB^{\frac{1}{3}} \qquad 5.7$$

where b = constant of proportionality.

B = magnetic field.

By plotting $\ln(n/B)$ versus $B^{\frac{1}{3}}$ they obtained values of $E_D(B)$ which were

in close agreement with other experiments. Beckman[83] et al also made use of the above approximation, they made the assumption that the impurity conduction was negligible compared to the band conduction and by plotting $\ln(R(H))$ versus $B^{1/3}$ deduced $E_D(B)$.

The greater the donor centre concentration, the greater is the magnetic field required to initiate freeze-out. The dependence of this threshold field on the concentration of donors was estimated by Beckman[83] et al who, defining freeze-out as the point at which the electronic wave-function becomes localised within the volume occupied by the donor atom, found that the critical field varied as

$$B_c \propto N_D^{0.8} \qquad 5.8$$

where B_c is the critical field required to initiate freeze-out and N_D equals the concentration of donor centres. It has been shown[82] that the resistivity of InSb in the ultra quantum limit approximates to the form

$$\sigma = \rho_{01}^{-1}\exp-(E_1/kT) + \rho_{02}^{-1}\exp(-E_2/kT) + \rho_{03}^{-1}\exp(-E_3/kT)$$

which, because of the tensor form of the resistivity is only valid for ρ_{zz}, the longitudinal magnetoresistance. On a logarithmic plot of resistivity versus reciprocal temperature, successive regions are revealed which have activation energies E_1 E_2 and E_3. Each of these regions has been interpreted as being due to a different process such that the total conductivity is the sum of contributions from each process. The region characterised by the activation energy E_1 has been associated with conduction due to electrons being excited from donor levels into conduction band, with the energy E_1 being equal to the donor binding energy E_D. The E_3 region has been associated with an activated hopping

process where the activation energy for the process, E_3, increases with increasing magnetic field. The E_2 region is associated with the excitation of electrons to extended conducting states, however most workers have agreed that the E_2 region has not been observed in InSb, whereas both the E_1 and E_3 regions have.

In some materials a fourth region has been observed below the E_3 region where the magnetoresistance increases less rapidly as the temperature is reduced than is expected for an activated process. At these temperatures it is considered that variable range hopping occurs in which nearest neighbour hopping is replaced by hopping to more remote centres. This process was considered by Mott[87] and was later developed for large magnetic fields by Shklovskii[88]. The possiblity that the electrons in a semiconductor might freeze-out into a Wigner lattice due to the effect of a magnetic field was suggested by Durkan et al[89] and numerical data for a magnetic field induced Wigner condensation for free carriers in a semiconductor at low temperatures was published by Kleppmann and Elliott[90]. Nimtz and Schlicht measured the magnetoresistance, as a function of temperature, in the ultra-quantum-limit, of three narrow gap semiconductors, HgCdTe, PbTe, and PbSnTe, materials in which the freeze-out of carriers can be avoided. In all three semiconductors a critical temperature and magnetic field was found at which a phase transition took place. The authors reported that the observed behaviour was in agreement with the features expected for a Wigner condensation, they did stress however, that the results did not represent definite proof that a Wigner condensation was taking place.

Striking anomalous effects have been observed in the magnetic freeze-out region in InSb. A change of sign in the Hall effect at fields greater than 2 Tesla depending on doping and temperature was first observed by Neuringer[94] and was subsequently studied in more detail by Fantner et al.[91-93]

They investigated several samples with doping densities ranging from $2x10^{14}$ to $3x10^{15}cm^{-3}$, all having different compensation ratios $K(=N_A/N_D)$, and found that for all samples the Hall coefficient reached a maximum, decreased, then underwent a change of sign. It was also found that the transverse magneto-resistance was nearly independent of B in the range where the sign change of R(H) occurred, with the longitudinal magnetoresistance showing similar behaviour. The critical magnetic field where the sign change occurred was found to decrease with decrease in temperature, increase with the degree of doping, and decrease with increasing K. The influence of the compensation ratio was shown to be much greater than the influence of the doping density, this was illustrated by the fact that with an impurity concentration of $4.2x10^{14}cm^{-3}$ and compensation ratio of 0.2 the sign reversal was at approximately 7 Tesla at $3^{o}K$, whereas with a much higher impurity concentration of $1x100^{15}cm^{-3}$ and $K\approx0.67$ the critical field was approximately 6.5 Tesla.

Several mechanisms which may have been responsible for the anomalies were dismissed by the authors. Free holes were thought not to be responsible since the holes have a large binding energy at acceptors (corresponding to approximately 80K), and magnetotransmission experiments upheld this. The existence of p-type inversion layers was not thought probable and to affirm this point they studied the influence of sample geometry, contact shape and surface treatment. Some indirect evidence against hopping conduction being responsible was quoted, eg, no frequency dependence of the Hall effect or transverse magnetoresistance was observed, as would have been expected if hopping conduction were taking place. Impurity band conduction was excluded because A) the sign changes were observed at magnetic fields where the overlapping of the impurity wave functions is much reduced making the formation of an impurity band improbable, B) the sign change was seen

for all compensation ratios.

The authors attributed their results to the mechanism of asymmetric scattering of spin-polarised electrons at ionised impurities known as skew scattering. They analysed their results in terms of this model (whose theoretical formalism is set-out in the paper by Biernat and Kriechbaum[95]) and found good agreement for some samples.

Mansfield and Kustzelan[32] (M/K) observed similar results to those obtained by Fantner et al. They found saturation of the transverse resistivity and a maximum in the Hall coefficeint occurring at a field of approximately 1 Tesla (temperature not given) in samples with $N_D \sim 4 \times 10^{14} cm^{-3}$ and $K \sim 0.25$. They attributed this to a surface conducting layer providing a conducting path which limited the resistance of the sample. This conducting layer was thought to have been caused by the soldering of the current leads to the sample and subsequent heating to $60^{\circ}C$ for two hours. Elimination of the layer was achieved by coating the current leads with a protective nail varnish and etching the sample with CP4, with the potential probes then being spot welded to the sample by condenser discharge. After this treatment the sample characteristics changed markedly with the transverse resistivity and Hall coefficient increasing by seven and five orders of magnitude respectively at 3 Tesla. Fantner and Kuchar carried out extensive investigations into the effect of the surface condition of their samples. They repeated the proceedure carried out by M & K, ie they soldered on contacts prior to, and after, etching, and observed no difference in the behaviour between the samples prepared in the two different manners, ie. the transverse resistivity saturated and the Hall coefficient changed sign, both at $2.2^{\circ}K$. They also found no difference between the results obtained with samples having an etched and polished surface and samples having a roughly ground surface.

They concluded that if there was a surface conducting layer then its origin was not associated with the heating of the sample during the soldering and that the proportionality of the transverse magnetoresistance with inverse sample cross section proved that the saturation of the resistance was a bulk effect.

5.2 EXPERIMENTAL DETAILS.

Measurements were carried out at $4.2^{o}K$ on two samples (G and H) having carrier concentrations of $5.3x10^{15}$ and $7.6x10^{15}cm^{-3}$ respectively, before annealing and $6.3x10^{15}$ and $1x10^{16}cm^{-3}$ after annealing. The doped samples were obtained as outlined in chapter 3. Contacting proceedures were such that the minimum of interference with the sample was achieved. After etching in 10% Bromine-Methanol, current contacts of pure Indium were soldered onto the ends of the sample, with potential and Hall probes, (on the face and sides respectively), being fabricated from the Silver preparation which merely involved applying the preparation at room temperature and allowing to dry for approximately 1-2 days, also at room temperature. Hence the heating the sample was subjected to during contacting was for the soldering on of the current leads and was very localised, lasting a matter of seconds.

D.C. magnetoresistance and Hall measurements were taken in the conventional manner of passing a constant current through the sample amplifying the output voltage from the potential or Hall probes before displaying the signal on a chart recorder as the magnetic field was swept. Measurement of the magnetic field was as described in Chapter 2 and was known to better than 2%. The possibility of hot electron effects was ruled out by checking that the current-voltage characteristics were linear over the magnetic field range used. Measurements were taken for both unannealed and annealed samples.

5.3 RESULTS.

Figure 5.1 shows the variation of the Hall voltage and transverse magnetoresistance of sample H with magnetic field. In the low field region the Hall voltage is linear with magnetic field, indicating that the Hall coefficient and hence the carrier concentration is constant in this region. As the field is increased a point is reached ($\sim$5 Tesla) at which the linear relationship begins to break down, ie the carrier concentration is no longer constant but decreases as the magnetic field increases. This is the onset of magnetic freeze-out and is also manifested in the resistivity by a marked increase of the magnetoresistance with increasing magnetic field. Measurements were taken up to 10 Tesla for both samples, with neither sample giving any indication of a sign change in the Hall coefficient, there was also no indication of the Hall coefficient approaching a maximum in either case. The transverse and longitudinal magnetoresistance were found to increase indefinitely with magnetic field and showed no tendancy to saturate. Figure 5.2 shows graphs of $\ln(V(HALL))$ versus $B^{1/3}$ for both samples. This illustrates that in the magnetic freeze-out region $\ln(V(HALL)) \propto (B^{1/3})$ ie. $B/n \propto \exp(B^{1/3})$, which by use of equation 5.1 it can be concluded that the donor binding energy has a $B^{1/3}$ magnetic field dependence. Comparison of the curves obtained for each sample reveals that the higher the donor concentration, the higher, is the magnetic field required to produce carrier freeze-out, in sample H a field of 5 Tesla was required whereas for sample G a field of 6 Tesla was needed. This is in agreement with the $B_c \propto N_D^{0.6}$ dependence.

A plot of ln(transverse magnetoresistance) versus ln(B) figure (5.3) in the region after the last oscillation and before the onset of freeze-out revealed a B^3 dependence of the transverse resistivity. This is in close agreement with theory[7] which predicts that for a degenerate distribution of electrons in the quantum limit when scattering by ionised impurities

TRANSVERSE MAGNETORESISTANCE AND HALL VOLTAGE AS A FUNCTION OF MAGNETIC FIELD
THE QUANTUM LIMIT(IONISED IMPURITY SCATTERING) AND ULTRA - QUANTUM LIMIT
(MAGNETIC FREEZE-OUT) REGIONS ARE INDICATED

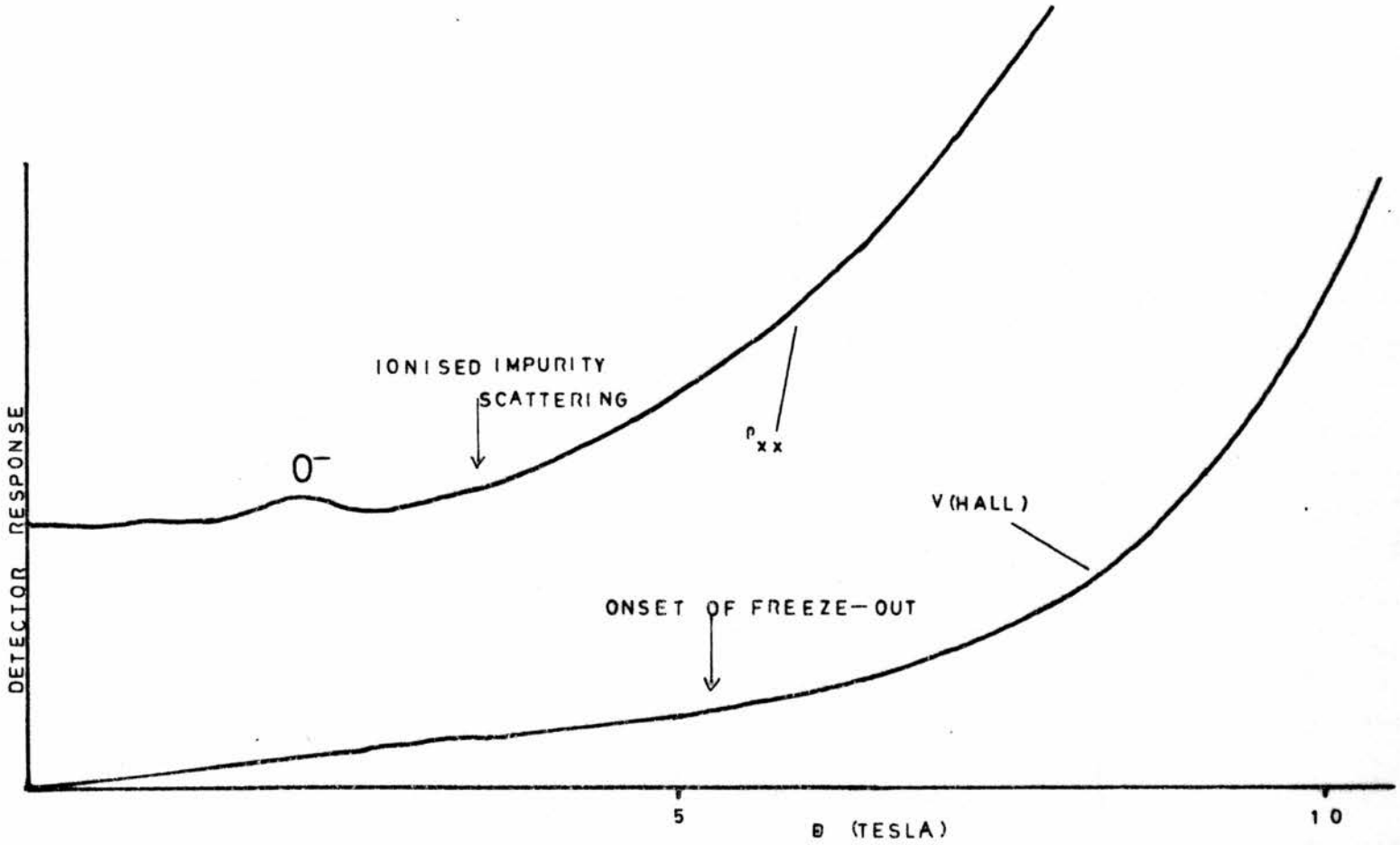

FIGURE 5·1

GRAPHS OF Ln(HALL VOLTAGE) VERSUS $B^{1/3}$ IN THE FREEZE-OUT REGION

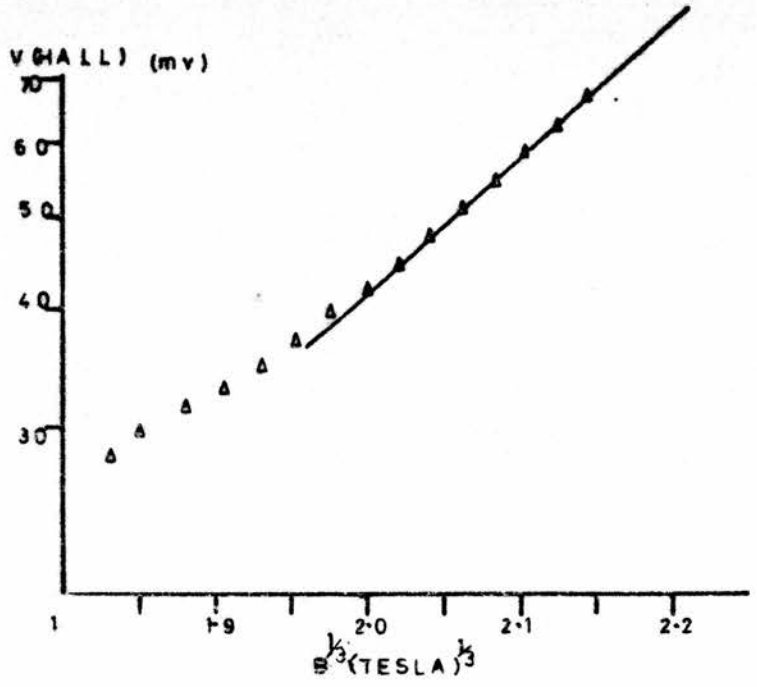

FIGURE 5·2 a

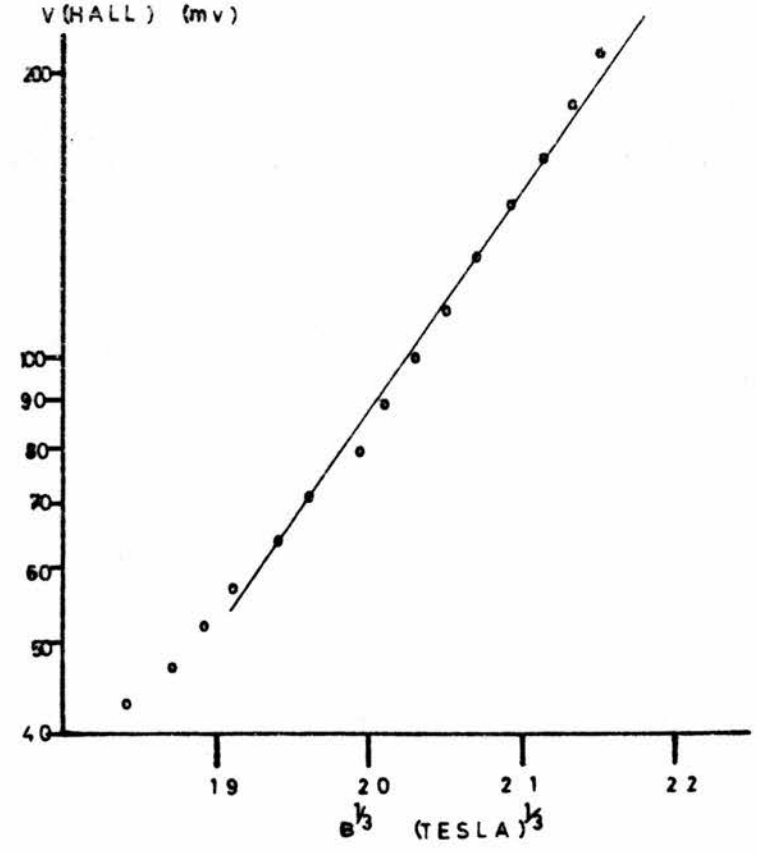

FIGURE 5·2 b

LOG(MAGNETORESISTANCE) VERSUS LOG(MAGNETIC FIELD)
IN THE QUANTUM LIMIT REGION i.e. BEFORE FREEZE-OUT

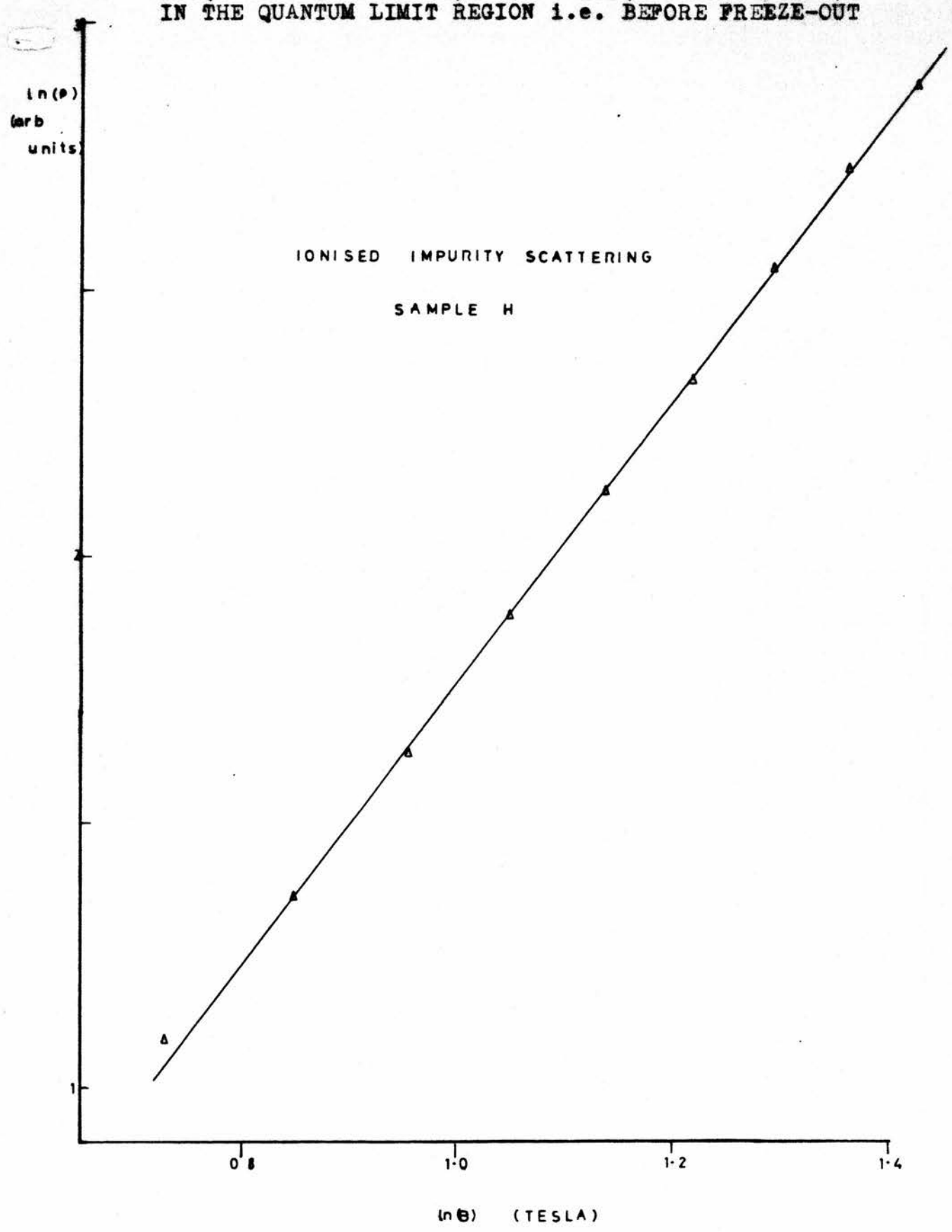

FIGURE 5·3

dominates $\rho(B) \sim B^3 T^0$ where T is temperature. Figure 5.4 is a plot of $\ln(\rho_{zz} B)$ versus $B^{1/3}$ for sample H after annealing and again illustrates the $E_D = bB^{1/3}$ relation. Values of the binding energy as a function of magnetic field were obtained from the graphs of $\ln(V(HALL))$ and $\ln(\rho_{zz} B)$ versus $B^{1/3}$ and equation 5.7. These are represented graphically in figure 5.5 along with the theoretical binding energy calculated from the formula given by Yafet, Keyes and Adams, who for a parabolic band found

$$E_D = \frac{1}{4}E^2\gamma + \sqrt{\frac{8}{\pi}}\, E\gamma^{1/2}$$

with E given by the solution of

$$\frac{\sqrt{\pi}\gamma^{1/2}}{2^{3/2}} = 2/E(\ln[2/E] - 1)$$

and $\gamma = \frac{\hbar\omega}{2R}$ where R is the Rydberg constant and ω = cyclotron frequency

In general results obtained after annealing were the same as the results for the unannealed samples with any difference due only to the differing carrier concentrations, eg the onset of freeze-out occurred at higher fields for a sample after annealing.

5.4 DISCUSSION.

The high magnetic field properties of the samples followed the characteristic pattern of freeze out as expected by theory and in agreement with most workers. The donor binding energy was calculated from the Hall data for both samples before annealing and from the Hall and longitudinal magnetoresistance for sample H after annealing. Several assumptions were made for these calculations. The contribution from the impurity conduction was assumed negligible and hence the value of n was taken to be given directly by the equation

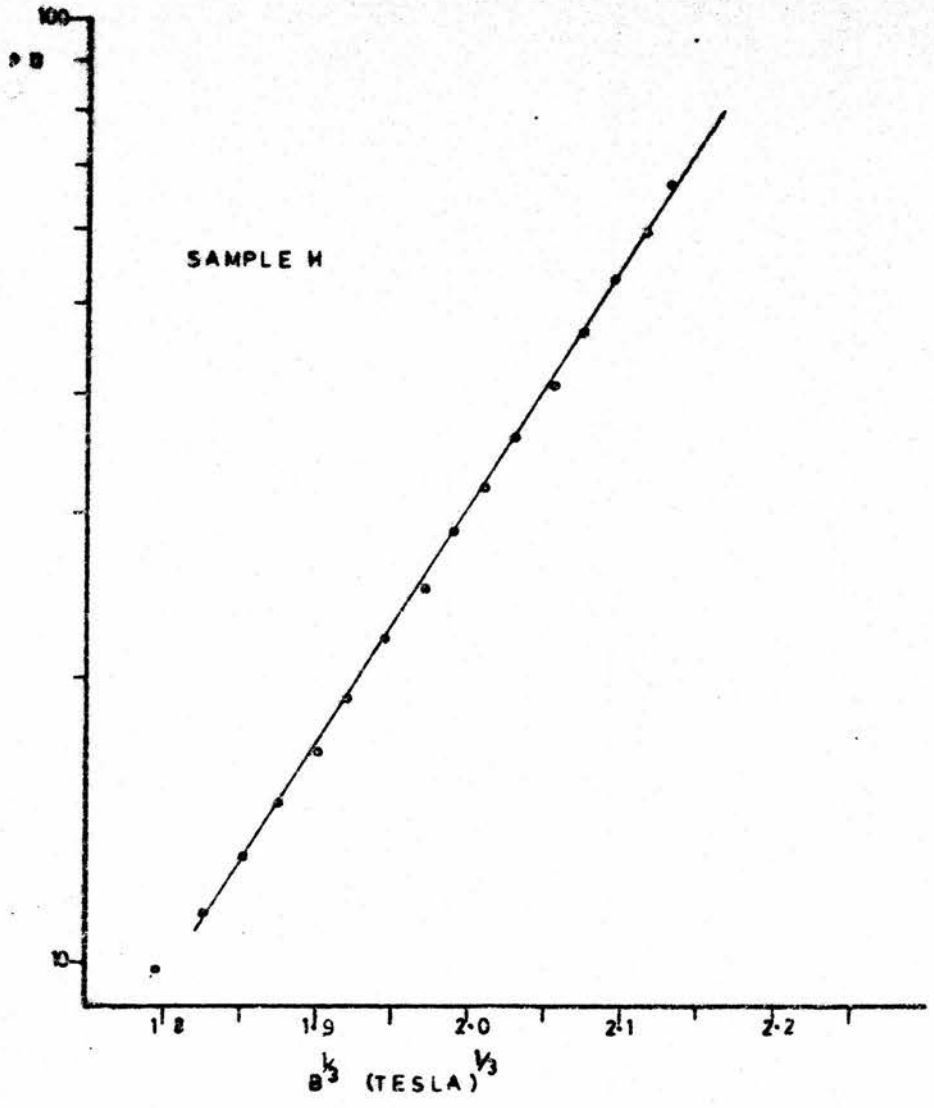

FIGURE 5·4

LOG(LONGITUDINAL MAGNETORESISTANCE X B)
VERSUS $B^{1/3}$ IN THE MAGNETIC FREEZE-OUT REGION

$$\sigma_{xy} = \rho_{xy}^{-1} = \frac{ne}{B} \qquad 5.9$$

The second approximation made was associated with the calculation of the binding energy from the longitudinal magnetoresistance, ie that of assuming a magnetic field independent mobility. This may be false for several reasons. Firstly a magnetic field independent mobility is only predicted for classical statistics, for the degenerate case the resistivity varies as approximately B^3, the variation being due only to the mobility. Immediately before freeze-out the resistivity obeys the power law predicted for a degenerate distribution (and ionised impurity scattering). As the magnetic field is increased and induces freeze-out, the degeneracy temperature falls and the electron distribution eventually becomes classical. However there may be part of the freeze-out region where the electron distribution is not to be described by either statistics and where the mobility is not independent of B. Secondly, freeze-out reduces the concentration of charged scattering centres which has the result of increasing the mobility, and also reduces the screening of the scatterers which has the effect of decreasing the mobility. Hence even in the limit of classical statistics the mobility may still be changing.

The donor binding energies were evaluated by obtaining the constant of proportionality b, (equation 5.7), from the gradients of the $\ln(\rho_{zz}B)$ and $\ln(V(HALL))$ versus $B^{1/3}$ graphs. As can be seen from figure 5.5 the values obtained from the Hall data exhibited the general trend of the higher the donor concentration, the lower the binding energy which was in agreement with previous experimental findings. Two curves were found to lie below that predicted by the YKA theory and one above. Comparison of the curves obtained from the Hall and longitudinal data of sample H after annealing reveals a difference in values of approximately 23% which is well outwith experimental error. This was

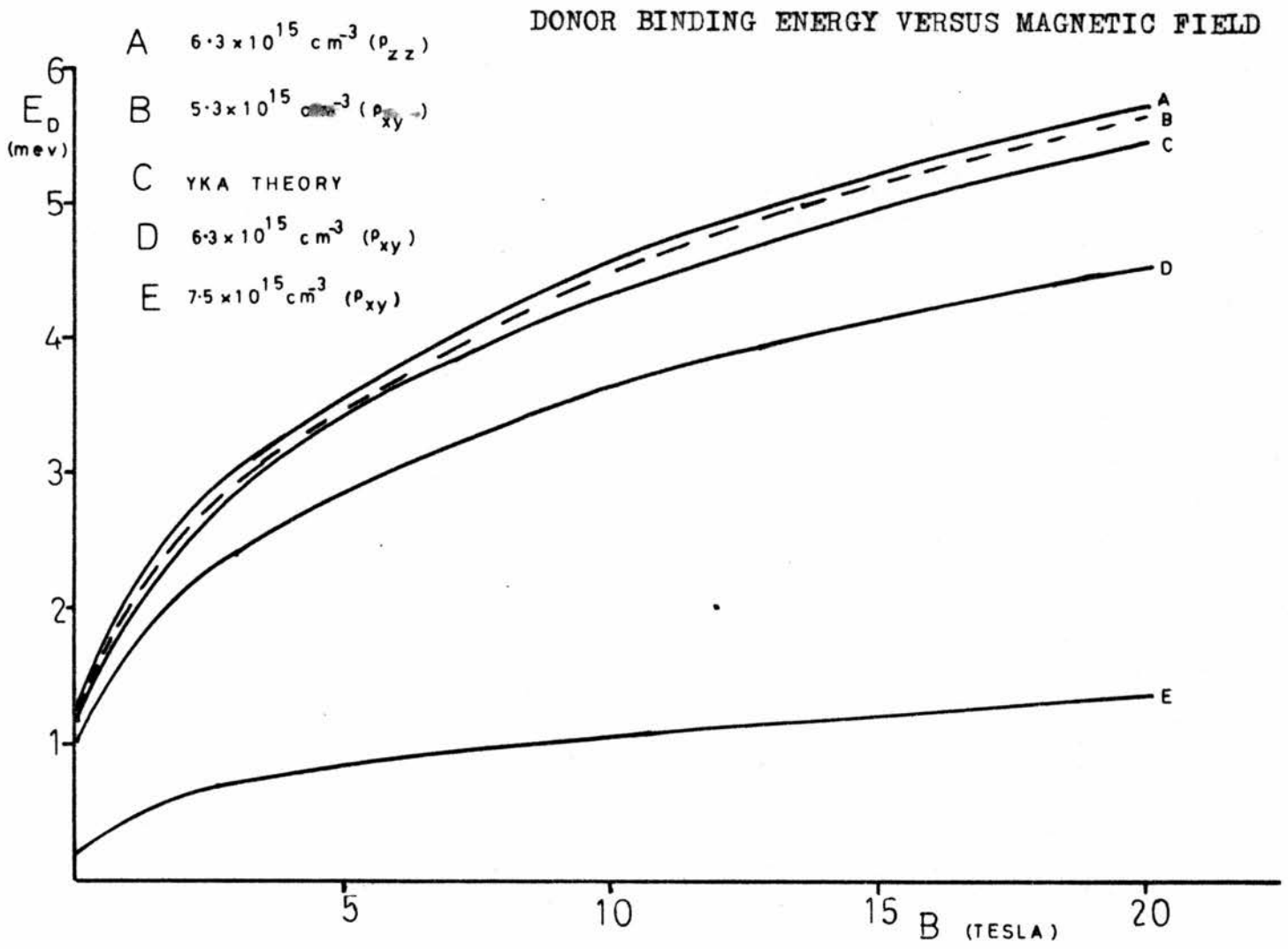
DONOR BINDING ENERGY VERSUS MAGNETIC FIELD
A 6·3 x 10^15 cm^-3 (ρzz)
B 5·3 x 10^15 cm^-3 (ρxy)
C YKA THEORY
D 6·3 x 10^15 cm^-3 (ρxy)
E 7·5 x 10^15 cm^-3 (ρxy)
E_D (mev)
6
5
4
3
2
1
5
10
15
20
B (TESLA)
A
B
C
D
E

FIGURE 5·5

also observed by Mansfield[80] who postulated that the difference was due to the variation of the mobility with magnetic field. In this case the difference is probably due to a combination of the mobility variation and the approximation of negligible contribution from impurity conduction.

The discrepancy between the experimental and theoretical values is the result of several effects which are not taken account of in the YKA theory. Screening of the impurity potential, non-parabolicity of the conduction band, band tailing and central cell effects serve to alter the binding energy. The effect of screening and non-parbolicity was treated by Ortenberg[97] who showed that they had opposing effects with the non-parabolicity increasing the binding energy and the screening reducing it. Figures 5.6 and 5.7 are graphs which were produced by Ortenberg showing the influence of both effects. At increasing impurity concentrations band tailing effects which decreases E_D, become non-negligible, as has been found experimentally in InSb.[98-99] Band tailing and its effect on the binding energy has been treated theoretically by Dyakonov et al. The influence of central cell effects was considered by Kaplan and Larsen[100] who adopted the approach of taking the shift, (to higher values), in the ground state energy, to be proportional to the charge density overlap with the ion core of the donor species. To accurately predict any donor binding energy in any semiconductor all the above effects must be included in the theory. To date, for InSb, theories exist which take account of one or two of these effects, but not all.

The Hall coefficient in all cases gave no indication of reversing sign and the transverse resistivity showed no tendency to saturate. Sample H has a impurity concentration very close to that of sample 7 investigated by Fantner et al (1976) which had an impurity concentration

GRAPHS SHOWING THE VARIATION OF CARRIER CONCENTRATION AND DONOR BINDING ENERGY WITH MAGNETIC FIELD IN THE FREEZE-OUT REGION. THE EFFECTS OF NON PARABOLICITY AND SCREENING ARE INCLUDED.

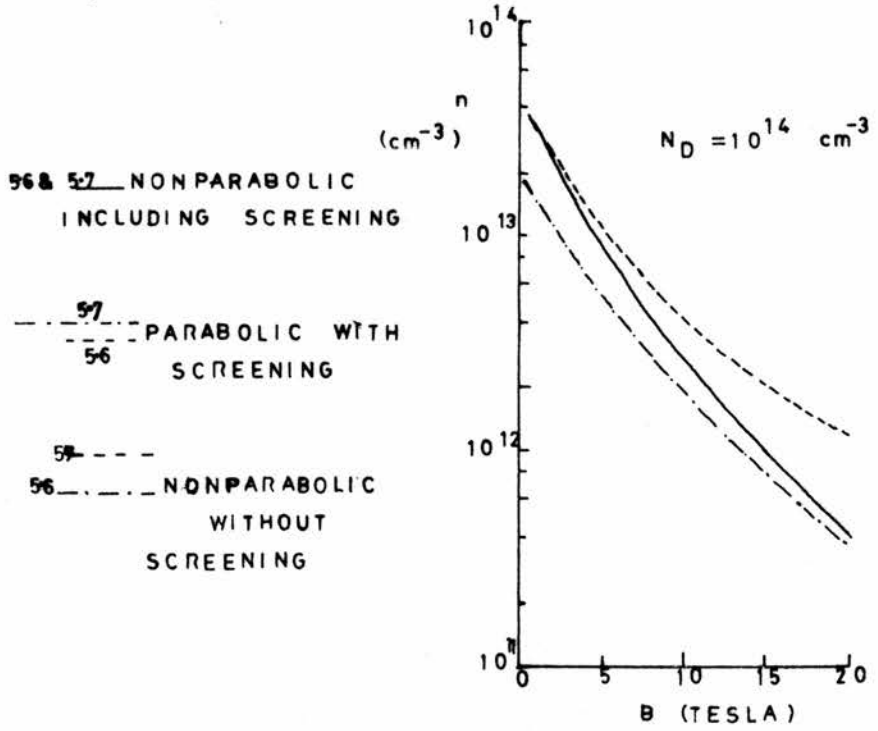

FIGURE 5·6

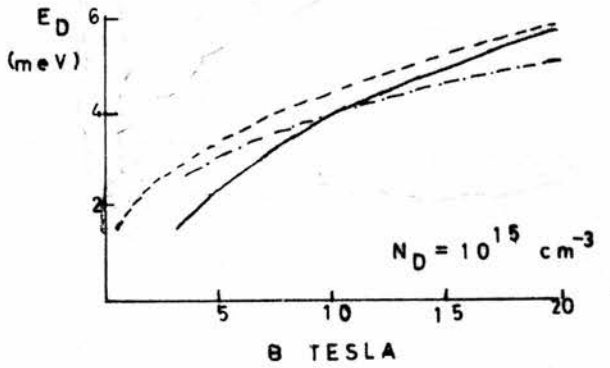

FIGURE 5·7

of $3x10^{15}cm^{-3}$ and a compensation ratio, K, of 0.65. Extrapolating the results of Fanter et al to 4.2°K it is found that for a sample having the characteristics of sample 7, the critical field at which the sign reversal takes place is approximately 10 Tesla. The transport properties of sample H were measured to this field and gave no sign of reproducing the behaviour seen by Fantner et al. This may be for two reasons: A) the impurity concentration of the sample in this work was higher, B) a difference in the compensation ratios. Although the K value for sample H is not accurately known it was estimated that it was not greater than 0.2. The former explanation seems unlikely since the impurity concentration difference is not large and the critical magnetic field does not appear to have a strong impurity concentration dependence. From the work of Fantner et al it is predicted that with the smaller value of K for sample H the critical magnetic field for the sign reversal should be higher than 10 Tesla. Hence basing the analysis on the results found by Fantner it was expected that the sign reversal of R(H) should occur at a field greater than was obtainable in these experiments. However, despite the larger impurity concentration and lower K value, both of which served to increase the critical magnetic field beyond 10 Tesla it was expected that if these experiments were to reproduce the Fantner results, the Hall coefficient would have given some evidence of approaching the maximum which preceeds the sign reversal.

SUMMARY.

The aim of this work was to revise the Shubnikov.de Haas effect as a technique for the determination of the band structure of semiconductors and to try to explain some of its anomalous behaviour.

Homogeneous N.T.D. samples were produced, all of which exhibited well defined oscillation profiles thus allowing detailed investigation of the magnetoresistance characteristics. The technique of double differentiation was employed to accentuate the higher harmonic components of the oscillations, this making possible the accurate measurement of the field positions of certain maxima. This in turn led to more accurate values for the electronic g-factor and also prompted the conclusion that the very small σ^- peak present in the longitudinal magnetoresistance is not due to the existence of transverse components of the current but is a true artefact of the longitudinal orientation.

The Dingle temperatures of the samples were determined at zero and high magnetic fields. In all cases it was found that the high magnetic field values exceeded the zero field values. This is in contradiction to the theory of Adams and Holstein which assumes a Dingle temperature independent of magnetic field.

Finally, the mechanism of magnetic freeze-out was observed and a $B^{1/3}$ dependence of the donor binding energy found. The variation of the Hall coefficient in the freeze-out region was investigated and contrary to the results of Kuchar et al no indication of a sign reversal was observed.

REFERENCES.

1) Landau L.D., (1930) Z. Physik Vol 64, P629.

2) de Haas W.J., Van Alphen P.M., (1930) Leiden Comm. 208d, 212d and (1933) 220d.

3) de Haas W.J., Shubnikov L., (1930) Leiden Comm. 207a, 207c, 207d, 210a.

4) Dresselhaus M.S., Mavroides J.G., (1964) Solid St. Comm. Vol. 2 P297.

5) Steele M.C., Babiskin J., (1955) Phys. Rev. Vol. 98 P359.

6) Kunzler J.E., Hsu F.S.L., Boyle W.S., (1962) Phys. Rev. Vol. 128, P1084.

7) Adams E.N., Holstein T.D., (1959), J. Phys. Chem. Solids Vol. 10, P254.

8) Kubo R., Hashitsume N., Miyake S.J., (1966) Solid St. Phys. Vol. 17, P269. (New York: Academic Press)

9) Gelmont B.L., Ivanov-Omskii V.I., Konstantinova N.N., Mashovets D.V., Parfeniev R.V., (1977) Proc. 3rd Int. Conf. on the Phys. Narrow Gap Semicond. Warsaw.

10) Narita, Suizu, (1975) Suppl. Prog. Theor. Phys. No. 57, P187.

11) Gavaleshko N.P., Dobrowolski W., Baj M., Dmowski L., Dietl T., Khomyak V.V., (1977) Proc. 3rd Int. Conf. on the Phys. of Narrow Gap Semicond. Warsaw.

12) Booth B.L., Ewald A.W., (1969) Phys. Rev. Vol. 186 No.3 P770.

13) Jay-Gerin J.P., Lakhani A.A., (1977) J. Low Temp. Phys. Vol. 28, No 1/2, P15.

14) Jaczynski M., Kossut J., Galazka R.R., (1977) Proc. 3rd. Int. Conf. on the Phys. Narrow-Gap Semicond. Warsaw.

15) Restorff J.B., Houston B., Allgaier R.S., Littlejohn M.A., Phatak S.B., (1980) J. Appl. Phys. Vol. 51 No 4 P2277.

16) Bliek L.M., Landwehr G., Von Ortenberg (1968) Proc. 9th Int. Conf. on Phys. Semicond. Vol. 2, Moscow, P710.

17) Dingle R.B., (1952 Proc. Roy. Soc. (London) A211 P517.

18) Bychkov Yu.A., (1961) Soviet Phys. JETP Vol.12, P977.

19) Luttinger J.M., (1961) Phys. Rev. Vol.121, P1251.

20) Argyres P.N., Adams E.N., (1956) Phys. Rev. Vol.104,P900.

21) Argyres P.N., Adams E.N., (1958) J. Phys. Chem. Solids. Vol.4, P19.

22) Barrie R. (1957) Proc. Phys. Soc. (London) B70 P1008.

23) Titeica S. (1935) Ann. Physik Vol.22 P129.

24) Kubo R., Hasegawa H., Hashitsame N., (1959) J. Phys. Soc. Japan Vol.14 P56.

25) Argyres P.N., Roth L.M., (1959) J. Phys. Chem. Solids Vol.12 P89.

26) Klinger M.I., (1961) Soviet Phys. Solid St. Vol.3 P974.

27) Kosevich A.M., Andreev V.V., (1960) Soviet Phys. JETP, Vol.11 P637.

28) Davydov B., Pomeranchuk I., (1940) J. Phys. USSR., Vol.2, P147.

29) Miyake S.J., (1965) J. Phys. Soc. Japan. Vol.20, P412.

30) Stradling R.A., Wood R.A., (1970) J. Phys. C : Solid St. Phys. Vol 3, P2425.

31) Wood R.A., (1970) D. Phil Thesis, Oxford University.

32) Blakemore J.S., Kennewell J.A., (1975) J. Phys C : Solid St. Phys., Vol. 8, P847.

33) Cleland J.W., Proc. Int. School of Physics. Enrico Fermi Course XVIII Radiation Damage in Solids, P384.

34) Kuchar F, Fantner E.J., Bauer G., (1974) Phys. Stat. Sol. a) Vol 24, P513.

35) Clark W.G., Isaacson R.A., (1966) J. Appl. Phys. Vol.38, No.5, P2284.

36) Lark-Horovitz K., Semiconducting materials, edited by H.K. Henisch (New York 1951), P47.

37) Cleland-J.W., Crawford J.H., (1954) Phys. Rev. Vol.95, No.5, P1177.

38) Gossick R.B., (1959) J. Appl. Phys. Vol.30, No. 8, P1214.

39) Vitovskii N.A., Dolgolenko A.P., Mashovets T.V., Oganesyan O.V., (1979) Sov. Phys. Semicond. Vol.13, No.10, P1141.

40) Vodop'yanov L.K., Kurdiani N.I., (1966) Sov. Phys. Semicond. Vol.1, No. 5, P541.

41) Abdullaev A., Vitovskii N.A., Mashovets T.V., Mustafakulov D., (1975) Sov. Phys. Semicond. Vol.9, No.2, P184.

42) Vitovskii N.A, Mashovets T.V., Oganesyan O.V., Pambukhchyan n.kh, (1978) Sov. Phys. Semicond. Vol.12, No.9, P1106

43) Bertolotti M., Radiation effects in semiconductors. (Proc. Sante Fe Conf., 1967, ed. by F.L. Vook), Plenum Press, New York (1968) P311.

44) Larson B.C., (1974) J. Appl. Phys. Vol.45, P514.

45) Bemski G., (1959) J. Appl. Phys. Vol.30, P1195.

46) Watkins G.D., Corbett J.W., Walker R.M., (1959) J. Appl. Phys. Vol.30, P1198.

47) Edmond J.T., (1960) J. Appl. Phys. Vol.31, No.8, P1428.

48) Bliek L.M., Landwehr G., (1969) Phys. Stat. Sol. Vol.31, P115.

49) Gurevich L.E., Efros A.L., (1963) Soviet Phys. JETP Vol,16, No.2, P402.

50) Amirkhanov Kh.I., Bashirov R.I., (1967) Soviet Phys. Solid St. Vol.8, No.7, P1739.

51) Antcliffe G.A., Stradling R.A., (1965) Physics Letters Vol.20, No.2, P119.

52) Gluzman N.G., Sabirzyanova L.D., Tsidil'kovskii I.M., (1979) Soviet Phys. Semicond. Vol.13, No.3, P275.

53) Dietl T., Dobrowski W., Galazka R.R., Iwanowskii R.J., (1976) Solid St. Commun. Vol, 20, P1133.

54) Stephens A.E., Seiler D.G., Sybert J.R., Mackey H.J., (1975) Phys. Rev. B, Vol.11, P4999.

55) Efros A.L., (1965) Sov. Phys. Solid St. Vol.7, P1206.

56) Galazka R.R., Dobrowolski W., Thuillier J.C., (1980) Phys. Stat. Sol. Vol.98, P97.

57) Traxler R.M., (1964) Ball. Am. Phys. Soc. Vol.9 P736.

58) Roth L.M., Lax B., Zwerdling S., (1959) Phys. Rev. Vol.114, P90.

59) Bowers R., Yafet Y., (1959) Phys. Rev. 115, P1165.

60) Kane E.O., (1957) J. Phys. Chem. Solids, Vol.1, P249.

61) Zawadzki W., (1963) Physics Letters Vol.4, No.3, P190.

62) Zwerdling et al, (1962) Proc. Int. Conf. on Phys. Semicond. (EXETER) P455.

63) Pidgeon C.R., Brown R.N., (1966) Phys. Rev. Vol.146, No. 2., P575.

64) Zawadzki W., Szymanska W., (1971) J. Phys. Chem. Solids Vol.32, P1151.

65) Ogg N.R., (1966) Proc. Phys. Soc. Vol.89, P431.

66) Pidgeon C.R., Mitchell D.L., Brown R.N., (1966) Phys. Rev. Vol.154, No.3, P737.

67) McCombe B.D., (1968) Solid State Commun. Vol.6, P533.

68) McCombe B.D., (1968) Phys. Rev. Vol.181, No.3, P1206.

69) Bemski G., (1960) Phys. Rev. Lett. Vol.4, P62.

70) Kaplan D., Konopka (1968) J., Proc. Int. Conf. on the Physics of Semicond. Moscow. Vol.2, P1146.

71) Isaacson R.A., (1968) Phys. Rev. Vol.169, P312.

72) Roth L.M., Argyres P.N., (1956) Semiconductors and Semi-metals Vol.1, P159.

73) Mason P.J., Private Communication

74) Hajdu Private Communication.

75) Stradling R.A., Private Communication.

76) Raymond A., Robert J.L., Bernard C., Bousquet C., Aulombard R., (1977) Proc. 3rd Int. Conf. Phys. Narrow-Gap Semicond. P331.

77) Keyes R.W., Sladek R.J., (1956) J. Phys. Chem. Solids Vol.17. P143.

78) Yafet Y., Keyes R.W., Adams L.M., (1956) J. Phys. Chem. Solids Vol.1, P137.

79) Mansfield R., Ahmad I., (1970) J. Phys. C., Solid State Phys. Vol.3, P423.

80) Mansfield R., (1971) J. Phys. C., Solid State Phys. Vol.4, P2084.

81) Robert J.L., Raymond A., Aulombard R.L., Bousquet C., (1980) Phil. Mag. B. Vol.42, P1003.

82) Mansfield R., Kustzelan (1978) J. Phys. C. Solid State Phys. Vol.11, P4157.

83) Beckman O., Hanamura E., Neuringer L.J., (1967) Phys. Rev. Lett. Vol.18, P773.

84) Wallis R.F., Boulden H.J., (1958) J. Phys. Chem. Solids vol.7, P78.

85) Kaplan R., (1967) J. Phys. Soc. Japan, (Suppl.) Vol.21, P249.

86) Robert J.L., Raymond A., Aulombard R, Bousquet C., Joullie A., (1973) Lecture Notes 3rd Int. Conf. Appl. High Magnetic Field in Semicond. Physics Wurzburgh P533.

87) Mott N.F., (1969) Phil. Mag. Vol.19, P835.

88) Shklovskii B.I., Soviet Phys. Semicond. Vol.6, P1053.

89) Durkan J. Elliott R.J., March N.H., (1968) Rev. Mod. Phys. Vol.40, P812.

90) Kleppmann W.G., Elliott R.J., (1975) J. Phys C., C8, P2729.

91) Fantner E.J., Kuchar F., Bauer G., Kriechbaum M., Biernat H., (1974) Proc XII. Int. Conf. Phys. Semicond. Stuttgart P249.

92) Fantner E.J., Kuchar F., Bauer G., (1976) Phys. Stat. Solidi b) Vol.78, P643.

93) Fantner E.J., Bauer G., (1973) Solid St. Commun. Vol.13, P629.

94) Neuringer L.J., (1968) Prox 1X Intern. Conf. Phys. Semicond. Moscow Vol2, P715.

95) Bierat H., Kriechbaum M., (1976) Phys. Stat. Sol. b) Vol.78, P653.

96) Fantner E.J., Kuchar F., (1980) J. Phys. C. Solid St. Phys. Vol.3, P461.

97) Ortenberg von. M., (1973) J. Phys. Chem. Solids. Vol.34, P397.

98) Ikoma H., (1971) J. Phys. Soc. Japan Vol.30, P1509.

99) Nakamura M. Hasegawa H., (1968) J. Phys. Soc. Japan Vol.25, P636.

100) Larsen D.M., (1974) Int. Conf. Appl. High. Mag. Fields Semicond Phys. Wurzburg P295.